EIDUNED
Escuela Internacional de Doctorado

PHD THESIS

2023

UPCOMING WILDFIRES:

Modeling Plant Moisture Dynamics Under Climate Change

Rodrigo Balaguer Romano

PhD PROGRAM IN SCIENCE

Rubén Díaz Sierra, Universidad Nacional de Estudios a Distancia
Víctor Resco de Dios, Universitat de Lleida

Universidad Nacional de Estudios a Distancia
Facultad de Ciencias
Dpto. de Física Matemática y de Fluidos

UPCOMING WILDFIRES:

Modeling Plant Moisture Dynamics Under Climate Change

RODRIGO BALAGUER ROMANO

Directores: Rubén Díaz Sierra & Víctor Resco de Dios

TESIS DOCTORAL

Esta tesis doctoral ha sido financiada por la beca PEJD-2019-PRE/AMB-15644, del Programa Operativo de Empleo Juvenil de la Comunidad de Madrid, asociada al proyecto de investigación RTI2018-094691-B-C31 (MCIU/AEI/FEDER, EU) y con un contrato predoctoral derivado de la beca UNED-SANTANDER. La estancia de tres meses realizada en la Western Sydney University requerida para obtener la Mención Internacional en el título de Doctor ha sido financiada por una ayuda de movilidad internacional del Banco de Santander para doctorandos matriculados en la EIDUNED.

MAYO 2023

AGRADECIMIENTOS

Han sido muchas las personas que me han ayudado con la tesis doctoral a lo largo de estos últimos tres años.

En primer lugar, quiero expresar mi mas sincero agradecimiento a mis directores Rubén Díaz Sierra y Víctor Resco de Dios, que, desde el primer hasta el último día, son quienes han hecho posible que esta tesis haya salido adelante. Rubén, muchas gracias por ofrecerme la oportunidad de hacer la tesis con vosotros, por hacer que me sienta acogido en la UNED desde el primer día, por facilitarme todo el equipo que he necesitado estos años, los fondos, los contactos, los papeleos, la posibilidad de ser tutor de TFG, la docencia, gracias por infundirme el interés por el mundo académico y la importancia de abordar la ciencia desde una perspectiva multidisciplinar. Víctor, muchas gracias por enseñarme a hacer ciencia, a enmarcar la tesis, a definir objetivos, a analizar y representar resultados, a escribir publicaciones, gracias por animarme a participar en cursos y congresos, por ponerme en contacto con tantos investigadores, por brindarme la oportunidad de ir de estancia a Australia, y, por motivarme a apuntar alto.

Durante mi estancia en *Hawkesbury Institute for the Environment* de la *Western Sydney University* he tenido el placer de conocer a Matthias Boer, el director del *NSW Bushfire and Natural Hazards Research Centre*. Matthias, muchas gracias por hacer mi estancia tan agradable, por todos los cafés que nos tomamos hablando de todo un poco y por ayudarme a definir y preparar la publicación del último capítulo de mi tesis. Espero que nos volvamos a ver algún día. También me gustaría agradecer a Rachael Nolan y a Hamish Clarke toda la ayuda que me han prestado.

De "la casa" (la Facultad de Ciencias de la UNED) me gustaría agradecer la ayuda que me ha prestado Daniel Rodríguez Pérez siempre que le he consultado alguna duda. También agradecer a Jaime Arturo de la Torre y Alejandro Pérez Rodríguez facilitarme el acceso al Centro de Computación de Alto Rendimiento (CCAR-UNED) y la asistencia técnica. A José Luis Martínez Guitarte (Tatu), su ayuda con todos los papeleos relacionados con las becas, la estancia, la tesis y su depósito. Al Servicio de Información Bibliográfica y Referencia por facilitar la publicación en acceso abierto del capítulo IV de esta tesis. Por último, agradecer a mis compañeros de despacho de los grupos de Biología y Toxicología Ambiental y de Biología Evolutiva su compañía durante estos años. Ane, Fer, Sori, Alberto, Andrea, Javi, Chicho, Ana Belén, Patri, Esther, Marina, Nacho, os deseo lo mejor.

Le estoy muy agradecido a Javier Madrigal (INIA), que me ayudó a encauzar los primeros pasos de esta tesis, colaborando en el primer artículo que publicamos. A Miquel De Cáceres (CREAF), por toda su ayuda para facilitar el trabajo con el modelo MEDFATE y pulir la publicación de los resultados. A Àngel Cunill Camprubí (UdL) por su ayuda con la obtención de los índices de vegetación espectral. A Jordi Voltas (UdL) por ayudarme con las publicaciones, con los análisis estadísticos y con la financiación de la asistencia a cursos y congresos (con sus papeleos correspondientes) a través del proyecto nacional RESILPINE.

Fuera del mundo académico, también tengo que agradecer el apoyo que me han dado día a día mis seres queridos. Mi madre y mi padre los primeros, gracias a vuestro ejemplo de trabajo, constancia, y esfuerzo estoy donde estoy. Vuestra sencillez, honradez, serenidad, practicidad, y saber vivir son una inspiración para mí, muchas gracias por todo. A mi hermano Nico del que estoy muy orgulloso. A mi abuela Jacinta, a mis tías, tíos primos y prima. A todos mis amigos y amigas, muchos de los cuales me lleváis acompañando más de media vida, viéndonos crecer los unos a los otros. A mi pareja Teresa, gracias por acompañarme en esta aventura y enseñarme que se puede sentir el mundo con otros ojos. A todos, os quiero.

INDEX

Figure Index

Table Index

Abbreviations

FM	Fuel Moisture
LFMC	Live Fuel Moisture Content
DFMC	Dead Fuel Moisture Content
I_0	Critical Surface Intensity
R_0	Critical Minimum Spread Rate
CBH	Canopy Base Height
CBD	Canopy Bulk Density
f_d	Canopy Dead Mass fraction
M_l	Canopy Live Matter Moisture
M_d	Canopy Dead Matter Moisture
M_w	Canopy Weighted Matter Moisture
CFB	Canopy Fraction Burned
LD	Lethal Thresholds
ROS	Fire Rate of Spread
DC	Drought Code
Ψ_{pd}	Predawn Leaf Water Potential
Ψ_{soil}	Soil Water Potential
LAI	Leaf Area Index
Tr	Trees
R-	Seeding shrubs
R+	Resprouting shrubs
EVI	Enhanced Vegetation Index
EWT	Equivalent Water Thickness
MODIS	Moderate Resolution Imaging Spectrometer
SLA	Specific Leaf Area
RCPs	Representative Concentration Pathways
GCMs	Global Climate Models
RCMs	Regional Climate Models
NPP	Net Primary Productivity
VPD	Vapor Pressure Deficit
d yr^{-1}	Days per year
$[CO_2]$	Atmospheric CO_2 concentration
FWI	Fire Weather Index
KBDI	Keetch-Byram Drought Index
Gt C	Giga Tons of Carbon
ΔSP	Net Sequestration Potential
EESF	Emissions Equivalent of Shortwave Forcing
NESC	Net Equivalent Carbon Stock Change
NEP	Net Ecosystem Productivity
IDW	Inverse Distance Weighted Interpolation
Mha	Million hectares
t C ha^{-1}	Tons of carbon per Hectare

Publications & Communications

1. Journal Articles

Balaguer-Romano, R., Díaz-Sierra, R., De Cáceres, M., Voltas, J., Boer, M. M., Resco de Dios, V. Global warming and associated drying of fuels threatens Spanish forest carbon sinks. Agricultural and Forest Meteorology. (Under Review)

Balaguer-Romano, R., Díaz-Sierra, R., De Cáceres, M., Cunill-Camprubí, À., Nolan, R. H., Boer, M. M., Voltas, J., Resco de Dios, V. (2022). A semi-mechanistic model for predicting daily variations in species-level live fuel moisture content. Agricultural and Forest Meteorology, 323, 323, 109022. https://doi.org/10.1016/j.agrformet.2022.109022

Balaguer-Romano, R., Díaz-Sierra, R., Madrigal, J., Voltas, J., & de Resco de Dios, V. (2020). Needle senescence affects fire behavior in Aleppo pine (*Pinus halepensis* Mill.) stands: A simulation study. Forests 11(10), 1054. https://doi.org/10.3390/f11101054

2. Conference Communications

Balaguer-Romano, R.; Diaz-Sierra, R.; Resco de Dios, V. Fuel moisture content dynamics under climate change in Spanish forests., in Proceedings of the 3rd International Electronic Conference on Forests: Exploring New Discoveries and New Directions in Forests, 15–31 October 2022, MDPI: Basel, Switzerland, doi:10.3390/IECF2022-13121

Balaguer-Romano, R.; Diaz-Sierra, R.; De Cáceres, M.; Voltas, J.; Resco de Dios, V. Un modelo semi-mecanicista para predecir las variaciones diarias de la humedad del combustible vivo a nivel de especie., in 8º Congreso Forestal Español, 27 June-1 July 2022, Sociedad Española de Ciencias Forestales: Lleida, España.

Balaguer-Romano, R.; Diaz-Sierra, R.; Voltas, J.; Resco de Dios, V. Linking Fuel Moisture with Plant Physiology: Coupling a water balance model with a LFMC model to predict species-specific LFMC values., in Proceedings of the 2nd International Electronic Conference on Forests: Sustainable Forests: Ecology, Management, Products and Trade, 1–15 September 2021, MDPI: Basel, Switzerland, doi:10.3390/IECF2021-10799

Balaguer-Romano, R.; Diaz-Sierra, R.; Madrigal, J.; Voltas, J.; Resco de Dios, V. Needle senescence affects fire behavior in Aleppo pine (*Pinus halepensis* Mill.) stands: a simulation study., in Proceedings of the 1st International Electronic Conference on Forests: Forests for a Better Future: Sustainability, Innovation, Interdisciplinarity, 15–30 November 2020, MDPI: Basel, Switzerland, doi:10.3390/IECF2020-08079

RESUMEN

La variación espacial y temporal del contenido de humedad de las plantas (humedad del combustible vivo; HCV) es un factor crítico en el desarrollo de los incendios forestales. La HCV condiciona la inflamabilidad de los ecosistemas al determinar la cantidad de biomasa vegetal (el combustible) susceptible de arder y su grado de conectividad espacial. A pesar de la importancia que supone monitorear la HCV para anticipar las amenazas asociadas a los incendios forestales, todavía existen importantes lagunas de conocimiento a la hora de estimar sus variaciones temporales y espaciales, sobre todo considerando las condiciones derivadas del calentamiento global. Por lo tanto, el objetivo principal de esta tesis doctoral es incrementar el realismo biológico de las estimaciones de la HCV, para evaluar con mayor precisión los efectos del cambio climático sobre la incidencia de incendios forestales. Para lograrlo, primero he simulado cómo afecta la variación estacional de la HCV al desarrollo de los incendios. A continuación, he desarrollado un modelo semi-mecanicista que considera los rasgos fisiológicos clave para estimar con precisión la HCV a nivel de especie. Luego, he aplicado el modelo desarrollado para pronosticar las tendencias de la HCV bajo las condiciones del cambio climático, evaluando los posibles aumentos en la incidencia de incendios forestales. Finalmente, he estimado hasta qué punto los aumentos en la incidencia de incendios forestales comprometen el potencial de las estrategias de reforestación a gran escala para mitigar el cambio climático a través del secuestro de carbono.

Los resultados de las simulaciones han permitido observar como las disminuciones en la HCV favorecen el desarrollo de incendios extremos, y, por lo tanto, no considerar la HCV a la hora de simular el comportamiento del fuego puede conducir a subestimar los riesgos asociados a los incendios forestales. El desarrollo del modelo semi-mecanicista para estimar la HCV a nivel de especie ha permitido observar que la inclusión de características fisiológicas de las plantas aumenta el realismo biológico y las capacidades predictivas de las estimaciones. El uso del modelo desarrollado para pronosticar las dinámicas de la HCV ha permitido proyectar aumentos significativos en la duración de las temporadas de incendios en amplias zonas forestales de la España peninsular. Estos aumentos han resultado ser inversamente proporcionales al gradiente de productividad de los ecosistemas. Finalmente, los aumentos que hemos proyectado en la incidencia de incendios forestales reducen la ya limitada capacidad de las reforestaciones para compensar las emisiones de CO_2. Los resultados indican que la capacidad de secuestro de carbono mediante programas de reforestación a gran escala está sobreestimada. En general, concluimos que podemos estar al borde de un drástico aumento en la incidencia de grandes incendios forestales a medida que las condiciones del cambio climático inducen bajos valores de la HCV durante periodos más frecuentes e intensos. Por lo tanto, es necesario seguir profundizando en el analisis de las dinámicas de la HCV con una perspectiva basada en procesos fisiológicos, que permita mejorar la anticipación y reducción de los impactos asociados a los incendios forestales en las próximas décadas.

ABSTRACT

Spatial and temporal variation in the moisture content of leaves, twigs, and small diameter branches (live fuel moisture content; LFMC) is a critical driver of the patterns of wildfire activity. LFMC conditions ecosystem flammability by affecting the availability of plant biomass (fuels) to fire and also the degree of spatial connectivity of dry patches. However, despite the crucial role of understanding LFMC dynamics for anticipating wildfire danger, there are still significant knowledge gaps regarding the estimation of temporal and spatial variations, particularly under ongoing global warming. The main purpose of this PhD Thesis is to improve current and future assessments of LFMC by adding more biological realism in LFMC estimations. To this end, I first simulated how seasonal variation in LFMC affects fire behavior. Secondly, I developed a semi-mechanistic model that considers key physiological traits to estimate species-specific LFMC dynamics. Then, I applied this model to forecast LFMC trends under climate change conditions assessing potential wildfire danger increases, including also estimates of dead fuel moisture content (DFMC). Finally, using a key driver of both LFMC and DFMC, I estimated how projected increases in fire danger under global warming may compromise the potential of reforestation strategies to mitigate climate change through carbon sequestration.

Simulation results indicated that LFMC declines increase the likelihood of extreme fire behavior and, therefore, disregarding LFMC from fire modeling would lead to wildfire risk underpredictions. The development of a new semi-mechanistic model to infer LFMC, considering plant physiological traits, significantly increased predictive capabilities. The application of this approach to forecast LFMC dynamics allows to project significant increases in the fire season over large parts of peninsular Spain, in a manner that was inversely proportional to the gradient in productivity. Finally, projected increases in future wildfire risks reduce the limited potential of reforestation strategies to offset anthropogenic CO_2 emissions, highlighting that, previous estimates on the potential carbon removal by plantations have been greatly overestimated. Overall, I conclude that we may be at the brink of a dramatical increase in the incidence of large wildfires, as fuel dry-down processes induced by climate change become more frequent and intense. The process-based understanding of LFMC dynamics proposed here may serve to anticipate critical transitions in forest flammability and consequently improve our preparedness for increased wildfire impacts in the coming decades.

Keywords: *Fuel Moisture, Fire Danger, Fire Modeling, Plant Hydraulics, Climate Change, Pyrophysiology.*

CHAPTER I:
INTRODUCTION

INTRODUCTION

I.1 Background

Wildfires have played a major role in shaping the structure and function of terrestrial ecosystems for the last 420 million years, following land plant expansion (Glasspool *et al.*, 2006). Wildfires affect the Earth system by altering the energy balance, the evolution of physiological traits and the oxygen cycle, among other processes (Resco de Dios, 2020). Thus, wildfires should be considered a key part of the environment, and sustainable wildfire management should aim to reduce risks to life and property while maintaining ecological functions, instead of attempting to eliminate all fires in ecosystems that are naturally fire-prone. A crucial aspect for achieving this objective relies on understanding the drivers of fire activity, from local to landscape scales. Wildfire activity is driven by four environmental triggers that need to occur simultaneously (Fig. I.1; Boer *et al.*, 2017; Bradstock, 2010). First, an accumulation of live and dead plant material with spatial continuity for fire propagation across the landscape is required. Then, this accumulated biomass (fuel) must dry out to become available to the fire. Once those conditions are met, the landscape is in a flammable state, and fires will readily start with an ignition. Finally, wildfires may reach major spread rates depending on the fire weather conditions, which are a combination of meteorological variables as wind, air temperature, precipitation, and relative humidity.

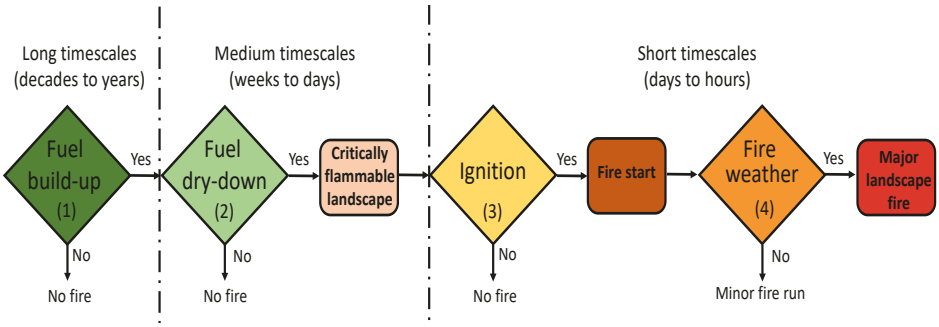

Figure. I.1: Wildfire drivers. Wildfire activity is drive by four environmental conditions. Modified from Boer *et al.*, 2017.

These four triggers operate at different timescales. On the one hand, while vegetation growth and the consequent accumulation of live and dead plant material take years to decades, the dry-down of these fuels varies seasonally, taking from weeks to days. On the other hand, ignitions are instantaneous and the meteorological conditions conducting to a fire weather show high variability at short timescales (Boer *et al.*, 2017). This PhD Thesis is focused on improving the modeling of fuel dry-down processes trough the inclusion of plant physiological mechanisms, with the aim of providing more accurate assessments of future wildfire risks.

I.2 Wildfire Modeling and Fuel Moisture

Despite wildfires being a natural component of many terrestrial ecosystems, they have become a threat to civil protection, public health, and national security in many different countries worldwide (Borchers-Arriagada *et al.*, 2021; Duane *et al.*, 2021; Karavani *et al.*, 2018; McDonald, 2020; Resco de Dios & Nolan, 2021; Tedim *et al.*, 2020). In this sense and following the advances in computational power in the last decades, fire behavior models have been developed to assist in wildfire management and prevention strategies. These models, implemented as software programs, mathematically describe the physical and chemical processes of wildfires to make quantitative evaluations of their onset and spread across the landscape (Sullivan, 2009a, 2009b, 2009c). Thus, fire behavior models play a crucial role in assisting fire extinction interventions, determining the locations where fire prevention actions will be more critical, and understanding the seasonal variation of fire activity and its drivers.

Modeling fire behavior characteristics and its effects involves describing fuel properties, meteorological conditions, and topographic features as inputs variables for model calculations (Andrews, 2018). Among fuel properties, fuel moisture (FM), defined as the water content per unit of dry weight, plays a crucial role in fire behavior because high moisture content values can significantly reduce fire ignition and propagation (Rothermel, 1983). Moreover, by determining the effective heat released when fuel burns, FM determines crucial fire attributes such as rate of spread, flame dimensions and fuel consumption (Anderson, 1970; McArthur, 1966). Therefore, monitoring and forecasting FM dynamics is a crucial aspect for understanding wildfire activity, and FM is a main input variable in almost all fire behavior models (Matthews, 2014).

The moisture contents of live and dead fuels are considered separately, as each fuel type shows its own temporal dynamics (Pimont *et al.*, 2019). Dead fuels such as leaves, bark, twigs, fallen limbs, and logs, are classified according to the thickness of their particles (<6 mm, 6-25 mm, 25-75 mm and >75 mm), since it determines the time lag needed to reach equilibrium with environmental humidity (1 h, 10 h, 100 h and 1000 h). Fine dead fuels (<25 mm) moisture content responds rapidly to atmospheric condition changes, transitioning from non-flammable to flammable states within hours, and thus causing a major impact over fire behavior (Resco de Dios, 2020). The effect of dead fuel moisture content (DFMC) on the behavior of surface fires has been well documented for decades (Anderson & Rothermel, 1965) and its estimation and monitorization has been largely addressed from different perspectives (Matthews, 2014; Viney, 1991). In contrast, there are significant knowledge gaps regarding the estimation and forecast of live fuel moisture dynamics.

I.3 Live Fuel Moisture Content

The term live fuels basically refer to plants' live foliage and small twigs. Fires across plant canopies propagate primarily through particles with a thickness smaller than 3 mm, and this is what constitutes the pool of live fuels. DFMC is a critical driver for the ignition and propagation of surface fires. Live fuel moisture content (LFMC) is equally important to determine fire spread across shrubs in surface fires. Furthermore, the probability and spread of high intensity crown fires are conditioned by LFMC (Van Wagner, 1977). The transition of fire from surface to crown fuel layers enables major landscape wildfire events in which fire intensity and severity increase dramatically, precluding extinction activities and causing severe ecological and socioeconomic impacts (Alexander & Cruz, 2016). Although the influence of LFMC on crown fire propagation has been questioned (Alexander & Cruz, 2013), several studies support that LFMC strongly affects fire activity at landscape scales (Dennison & Moritz, 2009; Nolan *et al.*, 2016; Pimont *et al.*, 2019; Ruffault *et al.*, 2018a). However, estimating and forecasting LFMC dynamics still poses significant difficulties.

LFMC exhibits temporal and spatial variations within and among plant species due to differences in anatomical and physiological traits that interact with environmental conditions across the soil-plant-atmosphere continuum (Resco de Dios, 2020, Kane *et al.*, 2023, Griebel *et al.*, 2023). While LFMC values in tree species remain nearly constant throughout the year, shrubs and herbs often show large seasonal variations (Martin-StPaul *et al.*, 2018; Nolan *et al.*, 2018; Pellizzaro *et al.*, 2007a; Yebra *et al.*, 2019). Nolan *et al.* (2018) proposed three major physiological processes to potentially explain the observed interspecific variability in LFMC temporal dynamics. One of them is access to water resources, which depends on root systems. Species with deeper root systems can access water resources from lower soil layers, buffering short-term fluctuations in shallow layers, and they therefore show a nearly constant LFMC throughout the year. In contrast, species with shallow root systems can only reach water resources from superficial soil layers, and thus display major seasonal LFMC variability. Other physiological mechanisms proposed to explain interspecific differences in LFMC dynamics rely on stomatal regulation processes, which affect leaf water potential, and osmotic and elastic adjustments, which affect turgor loss points and water storage capacities. Additionally, anatomical changes derived for instance from leaf phenology may also alter seasonal LFMC dynamics.

All these physiological processes can be considered to estimate LFMC dynamics through trait-based plant hydraulic models, but these mechanistic approaches are not used for managing wildfire danger as its development started only recently (Balaguer-Romano *et al.*, 2022; Ruffault *et al.*, 2022). However, the use of this mechanistic perspective to infer LFMC dynamics may potentially solve some of the limitations of current approaches as meteorological drought indices or remote sensing products.

Although drought indices were not developed to model fuel moisture, they are nonetheless used to predict LFMC through empirical relationships (Pellizzaro *et al.*, 2007b; Viegas *et al.*, 2001). The most popular ones are derived from fire weather and fire danger rating systems, such as the Drought Code (DC; Van Wagner, 1987) or the Keetch-Byram Drought Index (KBDI; Keetch & Byram, 1968). As these indices are based on daily weather data, which can be easily derived from meteorological datasets at locations of interest, they have been widely used to provide historical and projected estimations of LFMC dynamics. However, the use of drought indices to estimate species specific LFMC induces large spatial uncertainties as LFMC dynamics is species-dependent and drought indices cannot consider the physiological mechanisms involved in plant responses to water scarcity conditions (Ruffault *et al.*, 2018b). In contrast, LFMC values can be estimated through remote sensing approaches, as vegetation reflectance varies with water content. Thus, remotely sensed data are used for monitoring past and current LFMC dynamics over large areas at fine spatial and temporal resolutions (Yebra *et al.*, 2013; Yebra *et al.*, 2018). However, these approaches also show limitations as remotely sensed data require calibration and validation and they do not allow forecasting of future fuel moisture conditions.

Forecasting fuel moisture dynamics is crucial to anticipate future wildfire risks derived from climate change impacts. Global warming is expected to increase water scarcity, enhancing the frequency and intensity of droughts and fuel drying events (IPCC, 2021). Consequently, fire season duration and fire danger may increase as fuel moisture declines below critical dryness thresholds for longer periods. Furthermore, forested ecosystems with vast amounts of biomass that are currently fire-free due to high moisture content, may dry out and start experiencing large wildfire events in the coming decades (Resco de Dios *et al.*, 2021). In this context, it is important to understand the potential buffering effects derived from physiological mechanism that enhance plant species' resilience over climate aridity increases. Several attempts to estimate future fuel moisture dynamics and its effects on wildfire danger have been conducted based on drought indices, concluding that increased temperature and decreased precipitation would lead to global fire risk increases (Abatzoglou *et al.*, 2019; Dupuy *et al.*, 2020; Ellis *et al.*, 2022; Jones *et al.*, 2022; Rigo *et al.*, 2017). However, these studies do not consider to what extent can plant traits buffer climate change effects as physiological adjustments driving LFMC dynamics are ignored. Further research is needed in this sense to accurately estimate live fuel moisture dynamics under climate change conditions to assess future wildfire risks.

One of the main risks associated with wildfires is the potential impact over the global carbon cycle, through the release into the atmosphere of huge carbon amounts currently stored in forests (Anderegg *et al.*, 2020). Wildfire climate impacts do not only entail carbon emissions, as carbon sequestration potential is also reduced following forest cover losses. As photosynthetic carbon sequestration produces a

cooling effect by lowering atmospheric CO_2 concentration, the conservation of forest ecosystems is highlighted as a priority to face global warming (IPCC, 2021). In this sense, forest restoration is often proposed as a strategy for climate change mitigation (Bastin *et al.*, 2019). However, it remains uncertain to which extent climate change mitigation can be achieved through reforestation due to poor quantification of associated biogeophysical effects and future changes in wildfire risk. As fuel dry-down increases under global warming, accurate global assessments should be carried out to understand whether reforestation efforts to mitigate climate change are safe from projected wildfire danger increases.

The main purpose of this PhD Thesis is to shed some light into current knowledge gaps related to the effect of LFMC dynamics on fire behavior, the estimation of temporal and spatial LFMC variations, the forecasting of future LFMC trends under climate change conditions, and the potential feedbacks of changes in fuel moisture and fire danger on the potential of forest restoration actions proposed to mitigate climate change. To achieve it, first, I evaluated the influence of seasonal LFMC variations on large wildfire events through a simulation study. Second, I developed a semi-mechanistic model that considers key physiological traits to estimate species-specific LFMC dynamics overcoming the limitations of current approaches. Then, I applied this new approach to forecast future fuel moisture trends under climate change projections, taking into account plant physiological traits, in order to anticipate future changes in wildfire danger. Finally, I estimated to which extent projected changes in future wildfire danger would compromise the capacity of reforested lands to offset anthropogenic carbon emissions.

I.4 Structure of the PhD Thesis

The hypotheses and objectives of the PhD Thesis are presented in Chapter II. The main research of the thesis is described in the following four chapters, presented as scientific articles. In Chapter III, a simulation study is conducted to evaluate the effect of seasonal LFMC variations on the incidence of crown fire events in Mediterranean pinewoods. Chapter IV introduces a novel approach to estimate and forecast LFMC dynamics at species level. Chapter V assesses future wildfire risks by projecting Spain forests fuel moisture dynamics through the 21st century using the novel modeling approach developed in Chapter IV. Chapter VI spatially assess how increasing vapor pressure deficit, a key driver of fuel moisture and fire activity, could endanger the potential contribution of forest restoration activities to offset anthropogenic CO_2 emissions. Each chapter includes an introduction to the subject, a description of the methodology, a presentation of the results, a discussion of the results and the main conclusions. Chapter VII presents a general discussion of the principal achievements of the PhD Thesis. Finally, Chapter VIII summarizes the main research highlights. Bibliographic citations are provided, in separate sections, at the end of each chapter.

I.5 References

Abatzoglou, J. T., Williams, A. P., & Barbero, R. (2019). Global Emergence of Anthropogenic Climate Change in Fire Weather Indices. Geophysical Research Letters, 46(1), 326–336. https://doi.org/10.1029/2018GL080959

Alexander, M. E., & Cruz, M. G. (2013). Assessing the effect of foliar moisture on the spread rate of crown fires. International Journal of Wildland Fire, 22(6), 415–427. https://doi.org/10.1071/WF12008-CO

Alexander, M. E., & Cruz, M. G. (2016). Crown fire dynamics in conifer forests. USDA Forest Service - General Technical Report PNW-GTR, 163–258.

Anderegg, W. R. L., Trugman, A. T., Badgley, G., Anderson, C. M., Bartuska, A., Ciais, P., Cullenward, D., Field, C. B., Freeman, J., Goetz, S. J., Hicke, J. A., Huntzinger, D., Jackson, R. B., Nickerson, J., Pacala, S., & Randerson, J. T. (2020). Climate-driven risks to the climate mitigation potential of forests. Science 368(6497). https://doi.org/10.1126/science.aaz7005

Anderson, H. E. (1970). Forest fuel ignitibility. Fire Technology, 6(4), 312–319. https://doi.org/10.1007/BF02588932

Anderson, H. E., & Rothermel, R. C. (1965). Characteristics of Free-Burning Fires. 1009–1019.

Andrews, P. L. (2018). The Rothermel surface fire spread model and associated developments: A comprehensive explanation. USDA Forest Service - General Technical Report RMRS-GTR, 2018(371), 1–121.

Balaguer-Romano, R., Díaz-Sierra, R., De Cáceres, M., Cunill-Camprubí, À., Nolan, R. H., Boer, M. M., Voltas, J. & Resco de Dios, V. (2022). A semi-mechanistic model for predicting daily variations in species-level live fuel moisture content. Agricultural and Forest Meteorology, 323. https://doi.org/10.1016/j.agrformet.2022.109022

Bastin, J. F., Finegold, Y., Garcia, C., Mollicone, D., Rezende, M., Routh, D., Zohner, C. M., & Crowther, T. W. (2019). The global tree restoration potential. Science, 364(6448), 76–79. https://doi.org/10.1126/science.aax0848

Boer, M. M., Nolan, R. H., Resco de Dios, V., Clarke, H., Owen, F., & Bradstock, R. A. (2017). Changing Weather Extremes Call for Early Warning of Potential for Catastrophic Fire. Earth's Future, 5:1196–1202. https://doi.org/10.1002/eft2.274

Borchers-Arriagada, N., Bowman, D. M. J. S., Price, O., Palmer, A. J., Samson, S., Clarke, H., Sepulveda, G., & Johnston, F. H. (2021). Smoke health costs and the calculus for wildfires fuel management: a modelling study. The Lancet Planetary Health, 5(9), e608–e619. https://doi.org/10.1016/s2542-5196(21)00198-4

Bradstock, R. A. (2010). A biogeographic model of fire regimes in Australia: Current and future implications. Global Ecology and Biogeography, 19(2), 145–158. https://doi.org/10.1111/j.1466-8238.2009.00512.x

Dennison, P. E., & Moritz, M. A. (2009). Critical live fuel moisture in chaparral ecosystems: A threshold for fire activity and its relationship to antecedent precipitation. International Journal of Wildland Fire, 18(8), 1021–1027. https://doi.org/10.1071/WF08055

Duane, A., Castellnou, M., & Brotons, L. (2021). Towards a comprehensive look at global drivers of novel extreme wildfire events. Climatic Change, 165(3–4), 1–21. https://doi.org/10.1007/s10584-021-03066-4

Dupuy, J. L., Fargeon, H., Martin-StPaul, N., Pimont, F., Ruffault, J., Guijarro, M., Hernando, C., Madrigal, J., & Fernandes, P. (2020). Climate change impact on future wildfire danger and activity in southern Europe: a review. Annals of Forest Science, 77(2). https://doi.org/10.1007/s13595-020-00933-5

Ellis, T. M., Bowman, D. M. J. S., Jain, P., Flannigan, M. D., & Williamson, G. J. (2022). Global increase in wildfire risk due to climate-driven declines in fuel moisture. Global Change Biology, 28(4), 1544–1559. https://doi.org/10.1111/gcb.16006

Glasspool, I. J., Edwards, D., & Axe, L. (2006). Charcoal in the Early Devonian: A wildfire-derived Konservat-Lagerstätte. Review of Palaeobotany and Palynology, 142(3–4), 131–136. https://doi.org/10.1016/j.revpalbo.2006.03.021

Griebel, A., Boer, M. M., Blackman, C., Choat, B., Ellsworth, D. S., Madden, P., Medlyn, B., Resco de Dios, V., Wujeska-Klause, A., Yebra, M., Younes Cardenas, N., & Nolan, R. H. (2023). Specific leaf area and vapour pressure deficit control live fuel moisture content. Functional Ecology, 37(3), 719–731. https://doi.org/10.1111/1365-2435.14271

IPCC. (2021). Climate Change 2021: The Physical Science Basis. Contribution of Working Group I to the Sixth Assessment Report of the Intergovernmental Panel on Climate Change. Cambridge University Press, United Kingdom.

Jones, M. W., Abatzoglou, J. T., Veraverbeke, S., Andela, N., Lasslop, G., Forkel, M., Smith, A. J. P., Burton, C., Betts, R. A., van der Werf, G. R., Sitch, S., Canadell, J. G., Santín, C., Kolden, C., Doerr, S. H., & Le Quéré, C. (2022). Global and Regional Trends and Drivers of Fire Under Climate Change. Reviews of Geophysics, 60(3), 1–76. https://doi.org/10.1029/2020rg000726

Kane, J. M., Kerhoulas, L. P., & Goff, G. S. (2023). Conifer encroachment increases foliar moisture content in a northwestern California oak woodland. International Journal of Wildland Fire, 1–10. https://doi.org/10.1071/WF22184

Karavani, A., Boer, M. M., Baudena, M., Colinas, C., Díaz-Sierra, R., Pemán, J., de Luis, M., Enríquez-de-Salamanca, Á., & Resco de Dios, V. (2018). Fire-induced deforestation in drought-prone Mediterranean forests: drivers and unknowns from leaves to communities. Ecological Monographs, 88(2), 141–169. https://doi.org/10.1002/ecm.1285

Keetch, J. J., & Byram, G. M. (1968). A Drought Index for Forest Fire Control. US Departament of Agriculture, Forest Service, Southeastern Forest Experiment Station. 38, 1-32.

Martin-StPaul, N., Pimont, F., Dupuy, J. L., Rigolot, E., Ruffault, J., Fargeon, H., Cabane, E., Duché, Y., Savazzi, R., & Toutchkov, M. (2018). Live fuel moisture content (LFMC) time series for multiple sites and species in the French Mediterranean area since 1996. Annals of Forest Science, 75(3). https://doi.org/10.1007/s13595-018-0744-4

Matthews, S. (2014). Dead fuel moisture research: 1991-2012. International Journal of Wildland Fire, 23(1), 78–92. https://doi.org/10.1071/WF13005

McArthur, A. G. (1966). Weather and grassland fire behaviour. Australian Forestry and Timber Bureau Department of National Development, Leaflet 10, 1-23.

McDonald, M. (2020). After the fires? Climate change and security in Australia. Australian Journal of Political Science, 56(1), 1–18. https://doi.org/10.1080/10361146.2020.1776680

Nolan, R. H., Boer, M. M., Resco De Dios, V., Caccamo, G., & Bradstock, R. A. (2016). Large-scale, dynamic transformations in fuel moisture drive wildfire activity across southeastern Australia. Geophysical Research Letters, 43(9), 4229–4238. https://doi.org/10.1002/2016GL068614

Nolan, R. H., Hedo, J., Arteaga, C., Sugai, T., & Resco de Dios, V. (2018). Physiological drought responses improve predictions of live fuel moisture dynamics in a Mediterranean forest. Agricultural and Forest Meteorology, 263, 417–427. https://doi.org/10.1016/j.agrformet.2018.09.011

Pellizzaro, G., Duce, P., Ventura, A., & Zara, P. (2007a). Seasonal variations of live moisture content and ignitability in shrubs of the Mediterranean Basin. International Journal of Wildland Fire, 16(5), 633–641. https://doi.org/10.1071/WF05088

Pellizzaro, G., Cesaraccio, C., Duce, P., Ventura, A., & Zara, P. (2007b). Relationships between seasonal patterns of live fuel moisture and meteorological drought indices for Mediterranean shrubland species. International Journal of Wildland Fire, 16(2), 232–241. https://doi.org/10.1071/WF06081

Pimont, F., Ruffault, J., Martin-StPaul, N. K., & Dupuy, J. L. (2019). Why is the effect of live fuel moisture content on fire rate of spread underestimated in field experiments in shrublands? International Journal of Wildland Fire, 28(2), 127–137. https://doi.org/10.1071/WF18091

Resco de Dios, V. (2020). Plant-Fire Interactions. Applying Ecophysiology to Wildfire Management. Vol 36. Springer, Switzerland.

Resco de Dios, V., Hedo, J., Cunill, À., Thapa, P., Martínez, E., Martínez, J., Aragón, D., Antonio, J., Balaguer-Romano, R., Díaz-sierra, R., Yebra, M., & Boer, M. M. (2021). Climate change induced declines in fuel moisture may turn currently fi re-free Pyrenean mountain forests into fi re-prone ecosystems. Science of the Total Environment, 797, 149104. https://doi.org/10.1016/j.scitotenv.2021.149104

Resco de Dios, V., & Nolan, R. H. (2021). Some challenges for forest fire risk predictions in the 21st century. Forests, 12(4), 1–5. https://doi.org/10.3390/f12040469

Rigo, D. de, Libertà, G., Durrant, T. H., Vivancos, T. A., & San-Miguel-Ayanz, J. (2017). Forest fire danger extremes in Europe under climate change: variability and uncertainty. In Publication Office of the European Union.

Rothermel, R. C. (1983). How to predict the spread and intensity of forest and range fires. US Department of Agriculture, Forest Service, General Technical Report, INT-143. https://doi.org/10.2737/INT-GTR-143

Ruffault, J., Curt, T., Martin-Stpaul, N. K., Moron, V., & Trigo, R. M. (2018a). Extreme wildfire events are linked to global-change-type droughts in the northern Mediterranean. Natural Hazards and Earth System Sciences, 18(3), 847–856. https://doi.org/10.5194/nhess-18-847-2018

Ruffault, J., Martin-StPaul, N., Pimont, F., & Dupuy, J. L. (2018b). How well do meteorological drought indices predict live fuel moisture content (LFMC)? An assessment for wildfire research and operations in Mediterranean ecosystems. Agricultural and Forest Meteorology, 262, 391–401. https://doi.org/10.1016/j.agrformet.2018.07.031

Ruffault, J., Pimont, F., Cochard, H., Dupuy, J. L., & Martin-Stpaul, N. (2022). SurEau-Ecos v2.0: a trait-based plant hydraulics model for simulations of plant water status and drought-induced mortality at the ecosystem level. Geoscientific Model Development, 15(14), 5593–5626. https://doi.org/10.5194/gmd-15-5593-2022

Sullivan, A. L. (2009a). Wildland surface fire spread modelling, 1990–2007. 1: Physical and quasi-physical models. International Journal of Wildland Fire, 18(4), 387. https://doi.org/10.1071/wf06144

Sullivan, A. L. (2009b). Wildland surface fire spread modelling, 1990 - 2007. 2: Empirical and quasi-empirical models. International Journal of Wildland Fire, 18(4), 369. https://doi.org/10.1071/wf06142

Sullivan, A. L. (2009c). Wildland surface fire spread modelling, 1990 - 2007. 3: Simulation and mathematical analogue models. International Journal of Wildland Fire, 18(4), 387. https://doi.org/10.1071/wf06144

Tedim, F., Leone, V., & Mcgee, T. (2020). Extreme wildfire events and disasters: Root causes and new management strategies. Elsevier, Netherlands.

Van Wagner, C. E. (1977). Conditions for the start and spread of crown fire. Canadian Journal of Forest Research, 7(1), 23–34. https://doi.org/10.1139/x77-004

Van Wagner, C. E. (1987). Development and structure of the Canadian forest fire weather index system. Canadian Forest Service, Information Report 35.

Viegas, D. X., Piñol, J., Viegas, M. T., & Ogaya, R. (2001). Estimating live fine fuels moisture content using meteorologically-based indices. International Journal of Wildland Fire, 10(2), 223–240. https://doi.org/10.1071/WF01022

Viney, N. R. (1991). A review of fine fuel moisture modelling. International Journal of Wildland Fire, 1(4), 215–234. https://doi.org/10.1071/WF9910215

Yebra, M., Quan, X., Riaño, D., Rozas-Larraondo, P., Van Dijk, A. I. J. M., & Cary, G. J. (2018). Mapping live fuel moisture content and flammability for continental Australia using optical remote sensing. International Geoscience and Remote Sensing Symposium (IGARSS), 2018-July, 5903–5906. https://doi.org/10.1109/IGARSS.2018.8517662

Yebra, Marta, Dennison, P. E., Chuvieco, E., Riaño, D., Zylstra, P., Hunt, E. R., Danson, F. M., Qi, Y., & Jurdao, S. (2013). A global review of remote sensing of live fuel moisture content for fire danger assessment: Moving towards operational products. Remote Sensing of Environment, 136, 455–468. https://doi.org/10.1016/j.rse.2013.05.029

Yebra, Marta, Scortechini, G., Badi, A., Beget, M. E., Boer, M. M., Bradstock, R., Chuvieco, E., Danson, F. M., Dennison, P., Resco de Dios, V., Di Bella, C. M., Forsyth, G., Frost, P., Garcia, M., Hamdi, A., He, B., Jolly, M., Kraaij, T., Martín, M. P., Ustin, S. (2019). Globe-LFMC, a global plant water status database for vegetation ecophysiology and wildfire applications. Scientific Data, 6(1), 1–8. https://doi.org/10.1038/s41597-019-0164-9

CHAPTER II:
HYPOTHESES & OBJECTIVES

II.1 Hypotheses
II.2 Objectives

HYPOTHESES & OBJECTIVES

II.1 Hypotheses

H_0.1: Live fuel moisture content (LFMC) variation affects fire behavior.

H_0.2: Including plant physiological traits in LFMC modeling improves the estimation of species-specific temporal and spatial patterns.

H_0.3: Climate change is going to increase fuel-drying events, lengthening fire seasons, and enhancing wildfire danger throughout the 21st century.

H_0.4: Future wildfire activity would reduce the potential of large-scale reforestation strategies to mitigate climate change.

II.2 Objectives

Ob.1: Simulate the potential effects of Aleppo pine needle senescence on fire behavior, focusing on whether LFMC declines increase the incidence of crown fires development. Additionally, evaluate LFMC effects on fire behavior compared to the effect of other wildfire drivers, such as wind speed and DFMC.

Ob.2: Develop a semi-mechanistic model to infer species-specific LFMC dynamics and evaluate its capabilities by comparing the model estimations with field observed values. Then, compare this degree of agreement with estimations obtained under widely used approaches as meteorological drought indices and remote sensed data.

Ob.3: Apply semi-mechanistic models, using climate projections to forecast fuel moisture dynamics in peninsular Spain's forests. Analyze subsequent changes in fire season length by assessing the number of days per year with values below fuel dryness thresholds.

Ob.4: Assess the climate change mitigation potential of forest restoration by estimating global net carbon sequestration. Then, quantify the extent to which projected future wildfire danger could compromise this climate change mitigation potential.

CHAPTER III:
INTERACTIONS BETWEEN LFMC DYNAMICS AND WILDFIRES

INTERACTIONS BETWEEN LFMC DYNAMICS AND WILDFIRES

ABSTRACT

In this chapter, I evaluate the interaction between LFMC seasonal variation and wildfire danger by simulating the effect of Aleppo pine needle senescence process on the incidence of crown fire development. First, I introduce Aleppo pine needle senescence process as well as the different crown fire types, the variables affecting surface fires transition to crown fires and how these events are modelled. Then, I describe the methodology established to simulate fire behavior considering needle senescence seasonal effects over fuel moisture and structure in different Aleppo pine stands. Finally, I present and discuss the results arguing the effect of needle senescence over fire behavior relative to the effect of other wildfire drivers, such as wind speed and DFMC.

The research activities related in this chapter were published in the journal Forests in 2020 under the title: "Needle Senescence Needle senescence affects fire behaviour in Aleppo pine (Pinus halepensis mill.) stands: A simulation study" with Rubén Díaz-Sierra, Javier Madrigal, Jordi Voltas and Victor Resco de Dios as co-authors. https://doi.org/10.3390/f11101054

III.1 Introduction

Pine-dominated ecosystems are one of the major landscape types in the Mediterranean Basin, where they cover 25 % of the forest surface (Barbero *et al.*, 1998). One of the most abundant and widespread pine species in the Mediterranean Basin is *Pinus halepensis* Mill. (Aleppo pine), which covers 6.8 Mha, at low altitudes (<500 m) and near the coastline (Mauri *et al.*, 2016). Aleppo pine is a fire-embracer species meaning that it depends, at least partly, on fire for seed release from serotinous cones and consequent regeneration (Keeley, 2012; Resco de Dios *et al.*, 2018). Post-fire regeneration often results in dense thickets that show a high accumulation of ladder fuels leading to vertical fuel continuity (Palmero-Iniesta *et al.*, 2017). *P. halepensis* shows a low degree of self-pruning and thus, these forests are particularly prone to crown fires. Therefore, approximately one-third of the total annual burned area in the Mediterranean Basin occurs in *P. halepensis* stands (Quézel, 2000). There are different types of crown fires, ranging from individual tree torching, active crown fires and, under exceptional circumstance, independent crown fires that become decoupled from surface fuels may also occur (Van Wagner, 1977). Wildfire in *P. halepensis* stands often show potential for developing active crown fires beyond extinction capacity (Cruz & Alexander, 2017). The high rate of spread and intensity of crown fires in *P. halepensis* stands, combined with long range spotting are characteristics that pose a serious threat to life and property (Dimitrakopoulos *et al.*, 2007).

In order to understand potential wildfire behavior, mathematical models have been developed to account for the various interacting processes that drive fire behavior (Hoffman *et al.*, 2016). In North America and Europe, different models that link Rothermel (1991, 1972) surface and crown fire rate of spread predictions with Van Wagner (1977, 1993) crown fire transition and propagation criteria have often been used (Alexander & Cruz, 2016), including *BehavePlus* (Andrews, 2014), *FlamMap* (Finney, 2006) or *NEXUS* (Scott & Reinhardt, 2001). In these semi-empirical approaches, the onset of a crown fire is defined by the transition of a wildfire from surface to canopy fuels. This transition occurs when the surface fire intensity attains or exceeds a certain critical surface intensity (I_0) which, in turn, is determined by the interaction between live fuel moisture content (LFMC) and the canopy base height (CBH; Van Wagner, 1977):

$$I_0 = (0.01\ CBH\ (460 + 25.9\ LFMC))^{1.5} \quad \text{(III.1)}$$

After the transition from the surface to the canopy layer, a certain canopy bulk density (CBD) is needed to develop and maintain a solid flame front. If this CBD is not reached, the crown fire will passively torch isolated trees (or groups of trees), but it will not spread across the canopy (Scott & Reinhardt, 2001). Consequently, for active crown fire development, a critical minimum spread rate (R_0) which depends

on CBD, is needed to maintain continuous crowning (Rothermel, 1991):

$$R_0 = 3/CBD \quad \text{(III.2)}$$

Characterization of the fuel structure and its relevance for fire behavior has been a topic of much research (Keane, 2015). Variations in live fuel moisture are often taken into account, although some discussions are still active on its role in fire propagation (Alexander & Cruz, 2013). However, an aspect that has seldom been considered is the role of pre-programmed needle senescence, despite its potential to increase crown fire intensity and severity (Nolan *et al.*, 2020; Resco de Dios, 2020). Needle lifespan in *P. halepensis* is approximately three years, and three-years-old needles typically become dry and senesce towards the end of June or start of July (Fig. III.1A). This is immediately before the peak of the fire season in the Western Mediterranean basin, which often occurs in the first half of July (López-Santalla & López-Garcia, 2019; Fig. III.1B). Consequently, pre-programmed needle senescence (a developmental process that allows nutrient recycling in old leaves before shedding) potentially leads to one-third of the canopy (that is, all 3 years-old leaves) being dry right before the peak fire season (Karavani *et al.*, 2018). Some studies have addressed the role of LFMC on fire propagation (Alexander & Cruz, 2013). Others have addressed how canopy drying, following bark beetle attacks for instance, impacts fire behavior (Jenkins *et al.*, 2012; Reiner, 2017; Talucci & Krawchuk, 2019). However, the effects of partial canopy drying after needle senescence on crown flammability have not been quantified so far (Karavani *et al.*, 2018; Nolan *et al.*, 2020; Resco de Dios, 2020).

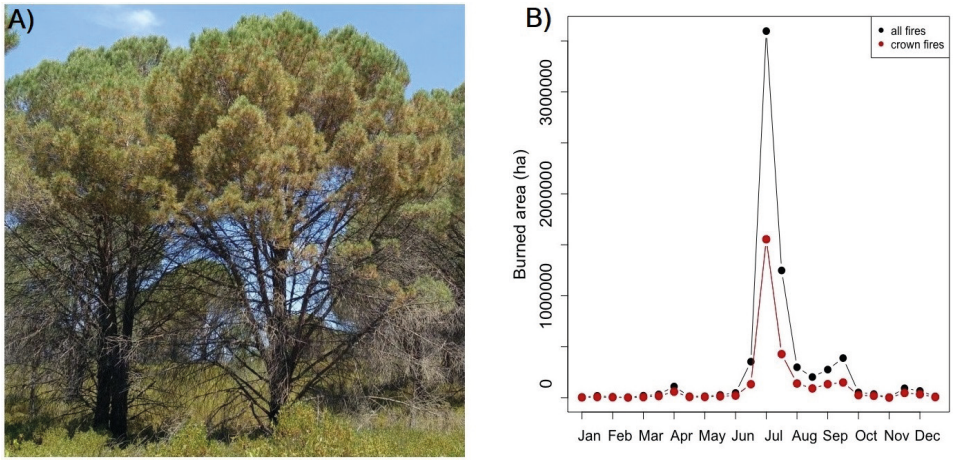

Figure III.1: Needle senescence and fire behavior. A: Needle senescence in *P. halepensis* affecting the old leaves cohort (3-years-old) typically occurs between the end of June or July and it drastically modifies the moisture of the canopy. Photo by Carles Arteaga. **B:** Temporal pattern of long-term average (1968–2015) burned area (black, all fires; red, crown fires) in the *Pinus halepensis* forests of the Mediterranean regions of Spain. (Data: Estadística General de Incendios Forestal provided by the Ministry of Agriculture, Fishing, and Food).

Temporal and spatial coincidence of low LFMC and high CBD creates optimal conditions to increase the probability of crown fire occurrence as well as their intensity and severity. High-intensity crown fires burn canopies by convection, leading to widespread defoliation and consequently plant death. Preprogrammed old needle senescence may thus enhance Aleppo pine mortality rates after wildfires, if it does affect intensity fire behavior (Resco de Dios, 2020). However, this effect only lasts for a few weeks, until leaf dropping (Nolan *et al.*, 2020). After shedding of senesced needles, the probability of crown fire activity declines as weighted LFMC increases and CBD decreases. Consequently, surface fires may become more intense after needle shedding due to an increase in surface fuel loads, but surface fires seldom reach intensities beyond extinction capacity. It is currently unknown why the brunt of the fire season occurs in early July in the Western Mediterranean Basin (Resco de Dios, 2020). During this time, LFMC in Mediterranean trees, shrubs and grasses is near its seasonal maximum (Nolan *et al.*, 2018) and fires occurring in late August, under much lower LFMC, often burn at lower intensity (Resco de Dios, 2020). Aleppo pine needle senescence could thus offer at least a partial explanation to such conundrum.

In this chapter, I seek to quantify the potential effects of needle senescence on fire behavior in *P. halepensis* stands. To achieve it, I simulated four scenarios that recreate the major annual physiological and structural changes in relation to needle senescence (that is, before, during and after leaf senescence, and later in the year after the onset of litter decomposition in the autumn). Each of the four simulations was ran for two highly contrasting *P. halepensis* fuel structures (representatives of very high and very low crown fire likelihood) that are dominant in Valencia (E-Spain), one of the most fire-prone regions in Mediterranean Spain. The main goal was to test the potential effects of needle senescence on crown and surface fire behavior in contrasting stand types, and also to establish its dependence and interactions with wind speed and dead fuel moisture content (DFMC), two well-known drivers of fire behavior. More specifically, in this chaptert I wanted to test: i) whether needle senescence increases the likelihood of transition from surface to crown fire; ii) whether once the transition to crown fire has occurred, the likelihood to develop an active crown fire increases with needle senescence in widely contrasting stand structures; iii) whether needle senescence increases mortality rates after wildfire activity; and iv) what is the importance of the effect of needle senescence on crown fire likelihood relative to wind speed and DFMC.

III.2 Materials and Methods

III.2.1 Senescence scenarios

Aleppo pine presents a tetracyclic annual shoot elongation process. Once senescence is active (end of June-beginning of July) needles have developed two thirds of the total annual elongation in current year shoots (Hover *et al.*, 2017).

Thus, considering a three-year needle life span, pre-programmed senescence leads to 1/3.6th, or 28 %, of the dried canopy (or dead mass fraction, f_d) if all 3 years old needles senesce at once. Four phenological scenarios were created to simulate annual canopy physiological and structural changes caused by needle senescence. The first one, scenario-A (Table III.1), represents spring leaf sprout. At this time there is an increase in canopy bulk density, canopy cover and live fuel moisture content. Scenario-B (Table III.1) represents the time of needle senescence, when about 28 % of the canopy is composed of dead matter at the beginning of July. To introduce these changes in LFMC, canopy live matter moisture (M_l) and canopy dead matter moisture (M_d) were weighed (M_w) considering f_d as in Rossa & Fernandes, (2018):

$$\text{LFMC} = M_w = f_d M_d + (1\text{-}f_d) M_l \quad \text{(III.3)}$$

Scenario-C simulates the time when needles have been shed, which reduce canopy bulk density. The reduction of dry needles in the crown increases weighted live fuel moisture content but needle shedding increases surface fine fuel loads. Finally, scenario-D (Table III.1) corresponds to autumn and winter periods when surface fine fuel loads decrease due to litter decomposition.

III.2.2 Stand structures and fuel features

Forest structure and fuel loads play a critical role in fire behavior and crown fire susceptibility. Fuel structure data were obtained from the fuel models developed by the Fire Service in Valencia, Spain (Generalitat Valenciana, 2020). The Valencian fuel model catalogue adapts the models from Scott and Burgan (2005) to E-Spain conditions. Models SH-9 (shrubland from now on; Tables III.1, III.2) and TU-3 (forest from now on; Tables III.1, III.2) were used. Model SH-9 is referred as a shrub fuel type, in the sense that it is short stature vegetation, but noting that it has two separate fuel layers (canopy fuels begin at 1 m above ground). It represents stands with a low proportion of large trees, extremely high tree density and horizontal fuel continuity. In contrast, TU-3 is a forest fuel type representing stands with two separated layers, high proportion of large trees, moderate tree density and moderate to low vertical and horizontal fuel continuity. Both models are considered as dynamic fuels, thus live herbaceous fuels become dead depending on their moisture content (Scott & Burgan, 2005). For initial model simulations, DFMC for scenarios A, B and C were established according to the lowest moisture values recorded after heat wave periods (Boer *et al.*, 2017; Jervis & Rein, 2016). As scenario-D represents autumn, DFMC values are higher due to more benign conditions. M_l was obtained from (Soriano-Sanchez & Quilez-Moraga, 2017) and M_d from (Jervis & Rein, 2016). Additionally, in order to understand the effect of leaf senescence relative to other drivers of fire behavior, a sensitivity analysis on how different values of 1-h DFMC (fine dead fuels moisture content) affected fire behavior was conducted. Canopy bulk density, canopy height and canopy base height were established according to

(Mitsopoulos & Dimitrakopoulos, 2007). Changes in canopy bulk density were established considering a reduction of 28 % among scenarios before and after senescence, as previously argued. Canopy base height values were considered stable among scenarios because the differences in height between 3 and 2 years-old needles are negligible (<10 cm) for the purpose of these simulations.

III.2.3 Fire behavior modeling

Wildland fire behavior simulation was done using *BehavePlus6* (Andrews, 2014) and crown fire was calculated using *Scott & Reinhardt* (Scott & Reinhardt, 2001) as input option. The input values used in each stand type and each scenario are detailed in Tables III.1 and III.2. Slope steepness was set to 0 % and 10 m open wind speed was established in a range from 0 to 30 km/h. Data analyses was carried out using *R* (R Development Core Team, 2021). Assessment of fire severity were performed using the lethal thresholds (LD) developed by (Resco de Dios, 2020). Thus, a crown fraction burned (CFB) between 0.4-0.8 eliminates 50 % of the population (LD_{50}), and CFB higher than 0.8-0.9 completely eliminates the population (LD_{100}). When CFB remains below 0.4 CFB mortality is negligible (LD_0; Resco de Dios, 2020).

Table III.1: Parameter values for each scenario. A, before senescence; B, during senescence; C, after shedding; D, in autumn. In Forest (TU-3) and Shrub (SH-9) fuel types.

Forest (TU-3)	A	B	C	D
Canopy Cover (%)	35	35	35	35
Canopy Height (m)	8	8	8	8
Canopy Base Height (m)	1.5	1.5	1.5	1.5
Canopy Bulk Density (kg/m3)	0.15	0.15	0.1	0.1
Fine Fuel Load (t/ha)	2.5	2.5	3	2.5
1-h DFMC (%)	6	5	5	9
10-h DFMC (%)	7	6	6	10
100-h DFMC (%)	8	7	7	11
LFMC (%)	105	74	100	100
Shrub (SH-9)	**A**	**B**	**C**	**D**
Canopy Cover (%)	100	100	100	100
Canopy Height (m)	5	5	5	5
Canopy Base Height (m)	1	1	1	1
Canopy Bulk Density (kg/m3)	0.22	0.22	0.15	0.15
Fine Fuel Load (t/ha)	10	10	10.7	10
1-h DFMC (%)	6	5	5	9
10-h DFMC (%)	7	6	6	10
100-h DFMC (%)	8	7	7	11
LFMC (%)	105	74	100	100

III.2.4 Dead mass fraction sensitivity analysis

A sensitivity analysis to assess how a varying proportion of f_d affected the transition ratio from a surface to crown layer was also conducted. This is important because, assuming that the biomass of each cohort is constant, the previously estimated 28 % of f_d would constitute a maximum potential value: needle senescence may start earlier in the year such that different values of f_d may occur when the fire season starts. Surface fire intensity was established from the mean surface intensity across scenarios with an intermediate wind speed of 15 km/h.

Table III.2: Parameter values for each fuel model. Forest (TU-3) and Shrub (SH-9).

Fuel Parameters	Fuel Model TU-3	Fuel Model SH-9
1-h Dead Fuel Load (t/ha)	2.5	10
10-h Dead Fuel Load (t/ha)	0.3	5.5
100-h Dead Fuel Load (t/ha)	0.5	0
Live Herbaceous Fuel Load (t/ha)	1.5	3.5
Live Woody Fuel Load (t/ha)	2.5	16
1-h SAV Ratio (cm^2/cm^3)	59.1	24.6
Live Herbaceous SAV Ratio (cm^2/cm^3)	52.5	59.1
Live Woody SAV Ratio (cm^2/cm^3)	45.9	49.2
Fuel Bed Depth (cm)	40	134
Dead Fuel Moisture of Extinction (%)	30	40
Dead Fuel Heat Content (KJ/kg)	18,622.3	18,622.3
Live Fuel Heat Content (KJ/kg)	18,622.3	18,622.3

III.3 Results

The results showed that maximum fire intensity and severity occurred in scenario-B under all wind speeds and fuel types (Table III.3). Fire intensity and severity values were higher in the shrub than in the forest fuel model. The highest estimated value of fire rate of spread (ROS) in scenario-B for the forest fuel type was 14.6 m/min at a wind speed of 30 km/h. This value was between 2 and 3 times higher than the peak ROS in the other scenarios (Fig. III.2.A). In the shrub fuel type, the highest ROS was 17.7 m/min, a value that was also reached in scenario-B with a wind speed of 30 km/h. ROS in scenario-B in the shrub fuel type was at least 1.4 times higher than in other scenarios (Fig. III.3.A). The highest fire line intensity reached in scenario-B was 5,924 kW/m in the forest stand and 17,179 kW/m in the shrub stand. Peak fire line intensity in scenario-B was 2-3 times higher in the forest fuel type and 1.5 times higher in the shrub fuel type compared to other scenarios (Table III.3). The highest flame

length occurred in scenario-B and took values of 8.7 m in the forest stand and 17.7 m in the shrub stand. Flame length remained between 2-3.3 m for the forest stand and between 10.1-14.4 m in the shrub stand in the other three scenarios (Table III.3).

The transition from surface to crown fire in the forest stand occurred with wind speeds higher than 11 km/h in scenario-B. For scenarios A, C and D, the wind speed thresholds necessary for crown fire development were 25, 18 and 26 km/h respectively. However, it is important to note that there were only transitions to passive crown fire development, not to active crown fires, in the forest fuel model TU-3. In the shrub fuel model SH-9, passive crown fires developed under all wind speed conditions. Active crown fire only developed in scenario-B when wind speeds were larger than 25 km/h.

Regarding fire severity, crown fraction burned (CFB) values were always higher in scenario-B for both fuel types and under all wind speed conditions (Figs. III.2.B and III.3.B). The relative effect of fuel type on CFB was higher in the forest stand than in the shrub stand since maximum CFB was 6 times larger in scenario-B (0.81) than in scenario-D (0.13). Importantly, the effect on CFB varied markedly with the moisture content of 1-h DFMC. For instance, in the forest, a CBD leading to (LD_{100}) in the scenario-B occurred either under a wind speed of 25 km/h and a 1-h DFMC of 4 % or with a wind speed of 30 km/h and 1-h DFMC of 10 %. LD_{50} was similarly reached with wind speeds above 15 km/h under minimum 1-h DFMC (4 %). In the remaining forest scenarios (scenarios A, C and D), increasing wind speed and lowering 1-h DFMC led to increases in CFB, but they always remained below LD_{50}.

In shrublands (Fig. III.3.B), at least some crown damage was recorded in all scenarios under any wind speed and 1-h DFMC conditions. CFB values ranged from 1 in scenario-B to 0.65 in scenario-D under the highest wind speed, indicating important differences depending on fuel phenology. Regarding lethal thresholds (LD), LD_{50} was reached in scenario-B, under a wind speed of 12 km/h when 1-h DFMC was at 12 %, or under 8km/h when 1-h DFMC was at 4 %. Further increases in wind speed in this scenario would lead to $LD_{100.}$ In the other scenarios, LD_{50} was recorded under an intermediate wind speed of 20 km/h and under critical wind speed conditions (30 km/h), LD_{100} also occurred in scenario A.

Finally, the sensitivity analysis on the effect of a varying f_d on the transition ratio was only performed in forest stands as critical transition to crown fires always occurred in the shrub fuel under any wind speed. Simulations indicated that the critical surface intensity to crown fire transition under a wind speed of 15 km/h occurred with a minimum fraction of 0.17 of the canopies composed of dead foliar fuels (Fig. III.4).

Table III.3: Simulation results. Simulated Rate of Spread (m/min), Fire Line Intensity (kW/m), Flame Length (m) and Crown Fraction Burned for each scenario (A, B, C, D) under four 10 m open wind speeds (0, 10, 20, 30 km/h).

FOREST (TU-3)	Wind Speed (km/h)	A	B	C	D
Rate of Spread (m/min)	0	0.3	0.5	0.4	0.3
	10	0.9	1.2	1.1	0.9
	20	1.7	5.1	2.6	1.7
	30	5.8	14.6	6.9	3.9
Fire Line Intensity (KW/m)	0	48	74	69	45
	10	130	200	183	121
	20	259	1384	462	240
	30	1,393	5,924	1,585	653
Flame Length (m)	0	0.5	0.6	0.5	0.4
	10	0.7	0.9	0.9	0.7
	20	1	3.3	1.6	1
	30	3.3	8.7	3.6	2
Crown Fraction Burned	0	0	0	0	0
	10	0	0	0	0
	20	0	0.35	0.06	0
	30	0.3	0.81	0.32	0.13
SHRUB (SH-9)	Wind Speed (km/h)	A	B	C	D
Rate of Spread (m/min)	0	0.7	1	0.8	0.7
	10	2.1	3.1	2.2	1.8
	20	5.7	8.6	5.5	4.4
	30	12.6	17.7	11.6	9.1
Fire Line Intensity (kW/m)	0	560	765	586	490
	10	1,752	2,615	1,679	1,330
	20	5,208	8,228	4,510	3,402
	30	12,562	17,179	10,074	7,372
Flame Length (m)	0	1.8	2.2	1.9	1.7
	10	3.9	5.1	3.8	3.2
	20	8	10.9	7.3	6
	30	14.4	17.7	12.4	10.1
Crown Fraction Burned	0	0.13	0.19	0.1	0.08
	10	0.34	0.44	0.27	0.23
	20	0.63	0.79	0.49	0.43
	30	0.95	1	0.75	0.65

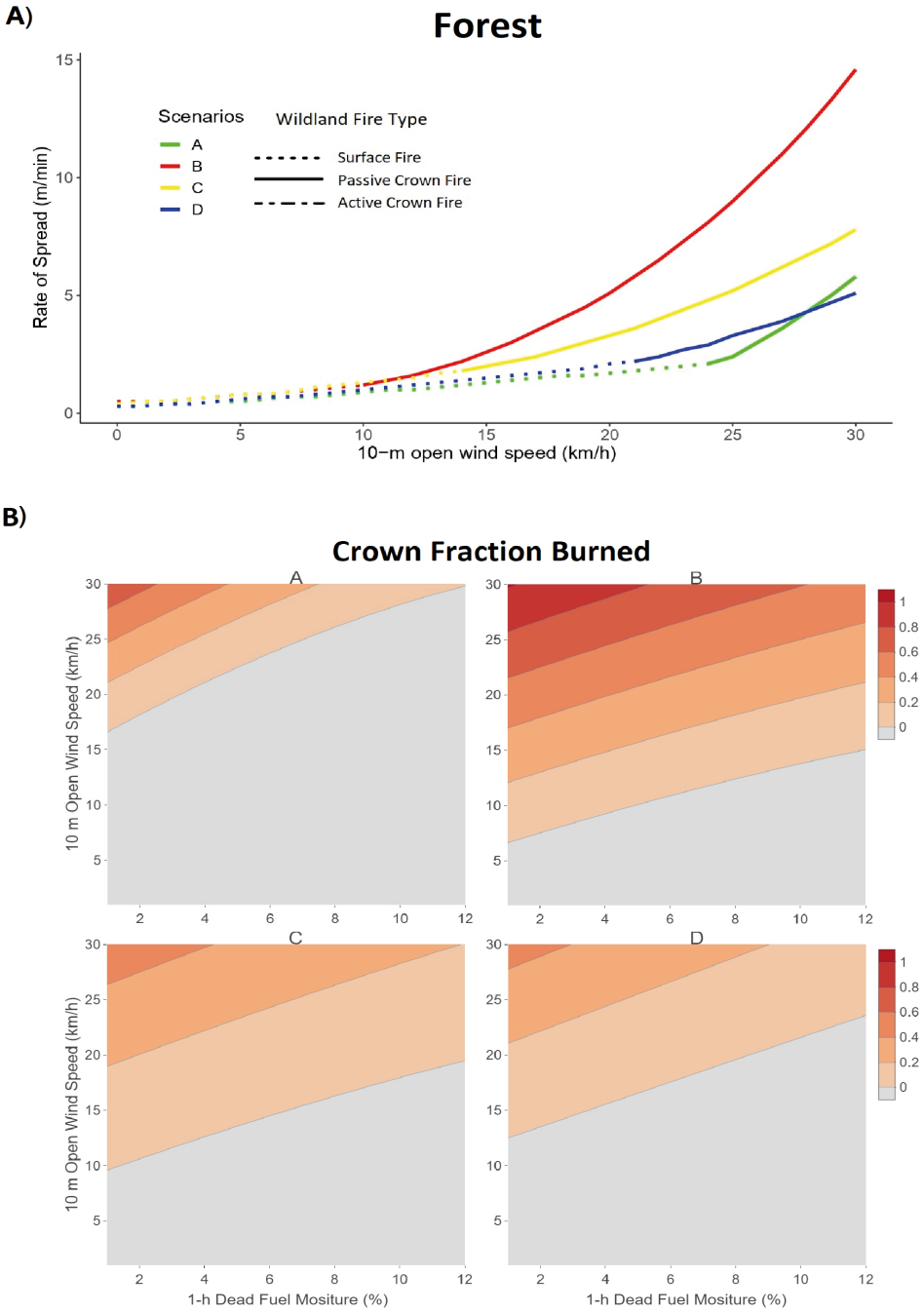

Figure III.2: Forest simulation results. A: Rate of Spread (m/min) in each scenario as a function of 10-m open wind speed in forest stands (TU-3 fuel model type). Dotted lines refer to surface fires, solid lines to passive crown fires. B: Crown Fraction Burned values as a function of 10-m open wind speed (km/h) and 1-h DFMC (%) for each scenario.

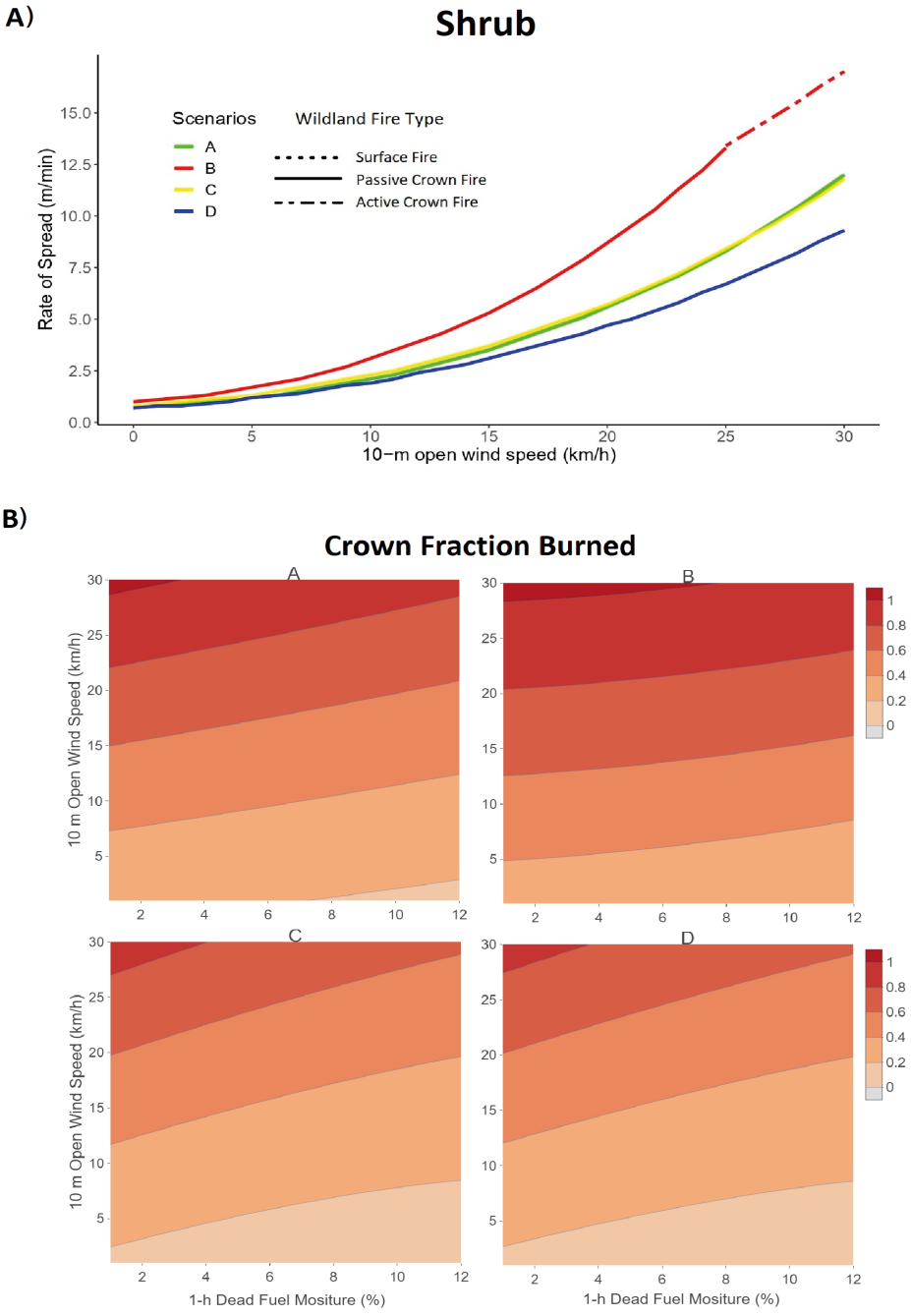

Figure III.3: Shrub simulation results. A: Rate of spread (m/min) in each scenario as a function of 10 m open wind speed in the shrub stand (SH-9 model type). Solid lines to passive crown fires and dot-dash lines to active crown fires. B: Crown Fraction Burned as a function of 10 m open wind speed (km/h) and 1-h DFMC (%) for each scenario.

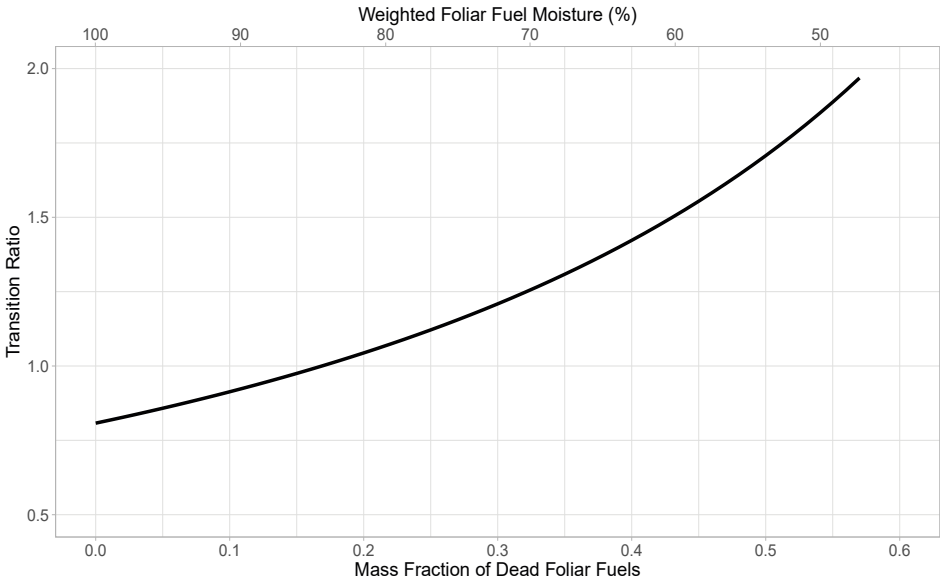

Figure III.4: Sensitivity analysis. Sensitivity analysis on the effects of a varying mass fraction of dead foliar fuels (f_d) and associated weighted foliar moisture on the Transition Ratio from a surface fire to the canopy layer on forest stands. Fire transition occurs when the transition ratio between the surface fire intensity (250 kW/m) and critical surface intensity (I_0, equation III.1) becomes equal or higher than 1.

III.4 Discussion

This chapter results suggest that Aleppo pine needle senescence significantly affects potential crown fire behavior. Simulations showed important differences in wildfire intensity and severity due to the physiological and structural changes caused by needle drying and shedding. However, the effect of needle senescence on fire behavior differed depending on fuel type and its interaction with wind speeds and DFMC. In other words, needle senescence by itself does not lead to active crown fire, but its presence lowers the critical wind speeds and 1-h DFMC values necessary to reach such transition point.

We can observe stronger crown fire activity under scenario-B in both stand types (Figs. III.2 and III.3). This scenario represents the process of needle senescence leading to a few-weeks period typically occurring towards the end of June or beginning of July (Karavani *et al.*, 2018) during which about one third of pine stand canopy is composed of dry needles (Fig. III.1A). Spatial and temporal coincidence of low foliar moisture content and high canopy bulk density favors the development of more intense and severe crown fires at lower

wind speed conditions, particularly for the shrub fuel type, where active crown fires may develop only under needle senescence. These results indicate that needle senescence could be a contributing factor to increasing fire intensity in Aleppo pine stands. Consequently, this mechanism could partly explain why the peak in burned area observed in the Western Mediterranean basin, where fires predominantly affect *P. halepensis*, occurs in early July (Fig. III.1B).

We can also observe that the relative effect of needle senescence was more noticeable in the forest fuel model than in the shrub fuel model. This is likely due to the fact that baseline flammability in shrublands is already very high: this fuel type presents a lower canopy base height which reduces, to some extent, the dependence of critical transitions to crown fire on LFMC (Equation III.1). Increasing canopy flammability in the shrubland stand would thus have, comparatively speaking, a smaller relative effect for extreme fire behavior than on the forest stand. In fact, crown fires would develop under any wind speed and canopy moisture in shrublands (Fig. III.3A). However, needle senescence did increase the probability of active crown fires. That is, the development of active fires in the shrubland stand only occurred under canopy senescence. These differences observed between fire behavior in shrub and forest stands are consistent with other studies (Alvarez *et al.*, 2012; Keeley *et al.*, 2005; Palmero-Iniesta *et al.*, 2017).

Needle senescence may influence crown fire behavior in, at least, two ways: affecting LFMC and CBD. In the forest stand simulation, the wind speed necessary for crown fire development decreased from 25 km/h to 10 km/h between scenarios A and B (Fig. III.1.A) because of decreasing LFMC from 105 % to 74 % (Table III.1). A lower LFMC reduces the influx of energy required to start the ignition, because a smaller amount of water needs to be evaporated. Needle senescence may thus enhance crown fire development, by reducing LFMC and hence the critical surface intensity threshold value at which surface fires become crown fires. Furthermore, as we can observed in the sensitivity analysis (Fig. III.4), the critical surface intensity to cause the transition from a surface fire to the canopy layer occurred as the dead foliar fractions increased over 17 %. It is important to point out that the actual role of LFMC in affecting the fire rate of spread is currently being discussed. Some authors argue that the role of LFMC is exaggerated in fire behavior models because the high convective and radiative fluxes produced by the flame are several orders of magnitude higher than the energy required to dry the fuel, which would render LFMC inconsequent (Alexander & Cruz, 2013). However, other studies consider that the effect of LFMC as a driver of fire spread has actually been underestimated (Pimont *et al.*, 2019; Rossa & Fernandes, 2018). Furthermore, empirical evidence across many biomes support that increases in burnt area occur under decreasing LFMC (Dennison *et al.*, 2008; Luo *et al.*, 2019; Nolan *et al.*, 2016; Pimont *et al.*, 2019).

The effect of needle senescence on fire behavior was dependent on DFMC. As figures III.2.B and III.3.B showed, senescence effects interact with variation in DFMC such that critical CFB values were reached in the senescence scenarios under low DFMC values. As previously stated, fire behavior is more affected, in relative terms, by the structural and physiological effects caused by needle senescence in forest stands compared to shrublands. Simulations showed that lethal thresholds varied from LD_0 which indicates negligible mortality in all forest scenarios, to LD_{100} which represents the death of the entire population in scenario-B under a wind speed of 30 km/h (Table III.3). These changes in tree mortality rates among scenarios were also noticeable in shrublands, where simulations showed that LD_{100} occurred in scenario-B after wind speeds as low as 21 km/h under low DFMC values. In the other shrubland scenarios, LD_{100} only occurred in scenario-A under a critical wind speed condition of 30 km/h. Therefore, while needle senescence is, by itself, not enough to reach critical fire severity thresholds, it lowers the need for critical wind speeds and DFMC values necessary to reach LD_{50} or LD_{100}.

The main problem that arises from this study is the way in which the effects of needle senescence on LFMC were inputted into the model. A weighted average of LFMC was used whereas, in reality, senesced leaves may form a layer of fuel that is effectively independent from LFMC. Future research should focus on building more realistic models to describe LFMC temporal and spatial dynamics. I conducted additional simulations considering only the CBD of dead canopy fuels, but the resulting CBD (0.05 kg/m^3 for forests and 0.07 kg/m^3 for shrublands) was not high enough to produce canopy fires (data not shown). Another problem with this study lies on the limitations of fire behavior modeling. Considering the complex dynamics behind wildland fires processes, fire models are very simplified, and this could lead to misleading predictions. Furthermore, considering climate change, it is difficult to predict extreme fire conditions accurately. There is some anecdotal evidence that needle senescence enhances crown flammability (M. Castellnou *pers. comm.*), but further work should confirm experimentally that needle senescence does enhance canopy flammability.

An important yet unresolved aspect is whether needle senescence serves an evolutionary role. It has been reported that pre-programmed needle senescence in the oldest cohort, at least in some temperate and boreal conifers, increases as new leaves develop (Kimmins, 2004). This would be a mechanism to recycle nutrients from old leaves into new, developing leaves. In this case, needle senescence co-occurs with the flush of current-year growth, and it could thus serve to support new needle growth. However, needle senescence also occurs as summer drought stress is starting to be important. Consequently, needle senescence could also serve as a water-saving mechanism that decreases transpirational area, at the expense of a transient increase in flammability (Karavani *et al.*, 2018). However, as climate change intensifies summer drought and wildfire activity, needle senescence could turn maladaptive by enhancing

crown fire likelihood. Further efforts towards quantifying the phenology of needle senescence and understanding its underlying drivers should be at the forefront of research efforts.

The results shown that not considering needle senescence can lead to misleading predictions on fire risk, potentially misestimating wildfire behavior in Aleppo pine stands and this could potentially lead to the application of suboptimal forest and fire management activities. While simulations are routinely performed in order to decide forest management and fire prevention operations, these simulations could incorporate the role of needle senescence because it significantly lowers the threshold for catastrophic fire behavior. To date, needle senescence effects may be underrated in fire behavior simulations due to the relatively short period that it represents each year. However, they occur at a critical time of the year and, as such, its cascading effects on fire behavior may be rather important, as it is anticipated in this work. An increased probability of extreme events has been forecasted for the next decades as a result of global change. According to predictions, fire seasons may be longer and drier, thereby producing more intense and severe wildfires (Resco de Dios, 2020). Changes in fire regimes represent a challenge to fire prone species and ecosystems. Aleppo pine post-fire regeneration strategy can be hard-pressed if wildfires return intervals become shorter than the time needed for trees to reach sexual maturity or to produce enough serotinous cones (Pausas, 2010). Also, extremely high wildfire intensity can damage serotinous seeds causing the decline of seedling recruitment and leading to populations collapse (Karavani *et al.*, 2018). We can thus expect important changes in ecosystem structure in the coming decades, which would have important interactions with changes in the fire regime. Furthermore, it would be relevant to simulate Aleppo pine-woods responses to predicted future climate conditions for the different scenarios tested in this study. A better understanding of pyrophysiology should therefore be at the forefront of our research.

III.5 Conclusions

• LFMC dynamics significantly affect wildfire danger, as the physiological changes that occur following needle senescence increase the probability of more intense and severe crown fires development.

• LFMC variation favors extreme fire behavior when environmental conditions (*e.g.*, high wind speed) and DFMC are also at critical levels.

• Disregarding LFMC from fire modeling attempts would lead to fire behavior underpredictions.

• Future research should focus on building more realistic models that describe LFMC temporal and spatial dynamics.

III.6 References

Alexander, M. E., & Cruz, M. G. (2013). Assessing the effect of foliar moisture on the spread rate of crown fires. International Journal of Wildland Fire, 22(6), 415–427. https://doi.org/10.1071/WF12008

Alexander, M. E., & Cruz, M. G. (2016). Crown fire dynamics in conifer forests. USDA Forest Service - General Technical Report PNW-GTR, 163–258.

Alvarez, A., Gracia, M., & Retana, J. (2012). Fuel types and crown fire potential in Pinus halepensis forests. European Journal of Forest Research, 131(2), 463–474. https://doi.org/10.1007/s10342-011-0520-6

Andrews, P. L. (2014). Current status and future needs of the BehavePlus Fire Modeling System. International Journal of Wildland Fire, 23(1), 21–33. https://doi.org/10.1071/WF12167

Barbero, M., Loisel, R., Quézel, P., Romane, F., & Richardson, D. M. (1998). Pines of the Mediterranean Basin. In Ecology and Biogeography of Pinus. Cambridge University Press, United Kingdom.

Boer, M. M., Nolan, R. H., Resco de Dios, V., Clarke, H., Owen, F., & Bradstock, R. A. (2017). Changing Weather Extremes Call for Early Warning of Potential for Catastrophic Fire. Earth's Future, 5:1196–1202. https://doi.org/10.1002/eft2.274

Cruz, M. G., & Alexander, M. E. (2017). Modelling the rate of fire spread and uncertainty associated with the onset and propagation of crown fires in conifer forest stands. International Journal of Wildland Fire, 26(5), 413–426. https://doi.org/10.1071/WF16218

Dennison, P. E., Moritz, M. A., & Taylor, R. S. (2008). Evaluating predictive models of critical live fuel moisture in the Santa Monica Mountains, California. International Journal Of Wildland Fire, 18–27. https://doi.org/10.1071/WF07017

Dimitrakopoulos, A. P., Mitsopoulos, I. D., & Raptis, D. I. (2007). Nomographs for predicting crown fire initiation in Aleppo pine (*Pinus halepensis* Mill.) forests. European Journal of Forest Research, 126(4), 555–561. https://doi.org/10.1007/s10342-007-0176-4

Finney, M. A. (2006). An overview of FlamMap fire modeling capabilities. Fuels Management—How to Measure Success: Conference Proceedings, 213–220.

Generalitat Valenciana, & Servei de Prevenció D'Incendis Forestals. (2020). Clave para la identificación de los modelos de combustible de la comunitat valenciana. Conselleria de Agricultura, Desarrollo rural, Emergencia Climática y Transición ecologica, 1–38.

Hoffman, C. M., Canfield, J., Linn, R. R., Mell, W., Sieg, C. H., Pimont, F., & Ziegler, J. (2016). Evaluating Crown Fire Rate of Spread Predictions from Physics-Based Models. Fire Technology, 52(1), 221–237. https://doi.org/10.1007/s10694-015-0500-3

Hover, A., Buissart, F., Caraglio, Y., Heinz, C., Pailler, F., Ramel, M., Vennetier, M., Prévosto, B., & Sabatier, S. (2017). Growth phenology in Pinus halepensis Mill.: apical shoot bud content and shoot elongation. Annals of Forest Science, 74(2). https://doi.org/10.1007/s13595-017-0637-y

Jenkins, M. J., Page, W. G., Hebertson, E. G., & Alexander, M. E. (2012). Fuels and fire behavior dynamics in bark beetle-attacked forests in Western North America and implications for fire management. Forest Ecology and Management, 275, 23–34. https://doi.org/10.1016/j.foreco.2012.02.036

Jervis, F. X., & Rein, G. (2016). Experimental study on the burning behaviour of Pinus halepensis needles using small-scale fire calorimetry of live, aged and dead samples. Fire And Materials, 40, 385–395. https://doi.org/10.1002/fam

Karavani, A., Boer, M. M., Baudena, M., Colinas, C., Díaz-Sierra, R., Pemán, J., de Luis, M., Enríquez-de-Salamanca, Á., & Resco de Dios, V. (2018). Fire-induced deforestation in drought-prone Mediterranean forests: drivers and unknowns from leaves to communities. Ecological Monographs, 88(2), 141–169. https://doi.org/10.1002/ecm.1285

Keane, R. E. (2015). Wildland fuel fundamentals and applications. Springer, Switzerland.

Keeley, J. E. (2012). Ecology and evolution of pine life histories. Annals of Forest Science, 69(4), 445–453. https://doi.org/10.1007/s13595-012-0201-8

Keeley, J. E., Pfaff, A. H., & Safford, H. D. (2005). Fire suppression impacts on postfire recovery of Sierra Nevada chaparral shrublands. International Journal of Wildland Fire, 14(3) 255-265. https://doi.org/10.1071/WF05049

Kimmins, J. P. (2004). Forest Ecology – A Foundation for Sustainable Forest Management and Environmental Ethics in Forestry. Prentice Hall, USA.

López-Santalla, A., & López-Garcia, M. (2019). Los incendios forestales en España. Decenio 2006-2015. Ministerio de Agricultura, Pesca y Alimentación Secretaría General Técnica Impresión, Madrid, 1, 166. https://www.mapa.gob.es/es/desarrollo-rural/estadisticas/incendios-decenio-2006-2015_tcm30-511095.pdf

Luo, K., Quan, X., He, B., & Yebra, M. (2019). Effects of live fuel moisture content on wildfire occurrence in fire-prone regions over southwest China. Forests, 10(10), 1–17. https://doi.org/10.3390/f10100887

Mauri, A., Di Leo, M., de Rigo, D., & Caudullo, G. (2016). Pinus halepensis and Pinus brutia in Europe: distribution, habitat, usage and threats. European Atlas of Forest Tree Species, March, 1, 122–123.

Mitsopoulos, I. D., & Dimitrakopoulos, A. P. (2007). Canopy fuel characteristics and potential crown fire behavior in Aleppo pine (Pinus halepensis Mill.) forests. Annals of Forest Science, 64(3), 287–299. https://doi.org/10.1051/forest:2007006

Nolan, R. H., Boer, M. M., Resco De Dios, V., Caccamo, G., & Bradstock, R. A. (2016). Large-scale, dynamic transformations in fuel moisture drive wildfire activity across southeastern Australia. Geophysical Research Letters, 43(9), 4229–4238. https://doi.org/10.1002/2016GL068614

Nolan, R. H., Hedo, J., Arteaga, C., Sugai, T., & Resco de Dios, V. (2018). Physiological drought responses improve predictions of live fuel moisture dynamics in a Mediterranean forest. Agricultural and Forest Meteorology, 263, 417–427. https://doi.org/10.1016/j.agrformet.2018.09.011

Nolan, R. H, Blackman, C. J., Resco de Dios, V., Choat, B., Medlyn, B. E., Li, X., Bradstock, R. A., & Boer, M. M. (2020). Linking Forest Flammability and Plant Vulnerability to Drought. Forests, 11(7), 779. https://doi.org/10.3390/f11070779

Palmero-Iniesta, M., Domènech, R., Molina-Terrén, D., & Espelta, J. M. (2017). Fire behavior in *Pinus halepensis* thickets: Effects of thinning and woody debris decomposition in two rainfall scenarios. Forest Ecology and Management, 404, 230–240. https://doi.org/10.1016/j.foreco.2017.08.043

Pausas, J. (2010). Fuego y evolución en el Mediterráneo. Investigación y Ciencia, 407, 56-63.

Pimont, F., Ruffault, J., Martin-StPaul, N. K., & Dupuy, J. L. (2019). Why is the effect of live fuel moisture content on fire rate of spread underestimated in field experiments in shrublands? International Journal of Wildland Fire, 28(2), 127–137. https://doi.org/10.1071/WF18091

Quézel, P. (2000). Taxonomy and biogeography of Mediterranean pines (Pinus halepensis and P. brutia). Ecology, Biogeography and Management of Pinus halepensis and Pinus brutia Forest Ecosystems in the Mediterranean Basin. Backhuys Publishers, Netherlands.

R Development Core Team. (2021). R: A language and environment for statistical computing. R Foundation for Statistical Computing. Austria. https://www.r-project.org/.

Reiner, A. L. (2017). Fire Behavior in Beetle-killed Stands: A brief review of literature focusing on early stages after beetle attack. US Forest Service Pacific Southwest Region: Vallejo, CA, USA, 2017; Volume 5, pp. 1–5.

Resco de Dios, V. (2020). Plant-Fire Interactions. Applying Ecophysiology to Wildfire Management. Vol 36. Springer, Switzerland.

Resco de Dios, V., Arteaga, C., Hedo, J., Gil-Pelegrín, E., & Voltas, J. (2018). A trade-off between embolism resistance and bark thickness in conifers: are drought and fire adaptations antagonistic? Plant Ecology and Diversity, 11(3), 253–258. https://doi.org/10.1080/17550874.2018.1504238

Rossa, C. G., & Fernandes, P. M. (2018). On the effect of live fuel moisture content on fire rate of spread. Forest Systems, 26(3), eSC08. https://doi.org/10.5424/fs/2017263-12019

Rothermel, Richard C. 1991. Predicting behavior and size of crown fires in the northern Rocky Mountains. Res. Pap. INT-RP-438. Ogden, UT: U.S. Department of Agriculture, Forest Service, Intermountain Research Station. 46 p.

Rothermell, R. C. (1972). A Mathematical Model for Predicting Fire Spread. Res. Pap. INT-115. Ogden, UT: U.S. Department of Agriculture, Intermountain Forest and Range Experiment Station. 40 p.

Scott, J. H., & Burgan, R. E. (2005). Standard fire behavior fuel models: A comprehensive set for use with Rothermel's surface fire spread model. USDA Forest Service - General Technical Report RMRS-GTR, 153 RMRS-GTR, 1–76. https://doi.org/10.2737/RMRS-GTR-153

Scott, J. H., & Reinhardt, E. D. (2001). Assessing crown fire potential by linking models of surface and crown fire behavior. USDA Forest Service - Research Paper RMRS-RP, 29 RMRS-RP, 1–62. https://doi.org/10.2737/RMRS-RP-29

Soriano-Sanchez, J., & Quilez-Moraga, R. (2017). Análisis de la humedad del combustible vivo en la Comunitat Valenciana 1/13. Sociedad Española de Ciencias Forestales, 1-14.

Talucci, A. C., & Krawchuk, M. A. (2019). Dead forests burning: the influence of beetle outbreaks on fire severity and legacy structure in sub-boreal forests. Ecosphere, 10(5). https://doi.org/10.1002/ecs2.2744

Van Wagner, C. E. (1977). Conditions for the start and spread of crown fire. Canadian Journal of Forest Research, 7(1), 23–34. https://doi.org/10.1139/x77-004

Wagner, C. E. Van. (1993). Prediction of crown fire behavior in two stands of jack pine. Canadian Journal of Forest Research, 23, 442–449. https://doi.org/10.1139/x93-062

CHAPTER IV:
MODELING LFMC DYNAMICS

MODELING LFMC DYNAMICS

ABSTRACT

In this chapter, I develop a semi-mechanistic model to estimate species-specific LFMC daily variations by considering key physiological traits. After introducing why spatial and temporal LFMC dynamics estimations are required and how these estimations are currently achieved, I explain the limitations of widely used approaches and how to overcome them. Then, I provide a detailed description of how species-specific physiological traits differences are considered in the developed approach, which is based on a water balance model that estimates predawn leaf water potential (Ψ_{pd}). After calibrating and validating the model, results showed that the developed approach has a better goodness of fit between the estimated and field observed values than widely used meteorological drought indices or remote sensed data. Finally, I discuss the results regarding model performance across different plant functional types and its applicability within large-scale fire danger forecast systems.

The research activities related in this chapter were published in the journal Agricultural and Forest Meteorology in 2022 under the title: "A semi-mechanistic model for predicting daily variations in species-level live fuel moisture content" with Rubén Díaz-Sierra, Miquel de Cáceres, Àngel Cunill-Camprubí, Rachael Nolan, Matthias M. Boer, Jordi Voltas and Victor Resco de Dios as co-authors. https://doi.org/10.1016/j.agrformet.2022.109022

IV.1 Introduction

A key aspect for fire prevention and management actions is understanding temporal and spatial moisture content variations of both, dead and live fuels. Wildfires can only occur once critical fuel dryness thresholds are crossed (Jurdao *et al.*, 2012; Luo *et al.*, 2019; Nolan *et al.*, 2016). Therefore, estimate fuel moisture dynamics provides a better knowledge of where and when live and dead fuels are in a critically dry state in order to anticipate large wildfire events (Moreno-Gutierrez *et al.*, 2011).

Wildfire activity depends on the interplay between biomass loads and connectivity along with the availability of such biomass to burn, which is strongly determined by moisture content (Boer *et al.*, 2021). While dead fuel moisture content (DFMC) variations have been far researched (Mathews, 2014), there are significant knowledge gaps regarding live fuel moisture content (LFMC) variations that can be addressed from a plant physiology perspective. LFMC, the water content in live foliage and small twigs on a dry mass basis, critically affects forest ignitability and likelihood of fire spread (Balaguer-Romano *et al.*, 2020; Gabriel *et al.*, 2021; Pimont *et al.*, 2019; Rossa, 2017). This is because the water content of live tissues acts as a heat sink, consequently reducing the intensity of fire and its rate of spread (Rothermel, 1983).

Many fire management agencies routinely monitor LFMC directly through time-consuming and expensive field inventories or indirectly through remote sensing products or meteorological drought indices. Remotely-sensing approaches, which include spectral vegetation indices and radiative transfer models, allow the monitoring of LFMC over large areas at fine spatial and temporal resolutions (Yebra *et al.*, 2013). Drought indices, such as the Drought Code (DC) from the Canadian Forest Fire Weather Index (Van Wagner, 1987), are based on daily air temperature and precipitation data and are designed to conceptually represent water dynamics in soil reservoirs. Common limitations to both indirect approaches are that they provide incomplete information on interspecific differences, at least without a priori calibrations, and that forecasting relies on empirical methods. Furthermore, a number of studies have cast doubt on the reliability of DC as an actual proxy of LFMC, at least in some plant functional types in the Mediterranean basin (Ruffault *et al.*, 2018; Soler-Martin *et al.*, 2017).

The degree of variation in LFMC within a fire season varies markedly across life-forms, at least in Mediterranean environments (Resco de Dios, 2020). This variation arises from differences in physiological and anatomical characteristics controlling LFMC such as stomatal control, the degree of sclerophylly, or rooting depth (Sánchez-Martínez *et al.*, 2020). Empirical studies have often observed how seasonal variation in LFMC is largest in seeding shrubs, intermediate in resprouting shrubs and lowest in trees (Nolan *et al.*, 2018; Pellizzaro *et al.*, 2007; Viegas *et al.*,

2001). Seeding shrubs often have shallow root systems which cannot reach deeper water sources (Nolan *et al.*, 2018), high resistance to embolism (Pausas *et al.*, 2016) and poor stomatal controls (Resco de Dios, 2020), which jointly lead to the lowest LFMC values during drought periods and the largest seasonal variation. Resprouting shrub species often have deeper roots and lower drought tolerance than seeders, leading to intermediate variation in LFMC (Resco de Dios, 2020). Tree species often have the deepest rooting systems and strong stomatal controls, which buffers against short term fluctuations in shallow water levels and, consequently, they often display nearly constant LFMC throughout the fire season (Nolan *et al.*, 2018; Viegas *et al.*, 2001).

Nolan *et al.* (2020) demonstrated that inter-species variation in LFMC could in principle be modelled as a function of predawn leaf water potential (Ψ_{pd}), given information on pressure-volume relationships. This approach can be further simplified and LFMC may be modelled from Ψ_{pd} using solely a linear regression when plants are operating below the turgor loss point, which is the most critical from the perspective of fire occurrence (Nolan *et al.*, 2018). In a case study using six species from a Mediterranean forest, the prediction of LFMC from Ψ_{pd} showed an overall goodness of fit that was better than that from existing drought indices (Nolan *et al.*, 2018). To scale up from local to larger areas, LFMC estimations would require predictions of Ψ_{pd} which, in turn, is strongly related to rhizosphere soil water potential (Ψ_{soil}). That is, Ψ_{pd} overnight equilibrates with Ψ_{soil} in the absence of nocturnal transpiration or significant disruptions in the soil-plant-atmosphere continuum (Ritchie & Hinckley, 1975). However, to our knowledge, no study has yet attempted large scale LFMC modeling by coupling a soil water balance model with a physiological model.

MEDFATE is a forest ecosystem model designed to simulate soil and plant water balances in forest stands with heterogeneous structure and composition (De Cáceres *et al.*, 2015, 2021). Aboveground stand structure is represented by total height, leaf area index and crown ratio of a set plant cohort. In MEDFATE, a plant cohort represents a set of plants that belong to the same species with similar structural characteristics, including root distribution, which is specified using the depths corresponding to cumulative 50 % and 95 % of fine roots. Soil is represented using a set of vertical layers with different depths and physical properties. Finally, the model requires daily weather data as inputs to simulate plant hydraulics and transpiration at subdaily time steps (De Cáceres *et al.*, 2015).

In this chapter, I seek to develop a novel approach for forecasting daily variations in LFMC across Mediterranean species by merging soil and plant water potential simulations from MEDFATE (De Cáceres *et al.*, 2015, 2021) with previously developed Ψ_{pd}-LFMC based models (Nolan *et al.*, 2018). More specifically, I seek to model LFMC variation across species grouped in three functional types (seeding

shrubs, resprouting shrubs and trees) from Ψ_{pd} values, and compare the results with current approaches such as the Drought Code and remotely sensed vegetation indices. To this end, I used the Spanish subset of a global LFMC database (Yebra *et al.*, 2019) for calibration and validation. The ultimate goal is to develop an approach that can be used within operational settings. Considering the usual trade-off between the degree of biological realism that is incorporated into a model and how applicable and easy to use the model will be, I seek to merge simplicity with biological realism to enhance applicability by making some simplifying assumptions on the biological differences across species.

IV.2 Materials and Methods

IV.2.1 Globe-LFMC database

Globe-LFMC is a global database of live fuel moisture content measured from 1,383 sampling sites in 11 countries (Yebra *et al.*, 2019). Each individual record represents an in situ destructive measurement of LFMC. All sites within Spain with species specific records were selected resulting in 40 sampling sites containing 2,511 individual records with observed LFMC. Data includes 37 species from 21 different genera covering a sampling period of 20 years from 1996 to 2017 (Methods S.IV.1, Table S.IV.1). Sampling sites selection cover many of the contrasting climates and ecoregions of peninsular Spain (Fig. IV.1). Mean annual air temperature varied from 10.9 to 17.8 ºC and mean annual precipitation from 243 to 1,345 mm across the selected sampling sites (Fig. IV.1.B-C, Table S.IV.1). Vegetation types and ecoregions ranged from xeric sclerophyll or Mediterranean pine forests to the more mesic Cantabrian mixed forests, dominated by temperate deciduous broad-leaf species (Fig. IV.1.A).

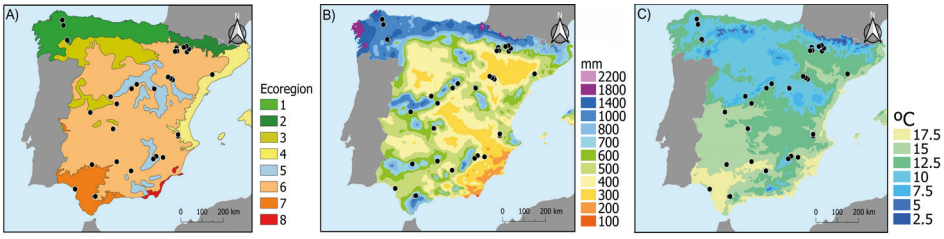

Figure IV.1: Sampling sites. Globe-LFMC sampling sites in Spain. a) Ecoregions, b) mean annual precipitation and c) mean annual air temperature. Black circles indicate the location of the study sites. Meteorological gradients from (Chazarra-Bernabé *et al.*, 2018). Ecoregion delimitations were obtained from WWF (Dinerstein *et al.*, 2017) and they indicate Cantabrian mixed Forests (1); Pyrenees conifer and mixed forests (2); Northwest Iberian Montane Forests (3); Northeast Spain Mediterranean forests (4); Iberian conifer forests (5); Iberian sclerophyllous and semi-deciduous forests (6); Southwest Iberian Mediterranean sclerophyllous and mixed forests (7); Southeast Iberian shrubs and woodlands (8).

IV.2.2 MEDFATE

MEDFATE (version 2.2.3) is a process-based soil-vegetation-atmosphere transfer model implemented in an *R* package, which uses soil, vegetation, and meteorological data to estimate moisture dynamics (De Cáceres *et al.*, 2021; Table S.IV.2). The model is based on the *BILJOU* and *SIERRA* water balance models (Granier *et al.*, 1999; Mouillot *et al.*, 2001) and estimates, at a daily time steps, the soil water content as a function of soil properties, stand structure and daily climatic variables. Thus, daily changes in soil water content are calculated as the difference between precipitation, the water input, and canopy interception, plant transpiration, bare soil evaporation, surface runoff and deep drainage (De Cáceres *et al.*, 2021, 2015). Also, the model estimates daily plant transpiration and photosynthesis rates. Based on Sperry *et al.* (2017), stomatal regulation of gas exchange is simulated at sub-daily steps involving detailed calculations of hydraulics, leaf energy balance and photosynthesis.

The soil was divided into four layers (0-10 cm, 10-20 cm, 20-60 cm, and 60-100 cm deep). When a given soil layer is filled, water percolates to the next layer below, except in the deepest layer where water is lost from the profile via deep drainage. Soil data inputs are bulk density, the percentage of clay, sand, organic matter, and rock fragment content, which were derived from the *Soil Grids System* at 250 m resolution (Hengl *et al.*, 2017). A previous sensitivity analysis has shown that modelled transpiration is more sensitive to meteorological or vegetation inputs such as annual rainfall and leaf area index (LAI) than to soil inputs such as soil depth of layers or soil texture variation from clayey soils to sandy soils (De Cáceres *et al.*, 2015).

Vegetation data inputs are species identity, tree density, shrub cover, plant height, tree diameter at breast height and plant rooting depth. All data except rooting depth were obtained from the nearest plot which includes the target species from the Third National Forest Inventory of Spain (Alberdi *et al.*, 2016), following the same approach as in previous publications (De Cáceres *et al.*, 2021). MEDFATE requires the rooting depth where the cumulative 50 % (Z50) and 95 % (Z95) of fine roots occur. Previous studies have incorporated species-specific differences from a model assuming that vegetation is at eco-hydrological equilibrium (Cabon *et al.*, 2018). However, to simplify model parameterization and diminish computational demands, it was assumed that Z50 and Z95 occurred at 10 cm and 20 cm for seeding shrubs (R-), at 20 cm and 75 cm for resprouting shrubs (R+) and at 20 cm and 100 cm for trees (Tr), respectively. These depths were chosen as they are consistent with previously defined soil depths and with our assumptions that seeding shrubs (R-) have shallow root systems that can only access shallow water resources; that tree (Tr) species have the deepest rooting systems and are able to extract water from superficial and also from deep layers; and that resprouting shrubs (R+) have an intermediate root distribution. MEDFATE also includes a set of species-specific

plant traits covering plant size, shrub, and tree allometric coefficients to predict biomass fuel loading, phenology and anatomy characteristics, tissue moisture, light extinction, transpiration, and photosynthesis (De Cáceres *et al.*, 2021). The default values for each species were applied with the aim of using a parsimonious parameterization to enhance the potential application of the model.

Temperature, precipitation, and wind speed were obtained for each sampling site (in a 0.1º x 0.1º grid) from the ERA-5 Land reanalysis dataset (Hersbach *et al.*, 2020), which provides hourly estimates of climate variables from the Copernicus Climate Change Service. Daily meteorological variables of relative humidity, incoming solar radiation, and potential evapotranspiration were then obtained using the *meteoland* R package (De Cáceres *et al.*, 2018). Relative humidity was estimated assuming that dew point temperature equals the minimum temperature, and potential solar radiation was estimated from latitude, slope, and aspect. Incoming solar radiation was then obtained following Thornton & Running (1999). Input data were then used to predict daily species-specific Ψ_{pd} values and simulations were ran with a one-year spin-up period to avoid interferences from initial conditions.

IV.2.3 Model calibration and validation

The Globe-LFMC database was divided into a calibration and a validation dataset. The calibration dataset was obtained by randomly sampling among sites and species using 34 % of the total dataset, that is, 852 data points. After obtaining Ψ_{pd} from MEDFATE, its relationship with LFMC was calibrated based on a linear regression where, following Nolan *et al.*, 2018, Ψ_{pd} had been logarithmically transformed. A single relationship between LFMC and Ψ_{pd} was used for all species in the entire dataset, instead of using separate relationships for each species, in order to increase model simplicity within operational settings and considering that not all the species present in the dataset had enough measurements for independent calibration. The validation dataset, containing the remaining 1,659 data points (representing 66% of the total), was used to validate the LFMC predictions. Model validation was performed by a linear regression between observed and predicted LFMC calculating the adjusted R-squared (R^2) to measure the goodness of fit of our predictions, as well as the intercept (β_0) and the slope (β_1), and their 95 % confidence interval, to test for model prediction biases. The root mean square error (RMSE) and the mean absolute error (MAE) were also estimated to quantify the accuracy of the predictions, and the mean biased error (MBE; Jolliff *et al.*, 2009) to assess to which extent the estimations underpredict or overpredict observed data.

IV.2.4 Drought Indices and Spectral Vegetation Indices

The goodness of fit of the developed approach was compared with estimations from existing drought indices and spectral vegetation indices using the same Globe-LFMC database validation dataset. Drought Code (DC) values were obtained using the Canadian Forest Fire Danger Rating System, as implemented in the *cffdrs* R package (Wang *et al.*, 2017), using the same meteorological data sources as those previously described for MEDFATE, and also leaving a one-year spin-up period to avoid interference from initial conditions.

Following Marino *et al.* (2020), nine spectral indices (Table S.IV.3) were calculated to infer LFMC using data from the Moderate Resolution Imaging Spectroradiometer (MODIS) MCD43A4 Collection 6 reflectance product produced acquired daily tiles at 500 m resolution. Data was downloaded from the NASA Land Processes Distributed Active Archive Center (LP DAAC, https://lpdaac.usgs.gov/). Then, it was extracted, for each sampling date and site, the values of each MODIS band as a simple pixel extraction which corresponded with the sampling site area. The spectral indices were regressed against observed LFMC to select the index with the highest adjusted R^2 in subsequent analyses (Enhanced Vegetation Index (EVI), R^2=0.33, Fig. S.IV.1). As EVI values included all the species present in the sampling site area, it was calculated the equivalent water thickness (EWT) from individual LFMC values to enhance comparability. EWT, which is a measure of water content per unit surface area of the vegetation (Sow *et al.*, 2013), was calculated following Chakroun *et al.* (2015):

$$EWT = \frac{1}{\rho_w}\frac{1}{N}\sum(LFMC_i)\left(\frac{1}{SLA_i}\right) \quad \text{(IV.1)}$$

where LFMC is the observed foliar moisture content recorded in the Globe-LFMC database, P_w is the density of pure water (1000 kg m^{-3}) and SLA is the specific leaf area. Species-specific SLA values were obtained from the MEDFATE plant traits set. The EWT values of N species contained in each study site for each sampling date were calculated by applying equation (IV.1) for i species. Finally, as vegetation index signals saturate in the upper ranges, EVI values were logarithmically transformed before regression against EWT.

IV.2.5 Statistical analysis

To assess for significant differences across the approaches used for calibration, an encompassing test of Davidson & Mackinnon (1993) was used with the *lmtest* R package (Zeileis & Hothorn, 2002). To compare two non-nested models, the test fits a third encompassing model which contains all regressors from both models. Then, the *encomptest()* function performs a Wald test for comparing each models against the encompassing model. If there are significant differences between each linear model against the encompassing model, the test indicates that both linear models are significantly different.

IV.3 Results

The dataset allowed for model testing and calibration under a wide range of LFMC values, which varied across functional groups as expected. That is, LFMC variation was largest in seeding shrubs (45-145 %, 5 and 95 % percentiles, respectively), and intermediate in resprouting shrubs (60-120 %). Average variations in trees (75-140 %) were larger than in shrubs due to physiological differences between *Pinus* and *Quercus*, although seasonal variations within each genus were smaller than those obtained for seeders and resprouters. Across all species and years, the average seasonal values varied between 125 % in spring to 80 % in summer.

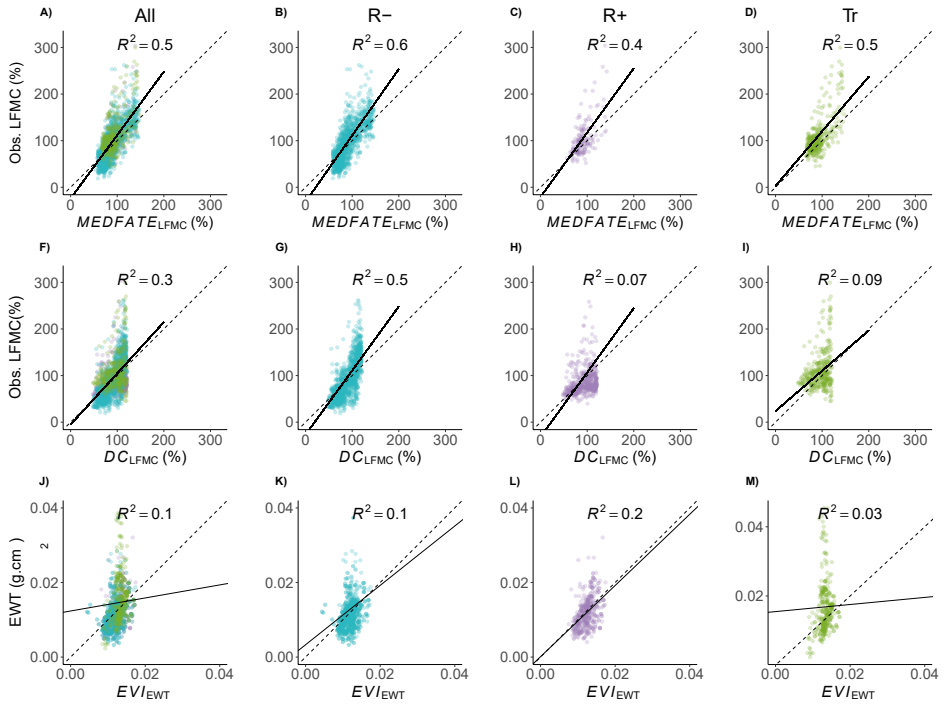

Figure IV.2: Models' performance. Observed LFMC against predicted values from $MEDFATE_{LFMC}$ (A-D) and Drought Code (DC_{LFMC}; F-I), and Equivalent Water Thickness against Enhanced Vegetation Index ($EVI_{EWT;}$ J-M) for all the data (A, F, J) or separately across functional types of seeding shrubs (R-; B, G, K) in blue, resprouting shrubs (R+; C, H, L) in purple and trees (Tr; D, I, M) in green. The line and the R^2 indicate the results of least squares fitting.

IV.3.1 Calibration, validation, and comparison of MEDFATE, DC and EVI

Using the calibration dataset, predicted Ψ_{pd} (logarithmically transformed) and DC values were regressed against observed LFMC while EVI (logarithmically

transformed) values were regressed against the equivalent water thickness (EWT) (Fig. S.IV.2). The encompassing test of Davidson & MacKinnon showed significant differences ($p < 0.001$) in the predictions of LFMC based on MEDFATE and on DC, against the encompassing model which contains all regressors from both models. The model showed significantly better fit than DC (Fig. S.IV.2). EVI could not be included in this analysis as the response variables were different (LFMC vs EWT). Then, the equations derived from these linear regressions were subsequently applied to Ψ_{pd} DC and EVI values obtained for the validation dataset. LFMC predictions using our approach ($MEDFATE_{LFMC}$) showed a substantial improvement over those based on the drought index (DC_{LFMC}) and the spectral vegetation (EVI_{EWT}) index (Table IV.1, Fig. IV.2).

IV.3.2 $MEDFATE_{LFMC}$ features

Despite the improvement of $MEDFATE_{LFMC}$ over DC_{LFMC} and EVI_{EWT} it is worth noting that the developed approach tended towards underprediction, particularly in the upper range of LFMC values (Fig. IV.2, Table IV.1). The slope of the observed *vs* predicted regression was 1.4 and the MBE was -8.8 %, indicating this tendency towards underprediction. The developed approach showed better goodness of fit for seeding shrubs ($R^2 = 0.6$, MAE = 21 %) than for trees ($R^2 = 0.5$, MAE = 23 %) or resprouting shrubs ($R^2 = 0.4$, MAE = 21 %). Also, MBE was lower for seeding shrubs (-5 %) than for resprouters (-13 %) or trees (-16 %; Table IV.1). Predictions of $LFMC_{LFMC}$ realistically captured the differences in temporal patterns of moisture content (Fig. S.IV.3), across genus (Table IV.2) and species (exemplified in Fig. IV.3).

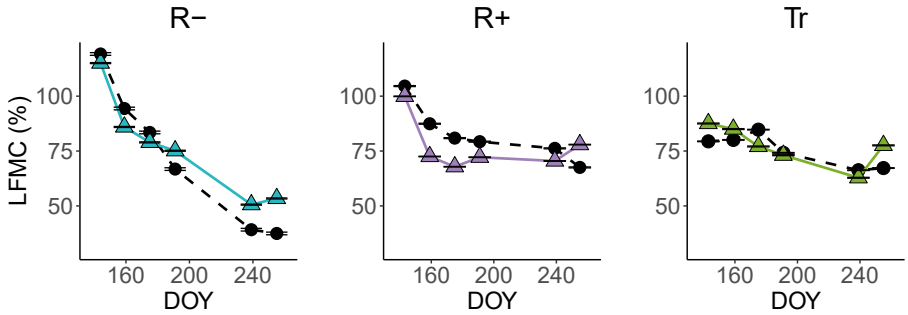

Figure IV.3: $MEDFATE_{LFMC}$ **performance.** Observed (black dashed line) and $MEDFATE_{LFMC}$ predicted (colour continuous line) LFMC seasonal dynamics across functional types, including a seeder (R-, *Genista scorpius*) in blue, a resprouting shrub (R+, *Quercus coccifera*) in purple and a tree (Tr, *Quercus ilex*) in green, in a representative sampling location (*AraCin12*). Error bars indicate standard error.

Table IV.1: Models performance. Goodness of fit statistics for the three approaches used in this study: $MEDFATE_{LFMC}$, Drought Code (DC_{LFMC}) used to predict LFMC, and Enhanced Vegetation Index (EVI_{EWT}) used to predict EWT, for each functional type (R-, seeding shrubs; R+, resprouting shrubs; Tr, trees). The adjusted R-squared (R^2), the intercept (β_0), and the slope (β_1), with each standard error in brackets, were calculated from the regression between observed and predicted LFMC, along with the root mean square error (RMSE), mean absolute error (MAE) and mean biased error (MBE).

	R^2	β_0	β_1	*RMSE*	*MAE*	*MBE*
$MEDFATE_{LFMC}$	0.5	-25.4 (±3.1)	1.4 (±0.0)	31.1	22.3	-8.8
R-	0.6	-28.9 (±3.4)	1.4 (±0.0)	28.7	21.5	-4.8
R+	0.4	-22.1 (±12.1)	1.4 (±0.1)	32.4	21.4	-12.9
Tr	0.5	-22.7 (±7.7)	1.4 (±0.1)	34.7	22.7	-15.8
DC_{LFMC}	0.3	-6.2 (±3.7)	1.1 (±0.0)	33.6	24.3	-3.4
R-	0.5	-46.7 (±4.3)	1.5 (±0.0)	31.3	23.4	-4.6
R+	0.07	49.5 (±5.9)	0.4 (±0.1)	31.2	22.5	6.5
Tr	0.09	44.2 (±11.1)	0.7 (±0.1)	41.6	29.5	-14.6
EVI_{EWT}	0.1	-0.001(±0.0)	1.0 (±0.0)	0.005	0.003	-0.0002
R-	0.1	0.001 (±0.0)	0.7 (±0.0)	0.002	0.001	0.0004
R+	0.2	-0.001 (±0.0)	0.9 (±0.1)	0.004	0.003	0.0004
Tr	0.03	-0.004 (±0.0)	0.9 (±0.4)	0.01	0.008	-0.0002

Table IV.2: $MEDFATE_{LFMC}$ performance. Goodness of fit statistics for each genus LFMC predicted with $MEDFATE_{LFMC}$. Sample size (n), adjusted R-squared (R^2), intercept (β_0) and slope (β_1), with each standard error in brackets, from regressing observed against predicted LFMC for all the data, and also separately for each functional type and each genus (when n > 20). The root mean squared error (RMSE), mean absolute error (MAE), and mean bias error (MBE).

	n	R^2	β_0	β_1	RMSE	MAE	MBE
Cistus (R-)	483	0.7	-5.3 (±3.5)	1.1 (±0.0)	20.7	16.1	-5.4
Lavandula (R-)	33	0.5	-149.6 (±50.6)	3.0 (±0.6)	68.4	52.9	-34.2
Salvia (R-)	473	0.6	-43.2 (±5.3)	1.5 (±0.1)	30.1	24	-5.6
Thymus (R-)	47	0.7	-251.2 (±31.3)	3.9 (±0.4)	41.8	33.6	4.9
Ulex (R-)	46	0.5	-19.4 (±23.1)	1.1 (±0.3)	24.2	20.5	10.7
Arbutus (R+)	29	0.5	-24.3 (±37.9)	1.7 (±0.3)	62.1	50.5	-49.1
Buxus (R+)	53	0.4	53.4 (±12.5)	0.5 (±0.1)	13.2	11.3	-4.3
Erica (R+)	43	0.3	4.5 (±18.1)	0.9 (±0.2)	21.2	17.6	3.4
Genista (R+)	30	0.6	-71.1 (±22.7)	1.7 (±0.3)	22.8	19.4	11.8
Pinus (Tr)	121	0.5	64.4 (±16.9)	0.4 (±0.2)	20.5	16.8	-7.2
Quercus (Tr)	347	0.6	-28.2 (±7.9)	1.5 (±0.1)	36.4	23.1	-17.5

The performance of the $MEDFATE_{LFMC}$ model generally increased when examining variations at the genus level. The best goodness of fit was observed across seeding genera like *Cistus* (R^2 = 0.7, MAE = 16 %), *Thymus* (R^2 = 0.7, MAE = 34 %), *Salvia* (R^2 = 0.6, MAE = 24 %), *Lavandula* (R^2 = 0.5, MAE = 53 %) and *Ulex* (R^2 = 0.5, MAE = 20 %). A higher β_1 for Thymus (3.9) and Lavandula (3.0) indicates a stronger underprediction of the model, but the slope remained between 1.1-1.5 for the other seeder shrubs. LFMC predictions for the two tree genera showed an R^2 =0.6 (*Quercus*) and R^2 =0.5 (*Pinus*) and MAE between 37 % (*Quercus*) and 17 % (*Pinus*). For resprouting shrubs, a larger variation in goodness of fit was observed, as the coefficient of correlation ranged from R^2 = 0.3 in *Erica* (MAE = 18 %), to R^2 = 0.5 in *Arbutus* (MAE = 50 %), R^2 = 0.5 in *Buxus* (MAE = 11 %) and R^2 = 0.6 in *Genista* (MAE = 20 %).

IV.4 Discussion

In this chapter I developed, calibrated, and validated a novel approach to predict daily values of LFMC across different species after modeling Ψ_{pd} using a plant-soil water balance model. The approach keeps a compromise between being mechanistic and operational, as it makes a series of simplifying assumptions on the rooting depth parameters which drive, among others plant traits, inter-specific and seasonal differences. Importantly, the novel approach was able to realistically capture seasonal variations (Fig. S.IV.3) in LFMC across individuals belonging to different species (Fig. IV.3), genus (Table IV.2) and functional types (Fig. IV.2), and, overall, it had a higher predictive ability than approaches based on remotely sensed spectral vegetation indices or drought indices (Table IV.1, Fig. IV.2).

The $MEDFATE_{LFMC}$ model was able to realistically capture the temporal patterns of variation in LFMC across functional types. Following expectations, species with shallower root systems, such as seeding shrubs, showed faster LFMC reductions during the summer dry period (Fig. IV.3). On the other hand, tree species with deeper root systems were less responsive to seasonal dryness, showing relatively little seasonal variation in LFMC, consistent with their larger dependence on deep soil water pools. Finally, resprouting shrub species show an intermediate dependence on shallow and deep-water pools between seeding shrubs and tree species, resulting in an intermediate level of seasonal LFMC variation (Nolan *et al.*, 2018).

We can observe a better performance for modeling LFMC in seeding shrubs and trees than for resprouting shrubs. This may be due to a lack of temporal continuity in resprouting shrub records at most sampling sites, as there were only two sites with more than three consecutive weekly measurements. Temporal discontinuity in the data can in turn decrease model performance due to poor data quality (Quan *et al.*, 2021). Another possibility for a poorer model performance in resprouters could

be the smaller temporal variation in LFMC records. At any rate, this method for predicting LFMC in resprouters presents a significant improvement over existing commonly used approaches based on optical remote sensing and drought indices (Fig. IV.2).

It is likely that LFMC predictions from the developed approach could be improved further by a more realistic description of the factors creating temporal variation as well as differences across species. Further studies using the model may derive LFMC from Ψ_{pd} as presented here (Fig. S.IV.2), but they are encouraged to develop their own calibration, particularly if dealing with very different vegetation types. Also, it is important that future studies consider the possibility of using species-specific pressure-volume curves to obtain LFMC estimates from Ψ_{pd} (Nolan *et al.*, 2020) to understand whether better predictions may be obtained.

LFMC depends on water content relative to dry mass (Pimont *et al.*, 2019), consequently, the incorporation of processes affecting dry mass may lead to further improvements (Jolly *et al.*, 2014). Seasonal changes in specific leaf area, for instance, may alter maximum LFMC (Nolan *et al.*, 2020). Similarly, differences in specific leaf area across species are likely to alter the relationship between LFMC and Ψ_{pd}. That is, at a given water potential (or water content), we can expect higher LFMC in species with larger specific leaf area because dry matter content will be lower. A more realistic description of rooting depth may also be achieved by coupling species-specific root depth models (Cabon *et al.*, 2018). However, I chose not to incorporate these variables in the current study because I sought to develop a relatively simple model that could be easily regionalized to work at national scales within operational settings. Further research could address to which extent model predictions could be improved by incorporating phenological as well as inter-specific differences in dry mass and rooting depth.

We can observe that DC provided reliable LFMC predictions for seeding shrubs, but not for trees or resprouting shrubs species (Fig. IV.2). In the case of EVI, always showed a poor relationship with EWT. LFMC varies over longer time-scales than the period between two consecutive MODIS measurements (Pellizzaro *et al.*, 2007; Resco de Dios *et al.*, 2021; Viegas *et al.*, 2001). The slight temporal mismatch between LFMC and MODIS measurements is thus unlikely to significantly affect the results. The goal was to develop a species-specific model, and, to that end, our approach showed a superior performance, allowing, for example, to model understory and overstory species separately, while remotely sensed models typically provide an integrated estimate. It is likely that EVI computed from remotely sensed imagery with higher spatial (*i.e.*, Sentinel 3), will show a stronger relationship with species-specific LFMC values than the one shown here, but as it is an empirical approach, predictive capabilities would continue to be limited. However, I used MODIS instead as it has a longer coverage for model validation and overlap with

the Globe-LFMC data set. It is worth noting that recent developments in the field of remote sensed Vegetation Optical Depth to detect vegetation response to water stress also allow for enhanced realism in LFMC predictions (Rao *et al.*, 2020). Understanding the potential for high resolution satellites remote sensed Vegetation Optical Depth approaches in monitoring species-specific variations in LFMC is another topic for future development.

Despite the large amount of input data required to run MEDFATE simulations (Table S.IV.1), much of the complexities of state variables and parameters can be hidden from the user in practical operational tools. The developed approach can be implemented within large scale fire danger forecast systems and may pave the way for a new generation of process-based models that are used for operational purposes within fire prevention scenarios.

IV.5 Conclusions

• The developed semi-mechanistic approach allows the estimation of species-specific LFMC seasonal changes and the forecast of future flammability conditions.

• Estimations showed better agreement with observed LFMC dynamics than commonly used drought indices or remote sensing vegetation indices, not only in general terms, but also by species functional types and genus.

• The approach can be implemented within large-scale fire danger forecast systems and may pave the way for a new generation of process-based models for operational purposes within fire prevention scenarios.

• The approach can be applied to improve estimations of climate change impacts on live fuel moisture dynamics as it considers plant physiological capabilities to adjust the moisture status.

IV.6 References

Alberdi, I., Sandoval, V., Condes, S., Cañellas, I., & Vallejo, R. (2016). The Spanish National Forest Inventory, a tool for the knowledge, management and conservation of forest ecosystems. Ecosistemas, 25(3), 88–97. https://doi.org/10.7818/ecos.2016.25-3.10

Balaguer-Romano, R., Díaz-Sierra, R., Madrigal, J., Voltas, J., & Resco de Dios, V. (2020). Needle senescence affects fire behavior in aleppo pine (Pinus halepensis mill.) stands: A simulation study. Forests, 11(10), 1054. https://doi.org/10.3390/f11101054

Boer, M. M., Resco de Dios, V., Stefaniak, E. Z., & Bradstock, R. A. (2021). A hydroclimatic model for the distribution of fire on earth. Environmental Research Communications, 3(3). https://doi.org/10.1088/2515-7620/abec1f

Cabon, A., Martínez-Vilalta, J., Martínez de Aragón, J., Poyatos, R., & De Cáceres, M. (2018). Applying the eco-hydrological equilibrium hypothesis to model root distribution in water-limited forests. Ecohydrology, 11(7). https://doi.org/10.1002/eco.2015

Chakroun, H., Mouillot, F., & Hamdi, A. (2015). Regional Equivalent Water Thickness Modeling from Remote Sensing across a Tree Cover/LAI Gradient in Mediterranean Forests of Northern Tunisia. Remote Sensing, 7(2), 1937–1961. https://doi.org/10.3390/rs70201937

Chazarra Bernabé, A., Flórez García, E., Peraza Sánchez, B., Tohá Rebull, T., Lorenzo Mariño, B., Criado Pinto, E., Moreno García, J. V., Romero Fresneda, R., & Botey Fullat, R. (2018). Mapas climáticos de España (1981-2010) y ETo (1996-2016). Agencia Estatal de Meteorología. https://doi.org/10.31978/014-18-004-2

Davidson, R., & MacKinnon, J. (1993). Estimation and Inference in Econometrics. Oxford University Press. United Kingdom.

De Cáceres, M., Martin-StPaul, N., Turco, M., Cabon, A., & Granda, V. (2018). Estimating daily meteorological data and downscaling climate models over landscapes. Environmental Modelling and Software, 108, 186–196. https://doi.org/10.1016/j.envsoft.2018.08.003

De Cáceres, M., Martínez-Vilalta, J., Coll, L., Llorens, P., Casals, P., Poyatos, R., Pausas, J. G., & Brotons, L. (2015). Coupling a water balance model with forest inventory data to predict drought stress: The role of forest structural changes vs. climate changes. Agricultural and Forest Meteorology, 213, 77–90. https://doi.org/10.1016/j.agrformet.2015.06.012

De Cáceres, M., Mencuccini, M., Martin-StPaul, N., Limousin, J. M., Coll, L., Poyatos, R., Cabon, A., Granda, V., Forner, A., Valladares, F., & Martínez-Vilalta, J. (2021). Unravelling the effect of species mixing on water use and drought stress in Mediterranean forests: A modelling approach. Agricultural and Forest Meteorology, 296, 108233. https://doi.org/10.1016/j.agrformet.2020.108233

Dinerstein, E., Olson, D., Joshi, A., Vynne, C., Burgess, N. D., Wikramanayake, E., Hahn, N., Palminteri, S., Hedao, P., Noss, R., Hansen, M., Locke, H., Ellis, E. C., Jones, B., Barber, C. V., Hayes, R., Kormos, C., Martin, V., Crist, E., Saleem, M. (2017). An Ecoregion-Based Approach to Protecting Half the Terrestrial Realm. BioScience, 67(6), 534–545. https://doi.org/10.1093/biosci/bix014

Gabriel, E., Delgado-Dávila, R., De Cáceres, M., Casals, P., Tudela, A., & Castro, X. (2021). Live fuel moisture content time series in Catalonia since 1998. Annals of Forest Science, 78(2). https://doi.org/10.1007/s13595-021-01057-0

Granier, A., Bréda, N., Biron, P., & Villette, S. (1999). A lumped water balance model to evaluate duration and intensity of drought constraints in forest stands. Ecological Modelling, 116(2–3), 269–283. https://doi.org/10.1016/S0304-3800(98)00205-1

Hengl, T., Jesus, J. M. De, Heuvelink, G. B. M., Ruiperez, M., Kilibarda, M., Blagoti, A., Shangguan, W., Wright, M. N., Geng, X., Bauer-marschallinger, B., Guevara, M. A., Vargas, R., Macmillan, R. A., Batjes, N. H., Leenaars, J. G. B., Ribeiro, E., Wheeler, I., Mantel, S., & Kempen, B. (2017). SoilGrids250m : Global gridded soil information based on machine learning. PLoS ONE 12(2): e0169748. https://doi.org/10.1371/journal.pone.0169748

Hersbach, H., Bell, B., Berrisford, P., Hirahara, S., Horányi, A., Muñoz-Sabater, J., Nicolas, J., Peubey, C., Radu, R., Schepers, D., Simmons, A., Soci, C., Abdalla, S., Abellan, X., Balsamo, G., Bechtold, P., Biavati, G., Bidlot, J., Bonavita, M. Thépaut, J. N. (2020). The ERA5 global reanalysis. Quarterly Journal of the Royal Meteorological Society, 146(730), 1999–2049. https://doi.org/10.1002/qj.3803

Jolliff, J. K., Kindle, J. C., Shulman, I., Penta, B., Friedrichs, M. A. M., Helber, R., & Arnone, R. A. (2009). Summary diagrams for coupled hydrodynamic-ecosystem model skill assessment. Journal of Marine Systems, 76(1–2), 64–82. https://doi.org/10.1016/j.jmarsys.2008.05.014

Jolly, W. M., Hadlow, A. M., & Huguet, K. (2014). De-coupling seasonal changes in water content and dry matter to predict live conifer foliar moisture content. International Journal of Wildland Fire, 23(4), 480–489. https://doi.org/10.1071/WF13127

Jurdao, S., Chuvieco, E., & Arevalillo, J. M. (2012). Modelling fire ignition probability fromsatellite estimates of live fuel moisture content. Fire Ecology, 8(1), 77–97. https://doi.org/10.4996/fireecology.0801077

Luo, K., Quan, X., He, B., & Yebra, M. (2019). Effects of live fuel moisture content on wildfire occurrence in fire-prone regions over southwest China. Forests, 10(10), 1–17. https://doi.org/10.3390/f10100887

Marino, E., Yebra, M., Guill, M., Algeet, N., Tom, L., Madrigal, J., Guijarro, M., & Hernando, C. (2020). Investigating Live Fuel Moisture Content Estimation in Fire-Prone Shrubland from Remote Sensing Using Empirical Modelling and RTM Simulations. Remote Sensing, 12(14), 2251. https://doi.org/10.3390/rs12142251

Matthews, S. (2014). Dead fuel moisture research: 1991-2012. International Journal of Wildland Fire, 23(1), 78–92. https://doi.org/10.1071/WF13005

Moreno-Gutiérrez, C., Barberá, G. G., Nicolás, E., De Luis, M., Castillo, V. M., Martínez-Fernández, F., & Querejeta, J. I. (2011). Leaf δ18O of remaining trees is affected by thinning intensity in a semiarid pine forest. Plant, Cell and Environment, 34(6), 1009–1019. https://doi.org/10.1111/j.1365-3040.2011.02300.x

Mouillot, F., Rambal, S., & Lavorel, S. (2001). A generic process-based simulator for meditERRanean landscApes (SIERRA): Design and validation exercises. Forest Ecology and Management, 147(1), 75–97. https://doi.org/10.1016/S0378-1127(00)00432-1

Nolan, R. H., Boer, M. M., Resco De Dios, V., Caccamo, G., & Bradstock, R. A. (2016). Large-scale, dynamic transformations in fuel moisture drive wildfire activity across southeastern Australia. Geophysical Research Letters, 43(9), 4229–4238. https://doi.org/10.1002/2016GL068614

Nolan, R. H., Hedo, J., Arteaga, C., Sugai, T., & Resco de Dios, V. (2018). Physiological drought responses improve predictions of live fuel moisture dynamics in a Mediterranean forest. Agricultural and Forest Meteorology, 263, 417–427. https://doi.org/10.1016/j.agrformet.2018.09.011

Nolan, R. H, Blackman, C. J., Resco de Dios, V., Choat, B., Medlyn, B. E., Li, X., Bradstock, R. A., & Boer, M. M. (2020). Linking Forest Flammability and Plant Vulnerability to Drought. Forests, 11(7), 779. https://doi.org/10.3390/f11070779

Pausas, J. G., Pratt, R. B., Keeley, J. E., Jacobsen, A. L., Ramirez, A. R., Vilagrosa, A., Paula, S., Kaneakua-Pia, I. N., & Davis, S. D. (2016). Towards understanding resprouting at the global scale. New Phytologist, 209(3), 945–954. https://doi.org/10.1111/nph.13644

Pellizzaro, G., Cesaraccio, C., Duce, P., Ventura, A., & Zara, P. (2007). Relationships between seasonal patterns of live fuel moisture and meteorological drought indices for Mediterranean shrubland species. International Journal of Wildland Fire, 16(2), 232–241. https://doi.org/10.1071/WF06081

Pellizzaro, G., Duce, P., Ventura, A., & Zara, P. (2007). Seasonal variations of live moisture content and ignitability in shrubs of the Mediterranean Basin. International Journal of Wildland Fire, 16(5), 633–641. https://doi.org/10.1071/WF05088

Pimont, F., Ruffault, J., Martin-StPaul, N. K., & Dupuy, J. L. (2019). Why is the effect of live fuel moisture content on fire rate of spread underestimated in field experiments in shrublands? International Journal of Wildland Fire, 28(2), 127–137. https://doi.org/10.1071/WF18091

Quan, X., Yebra, M., Riaño, D., He, B., Lai, G., & Liu, X. (2021). Global fuel moisture content mapping from MODIS. International Journal of Applied Earth Observation and Geoinformation, 101, 102354. https://doi.org/10.1016/j.jag.2021.102354

Rao, K., Williams, A. P., Flefil, J. F., & Konings, A. G. (2020). SAR-enhanced mapping of live fuel moisture content. Remote Sensing of Environment, 245, 111797. https://doi.org/10.1016/j.rse.2020.111797

Resco de Dios, V. (2020). Plant-Fire Interactions. Applying Ecophysiology to Wildfire Management. Vol 36. Springer, Switzerland.

Resco de Dios, V., Hedo, J., Cunill, À., Thapa, P., Martínez, E., Martínez, J., Aragón, D., Antonio, J., Balaguer-Romano, R., Díaz-sierra, R., Yebra, M., & Boer, M. M. (2021). Climate change induced declines in fuel moisture may turn currently fi re-free Pyrenean mountain forests into fi re-prone ecosystems. Science of the Total Environment, 797, 149104. https://doi.org/10.1016/j.scitotenv.2021.149104

Ritchie, G. A., & Hinckley, T. M. (1975). The Pressure Chamber as an Instrument for Ecological Research. Advances in Ecological Research, 9, 165–254. https://doi.org/10.1016/S0065-2504(08)60290-1

Rossa, C. G. (2017). The effect of fuel moisture content on the spread rate of forest fires in the absence of wind or slope. International Journal of Wildland Fire, 26(1), 24–31. https://doi.org/10.1071/WF16049

Rothermel, R. C. (1983). How to predict the spread and intensity of forest and range fires. US Department of Agriculture, Forest Service, General Technical Report, INT-143. https://doi.org/10.2737/INT-GTR-143

Ruffault, J., Martin-StPaul, N., Pimont, F., & Dupuy, J. L. (2018). How well do meteorological drought indices predict live fuel moisture content (LFMC)? An assessment for wildfire research and operations in Mediterranean ecosystems. Agricultural and Forest Meteorology, 262, 391–401. https://doi.org/10.1016/j.agrformet.2018.07.031

Sanchez-Martinez, P., Martínez-Vilalta, J., Dexter, K. G., Segovia, R. A., & Mencuccini, M. (2020). Adaptation and coordinated evolution of plant hydraulic traits. Ecology Letters, 23(11), 1599–1610. https://doi.org/10.1111/ele.13584

Soler-Martin, M., Bonet, J. A., Martínez De Aragón, J., Voltas, J., Coll, L., & Resco De Dios, V. (2017). Crown bulk density and fuel moisture dynamics in Pinus pinaster stands are neither modified by thinning nor captured by the Forest Fire Weather Index. Annals of Forest Science, 74(3). https://doi.org/10.1007/s13595-017-0650-1

Sow, M., Mbow, C., Hély, C., Fensholt, R., & Sambou, B. (2013). Estimation of Herbaceous Fuel Moisture Content Using Vegetation Indices and Land Surface Temperature from MODIS Data. Remote Sensing, 2617–2638. https://doi.org/10.3390/rs5062617

Sperry, J. S., Venturas, M. D., Anderegg, W. R. L., Mencuccini, M., Mackay, D. S., Wang, Y., & Love, D. M. (2017). Predicting stomatal responses to the environment from the optimization of photosynthetic gain and hydraulic cost. Plant Cell and Environment, 40(6), 816–830. https://doi.org/10.1111/pce.12852

Thornton, P. E., & Running, S. W. (1999). An improved algorithm for estimating incident daily solar radiation from measurements of temperature , humidity , and precipitation. Agricultural and Forest Meteorology, 93(4), 211-228. https://doi.org/10.1016/S0168-1923(98)00126-9.

Van Wagner, C. E. (1987). Development and structure of the Canadian forest fire weather index system. Canadian Forest Service, Information Report 35.

Viegas, D. X., Piñol, J., Viegas, M. T., & Ogaya, R. (2001). Estimating live fine fuels moisture content using meteorologically-based indices. International Journal of Wildland Fire, 10(2), 223–240. https://doi.org/10.1071/WF01022

Wang, X., Wotton, B. M., Cantin, A. S., Parisien, M. A., Anderson, K., Moore, B., & Flannigan, M. D. (2017). cffdrs: an R package for the Canadian Forest Fire Danger Rating System. Ecological Processes, 6(1). https://doi.org/10.1186/s13717-017-0070-z

Yebra, M., Dennison, P. E., Chuvieco, E., Riaño, D., Zylstra, P., Hunt, E. R., Danson, F. M., Qi, Y., & Jurdao, S. (2013). A global review of remote sensing of live fuel moisture content for fire danger assessment: Moving towards operational products. Remote Sensing of Environment, 136, 455–468. https://doi.org/10.1016/j.rse.2013.05.029

Yebra, M., Scortechini, G., Badi, A., Beget, M. E., Boer, M. M., Bradstock, R., Chuvieco, E., Danson, F. M., Dennison, P., Resco de Dios, V., Di Bella, C. M., Forsyth, G., Frost, P., Garcia, M., Hamdi, A., He, B., Jolly, M., Kraaij, T., Martín, M. P., Ustin, S. (2019). Globe-LFMC, a global plant water status database for vegetation ecophysiology and wildfire applications. Scientific Data, 6(1), 1–8. https://doi.org/10.1038/s41597-019-0164-9

Zeileis, A., & Hothorn, T. (2002). Diagnostic Checking in Regression Relationships. R News, 2(3), 7–10.

CHAPTER V:
FUEL MOISTURE DYNAMICS UNDER CLIMATE CHANGE

FUEL MOISTURE DYNAMICS UNDER CLIMATE CHANGE

ABSTRACT

In this chapter, I use semi-mechanistic models to forecast fuel moisture dynamics during the 21st century under different projected greenhouse gas emission scenarios (RCP4.5 and RCP8.5). First, I introduce why the use of semi-mechanistic approaches improves future fuel moisture dynamics estimations under climate change conditions and how future climate is simulated. Then, I describe the methodologies followed to establish study sites, to obtain climate projections, to apply the semi-mechanistic models and to analyze the data. Results show that both live and dead fuels moisture content are expected to decline in the coming decades, increasing the annual frequency of days with fuel moisture values below wildfire occurrence thresholds and thus lengthening fire seasons. Finally, I discuss the implications of fuel moisture declines on future wildfire danger.

V.1. Introduction

Water scarcity is projected to increase in Europe, amongst other parts of the world, as a result of climate change (IPCC, 2021). In ecosystems where plant biomass (*i.e.*, fuel) is abundant enough to sustain a fire, fire activity is primarily constrained by fuel availability which is determined by the frequency and duration of hot and dry weather periods (Boer *et al.*, 2021). Consequently, climate change may increase the duration of the fire season as well as fire activity in many European regions, including currently fire-free zones like the Pyrenees or the Alps, as fuel moisture declines below critical dryness thresholds for longer periods (Carnicer *et al.*, 2022; Jolly *et al.*, 2015; Resco de Dios *et al.*, 2021).

Many studies assessing future changes in wildfire danger are primarily based on fire weather indices as they can easily incorporate climate projections (Rigo *et al.*, 2017; Dupuy *et al.*, 2020; Ellis *et al.*, 2022; Gannon & Steinberg, 2021). But, while fire weather indices can reasonably assess future changes in DFMC (Mathews, 2014), they make simplifying assumptions about how LFMC will change under a warming climate. That is, they usually infer LFMC from changes in weather conditions and, consequently, they ignore species-level physiological capabilities to adjust the moisture status of live tissues as well as soil effects. Furthermore, previous work has indicated that fire weather indices are not reliable proxies for LFMC, particularly for resprouting shrubs and tree species from the Mediterranean region (Balaguer-Romano *et al.*, 2022; Ruffault *et al.*, 2018). Inferring potential changes in fire activity based only on fire weather may thus exaggerate future fire danger as physiological adjustments driving LFMC dynamics are ignored. One of the key factors that may delay or prevent critical dryness transitions in live fuels is increasing atmospheric CO_2 concentrations. Stomatal aperture often responds negatively to increasing CO_2 concentrations (Wullschleger *et al.*, 2002), and that may serve as a water conserving mechanism that enhances water use efficiency and thus LFMC. Otherwise, future drier conditions may also change the proportion of live and dead fuels, due to mortality increases derived from drought-induced cavitation (McDowell *et al.*, 2022). There is a wide variety of physiological adjustments that interact with environmental conditions and, understanding future variations in LFMC thus requires mechanistic modeling.

Climate shapes global fire distribution as it constrains the amount and timing of plant available water which, in turn, drives biomass production and fuel dryness, the main conditions for wildfire occurrence (Boer *et al.*, 2021). In other words, fire activity varies unimodally across productivity/aridity gradients, reaching peak values at intermediate productivity levels and decreasing towards extremes. This is because arid ecosystems may not have biomass loads high

enough to sustain a fire, and because very mesic ecosystems may be too wet to sustain fires (Pausas & Ribeiro, 2013). Climate change is expected to shift this fire maximum towards more productive ecosystems as climate aridity increases the frequency and intensity of droughts and fuel drying events in those productive ecosystems. Thus, forested ecosystems that are currently fire-free, with vast amounts of biomass that are not available to burn due to high moisture content, may dry below critical thresholds and start experiencing large wildfires in the coming decades (Ellis *et al.*, 2022; Resco de Dios *et al.*, 2021), potentially switching those mesic forest from a net carbon sink to a net carbon source (Anderegg *et al.*, 2020). Whether this switch is likely to occur, depends, first of all, on the extent to which increasing climate aridity affects fuel moisture dynamics. But current Land Surface Models and Fire-enabled Dynamic Global Vegetation Models (Hantson *et al.*, 2016; Rabin *et al.*, 2017; Teckentrup *et al.*, 2019) cannot yet fully account all relevant climate-vegetation-fire interactions.

General Climate Models (GCMs), which represent the major climate system components and their interactions (Taylor *et al.*, 2012) together with Representative Concentration Pathways (RCPs), which describe different future greenhouse gas emission scenarios (Moss *et al.*, 2010), are the main tools to simulate future climates (Rodriguez & Gutierrez, 2018). Several projections of climate change impacts on future wildfire hazard have been conducted using different GCM and RCP, concluding that increased temperature and decreased precipitation would lead to global increases in fire risk and longer fire seasons (Abatzoglou *et al.*, 2019; An *et al.*, 2015; Fargeon *et al.*, 2020; Gao *et al.*, 2021; Jones *et al.*, 2022; Varela *et al.*, 2019). Projected increases in the incidence of severe fire weather and its proxies for live and dead fuel moisture, together with existing empirical relationships between LFMC and climate, indicate that fuel moisture is likely to decline below critical thresholds for longer periods of time during later decades of the 21st century (Dupuy *et al.*, 2020; Ellis *et al.*, 2022; Ma *et al.*, 2021; Mathews *et al.*, 2011; Vilar *et al.*, 2021). Even relatively minimum fuel moisture decreases can have disproportionally consequences as the relationship between fuel moisture and fire size is exponential. Proportionally small decreases of fuel moisture led to larger proportions of extreme wildfires that causes vast increases in the area burned (Resco de Dios *et al.*, 2022). Besides the importance of the correctly characterization of fuel moisture dynamics under climate change, no study has so far provided future LFMC estimates using physiologically-based models for a wide range of species and sites distributed across broad climatic and productivity gradients.

In this chapter, I sought to test the general hypothesis that climate change will cause increasing fuel dryness, and consequently increasing fire season length, across Spain's forests regions during the 21st century. I also hypothesize that climate change effects over fuel dryness will depend on

vegetation productivity, and that enhanced water use efficiency derived from increased CO_2 effects will not fully compensate for changes in temperature and precipitation. Four different GCM projections during the 21st century under different RCPs (RCP4.5 and RCP8.5) were used as inputs for a physiologically-based LFMC model (Balaguer-Romano *et al.*, 2022) and a semi-mechanistic DFMC model (Resco de Dios *et al.*, 2015). Then I address LFMC and DFMC dynamics analyzing subsequent changes in fire season length by assessing the number of days per year with values below fuel dryness thresholds. Then I study how changes in fuel moisture and fire season length vary across gradients of net primary productivity (NPP), to assess whether changes in the potential fire season will be amplified or reduced across productivity gradients. Finally, I analyze CO_2 effects on LFMC dynamics to test the hypothesis that increasing CO_2 concentrations will enhance the water-use efficiency of the vegetation, thus counteracting the negative effects of the increases in water stress due to more frequent and intense drought events under global warming. Overall, this represents the first effort to quantify changes in fuel moisture under climate change over broad climate and productivity gradients using process-based models.

V.2 Materials and Methods

V.2.1 Study sites

Live and dead fuel moisture content variation was assessed across many of the contrasting climates and ecoregions of peninsular Spain (Fig. V.1). Study site locations correspond with plots from the Third National Forest Inventory of Spain (Alberdi *et al.*, 2016) and they are monospecific stands of six broadleaf species (*Fagus sylvatica* L.*, Quercus ilex* L.*, Quercus suber* L.*, Quercus robur* L.*, Quercus pyrenaica* Willd. *or Quercus faginea* Lam) and of six conifer species (P*inus halepensis* Mill.*, Pinus nigra* Arnold.*, Pinus sylvestris* L.*, Pinus pinea* L.*, Pinus pinaster* Ait. *or Pinus uncinata* Ramond.), selecting three plots per species which result in 36 study sites (Table S.V.1, Fig. S.V.1). Across the study sites, mean annual air temperature varied from 10 to 18 ºC (Fig. V.1.A, Table S.V.1) and mean annual precipitation from 375 to 2200 mm (Fig. V.1.B, Table S.V.1). Vegetation types and ecoregions ranged from xeric sclerophyll or Mediterranean pine forests to the more mesic Cantabrian forests, dominated by temperate deciduous broad-leaf species, or high mountain conifer forests (Fig. V.1.C). MODIS product (MOD17A3HGF, Running & Zhao, 2019) with a spatial resolution of 500 m was used to estimate average annual net primary productivity (kg C m^{-2}) between 2010-2020. Long term average annual productivity of study sites ranged from 3,870 to 15,031 kg C m^{-2}, showing a strong south-north productivity gradient (Fig. V.1.D, Table S.V.1).

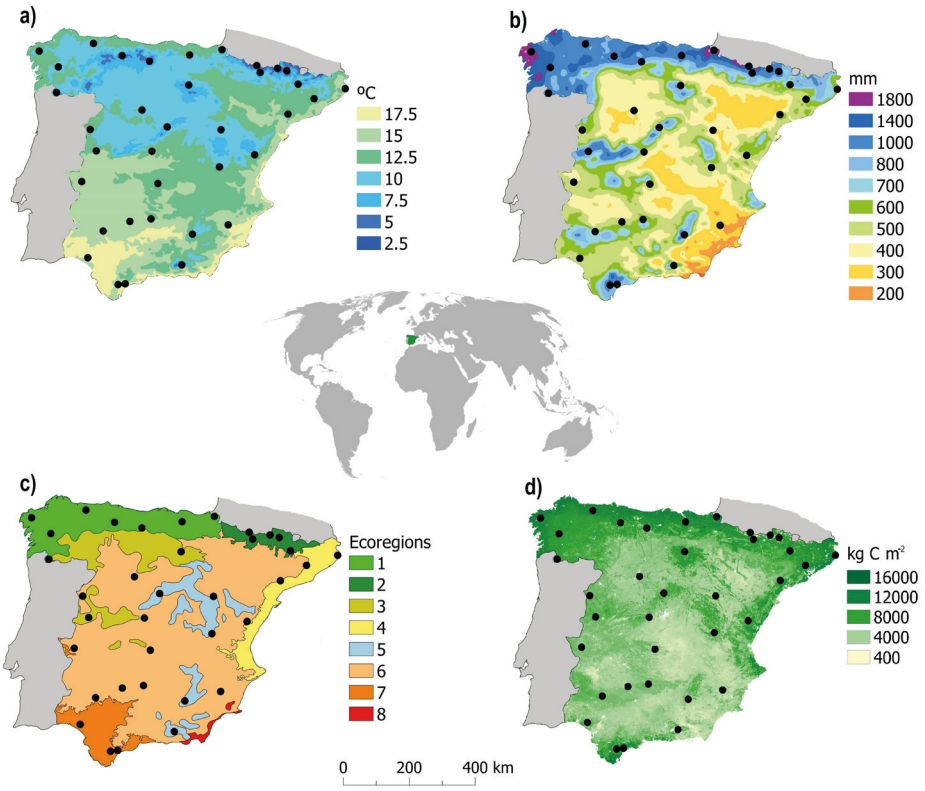

Figure V.1: Study sites. Study site locations (black dots) and main bioclimatic properties: A) mean annual air temperature (ºC), B) mean annual precipitation (mm), C) ecoregions, D) mean annual net primary productivity (kg C m^{-2}) between 2010 and 2020. Ecoregion delimitations were obtained from WWF (Dinerstein *et al.*, 2017) and they indicate Cantabrian mixed Forests (1); Pyrenees conifer and mixed forests (2); Northwest Iberian Montane Forests (3); Northeast Spain Mediterranean forests (4); Iberian conifer forests (5); Iberian sclerophyllous and semi-deciduous forests (6); Southwest Iberian Mediterranean sclerophyllous and mixed forests (7); Southeast Iberian shrubs and woodlands (8). Meteorological data is from Chazarra-Bernabé *et al.* (2018) and mean annual net primary productivity values are from Running & Zhao (2019).

V.2.2 Climate projections

Daily precipitation and daily maximum and minimum air temperature projections from 2010 to 2100 were obtained from the Euro-CORDEX adjusted grid at 0.11º resolution (Kotlarski *et al.*, 2014). Four different Global Climate Models (GCM) coupled within Regional Climate Models (RCM) were selected maximizing model spread for relevant variables and avoiding duplications in order to reduce model predictions biases (Table S.V.2, Rodríguez & Gutiérrez, 2018). The selected GCMs have been evaluated over western Europe and

exhibit significant differences in predictions of summer temperature and precipitation (Table S.V.2, McSweeney *et al.*, 2015). Both medium and high greenhouse gas emission scenarios (RCPs 4.5 and 8.5) were considered for each GCM. Projections bias corrections was performed using standard methods based on daily mean bias for temperature and quantile mapping for precipitation (Ruffault *et al.*, 2014). Data from the Spanish Meteorological Agency (AEMET) from 2010 to 2020 were used as reference observational data for GCM projection bias corrections and all analyses were performed using the *R* package *meteoland* (De Cáceres *et al.*, 2018). GCM climate projection across all study sites showed that, from 2010 to 2100, mean annual temperature is expected to increase by 1.5 ºC under RCP4.5 and by 4 ºC under RCP8.5, while mean annual precipitation is expected to decrease by 100 mm under RCP4.5 and by 150 mm under RCP8.5 (Fig. S.V.2). Relative humidity, incoming solar radiation, and potential evapotranspiration were daily predicted using *meteoland* (De Cáceres *et al.*, 2018). Relative humidity was estimated assuming that dew point temperature equals the minimum temperature. Potential solar radiation was estimated from latitude, slope and aspect and incoming solar radiation was then obtained following Thornton & Running (1999). Projections of annual atmospheric CO2 concentrations were obtained for each RCP scenario from Meinshausen *et al.* (2011).

V.2.3 LFMC modeling

Daily variations in species-level LFMC were estimated applying the approach developed in Chapter IV. The approach predicts daily plant transpiration and photosynthesis rates. Stomatal regulation of gas exchange is simulated at sub-daily steps involving detailed calculations of hydraulics, leaf energy balance and photosynthesis based on Sperry *et al.*, (2017). This approach is based on MEDFATE which predicts the trajectory of stomatal responses to changes in environment across time by considering that at any given instant the stomatal aperture adjusts to maximize the instantaneous difference between photosynthetic gain and hydraulic cost.

Soil and vegetation data were imputed following Chapter IV protocols. In short, the soil was divided into four layers (0-10 cm, 10-20 cm, 20-60 cm, and 60-100 cm deep), and data inputs regarding bulk density, the percentage of clay, sand, organic matter, and rock fragment content were extracted for plot locations from the Soil Grids System at 250 m resolution (Hengl *et al.*, 2017). Vegetation data inputs were species identity, tree density, shrub cover, plant height, tree diameter at breast height and plant rooting depth. All data except rooting depth were obtained for the selected plots from the Third National Forest Inventory of Spain (Alberdi *et al.*, 2016). Rooting depth, classified as the depth at which cumulative 50 % (Z50) and 95 % (Z95) of fine roots occur, which was set at

20 cm and 100 cm for tree species and at 10 cm and 20 cm for shrub species as previously discussed (Balaguer-Romano *et al.*, 2022). MEDFATE also includes a set of species-specific plant traits covering plant size, plant phenology and anatomy characteristics, and shrub and tree allometric coefficients to predict plant biomass loading, foliage and small twigs tissue moisture, light extinction, transpiration, and photosynthesis (De Cáceres *et al.*, 2021). Default package values (ver. 2.7.3) were used for each selected species. Following Chapter IV, soil and vegetation data inputs were used along with meteorological projections to predict daily species-specific Ψ_{pd} values and corresponding daily LFMC for all study sites. To do this equation (V.1) was applied:

$$LFMC = 91.87 - 31.12 \log10(-\Psi_{pd}) \quad (V.1)$$

Finally, a second round of simulations was run for each species (Table S1), considering a stable atmospheric CO_2 concentration of 386 ppm (2000-2020 mean) in order to quantify the potential mitigatory effect of CO_2 on LFMC dynamics.

V.2.4 DFMC modeling

Daily minimum DFMC was predicted from vapor pressure deficit (VPD) values in each study site applying the equation (V.2) derived from the semi-mechanistic model developed by Resco de Dios *et al.* (2015):

$$DFMC = DFMC_0 + DFMC_1 e^{(-mVPD)} \quad (V.2)$$

where $DFMC_0$ and $DFMC_1$ represent the minimum and maximum moisture content values, respectively, and m is the rate of change in DFMC with VPD. Values for $DFMC_0$ (6.79), $DFMC_1$ (27.43) and m (1.05) were obtained from (Nolan *et al.*, 2016a), and the Resco *et al.* (2015) DFMC model that has been previously used and validated in Spain (Resco de Dios *et al.*, 2022). Daily VPD values were estimated using the *plantecophys* R package (Duursma, 2015) from daily minimum relative humidity and daily maximum air temperature previously obtained from meteorological projections, which leads to the lowest DFMC daily value (Resco de Dios *et al.*, 2015).

V.2.5 Data Analyses

Live and dead fuel moisture content values were analysed over three decadal time periods, ranging from 2010 to 2020, from 2040 to 2050 and from 2090 to 2100. To analyse fuel moisture content dynamics, LFMC and DFMC summer mean (from June 21st to September 21st) were estimated for each year, as this

period concentrate the bulk of the fire activity in peninsular Spain (Resco de Dios *et al.*, 2022). To account for a potential lengthening of the fire season under global warming, the fire season length was estimated as the total number of days per year (d yr^{-1}) when moisture content values fell below wildfire occurrence thresholds. LFMC typically ranges between 40-150 % during the fire season for key woody plant species in peninsular Spain (Balaguer-Romano *et al.*, 2022; Nolan *et al.*, 2018) while DFMC variation ranges between 4-30 % (Mathews, 2014; Nolan *et al.*, 2016b). Previous publications were followed to establish the minimum, critical and extreme threshold values of fuel moisture content associated with fire activity in the Mediterranean and temperate broadleaf and mixed forest ecoregions at 120, 100 and 80 % for LFMC and at 12, 10 and 8 % for DFMC, respectively (Boer *et al.*, 2017; Ellis *et al.*, 2022; Ma *et al.*, 2021; Nolan *et al.*, 2016b; Resco de Dios *et al.*, 2022). The minimum fuel moisture threshold is defined as the level associated with the onset of wildfire occurrence (Boer *et al.*, 2017; Ellis *et al.*, 2022), while fuel moisture levels below the critical thresholds set the stage for vigorous fire spread (Ellis *et al.*, 2022; Nolan *et al.*, 2016b; Resco de Dios *et al.*, 2022). Lastly, the extreme fuel moisture threshold is defined as the level at which large wildfire events exhibiting exponential growth of the burned area is observed (Ma *et al.*, 2021; Nolan *et al.*, 2016b).

To assess LFMC and DFMC responses to climate change conditions, linear mixed-effects models were fitted with the *lme4 R* package (Bates *et al.*, 2015). The fitted models had a double factorial structure with *Period* and *RCP* as fixed factors and *Site* and *Year* as random effects, with *Year* being a replicate for *Period*. The response variables were fuel moisture values (%) and fire season length (d yr^{-1}). LFMC critical threshold values were squared root transformed in order to meet model assumptions. Results for LFMC extreme fuel moisture threshold data are not shown as the fitted model did not meet normality assumptions. Then moisture content dynamics and fire season lengths were correlated with each study sites mean annual net primary productivity (NPP) to assess whether changes in fuel moisture and in the potential fire season length will be amplified or reduced across productivity gradients. Finally, to test for CO_2 effects on LFMC and fire season length, it was performed a dependent samples sign test from the *R* package *BSDA* (Arnholt, 2022). A non-parametric test was used as linear models fitted with constant and increasing CO_2 databases values did not meet normality assumptions. In this way, it was assessed whether median LFMC (%) and fire season length (d yr^{-1}) values estimated under constant or increasing atmospheric CO_2 concentrations were significantly different.

V.3 Results

V.3.1 Fuel moisture dynamics

Summer mean moisture content ranged from 62 to 135 % in the case of live fuels and from 7 to 15 % in the case of dead fuels, with a mean LFMC of 114 % and a mean DFMC of 9 % across all study sites and throughout all time periods while considering both RCP scenarios. Declines in LFMC and in DFMC were projected in the three decadal periods, from 2010-2020 (1st period) to 2040-2050 (2nd period) and from 2010-2020 to 2090-2100 (3rd period) under both RCP scenarios.

There was a significant effect of *RCP, Period*, and their interactions on LFMC variation (Table S.V.3). Bonferroni corrected post hoc comparisons (Table S.V.4.1) revealed that, under the moderate greenhouse gas emission scenario (RCP4.5, Fig. V.2a-c-e), there were only significant differences between the 1st and 3rd decadal periods ($p < 0.001$) where summer mean LFMC across all sites was predicted to decline from 116 % (Fig. V.2.A) to 113 % (Fig. V.2.E). The trends of declining mean summer LFMC were more pronounced under high greenhouse emission scenario (RCP8.5, Fig. V.2.B-D-F), where differences between periods were always significant. Projections showed a mean decline from 116 % in 2010-2020 (Fig. V.2.B) to 112 % for 2040-2050 (Fig. V.2.D) and to 106 % for 2090-2100 (Fig. V.2.F). Regarding RCP comparisons (Fig. S.V.3, Table S.V.4.1), there were non-significant differences between predicted mean summer LFMC during the 1st period for both RCPs, and between RCP4.5 for the 3rd period and RCP8.5 for the 2nd period. The rest of pairwise comparisons involving RCP and Period were significantly different (Fig. V.2, Fig. S.V.3, Table S.V.4.1). Finally, the effect of the random Site factor indicated significant and widespread variability across sites (Table S.V.4.2).

DFMC analyses also showed significant effects of *Period, RCP* and their interaction on DFMC variation (Table S.V.5). Bonferroni corrected post hoc comparisons revealed that all pairwise differences between periods in both RCP scenarios were significant (Fig. S.V.4, Table S.V.6.1). Summer mean DFMC levels across the study sites (Fig. V.3) predicted under RCP4.5 showed a decline from 10 % in 2010-2020 (Fig. V.3.A) to 9.5 % in 2040-2050 (Fig. V.3.C), and to 9 % in 2090-2100 (Fig. V.3.E). Under RCP8.5, predicted mean summer values showed a mean decline from 10 % in 2010-2020 (Fig. V.3.B) to 9.25 % in 2040-2050 (Fig. V.3.D), and to 8.5 % in 2090-2100 (Fig. V.3.F). Differences in predicted mean summer DFMC values across all sites between both RCPs for the 2nd periods were not significant, but DFMC was significantly lower in RCP8.5 than in RCP4.5 in the rest of pairwise comparisons across periods (Fig. S.V.4, Table S.V.6.1). Again, the effect of the random Site factor indicated significant and widespread variability across sites (Table S.V.6.2).

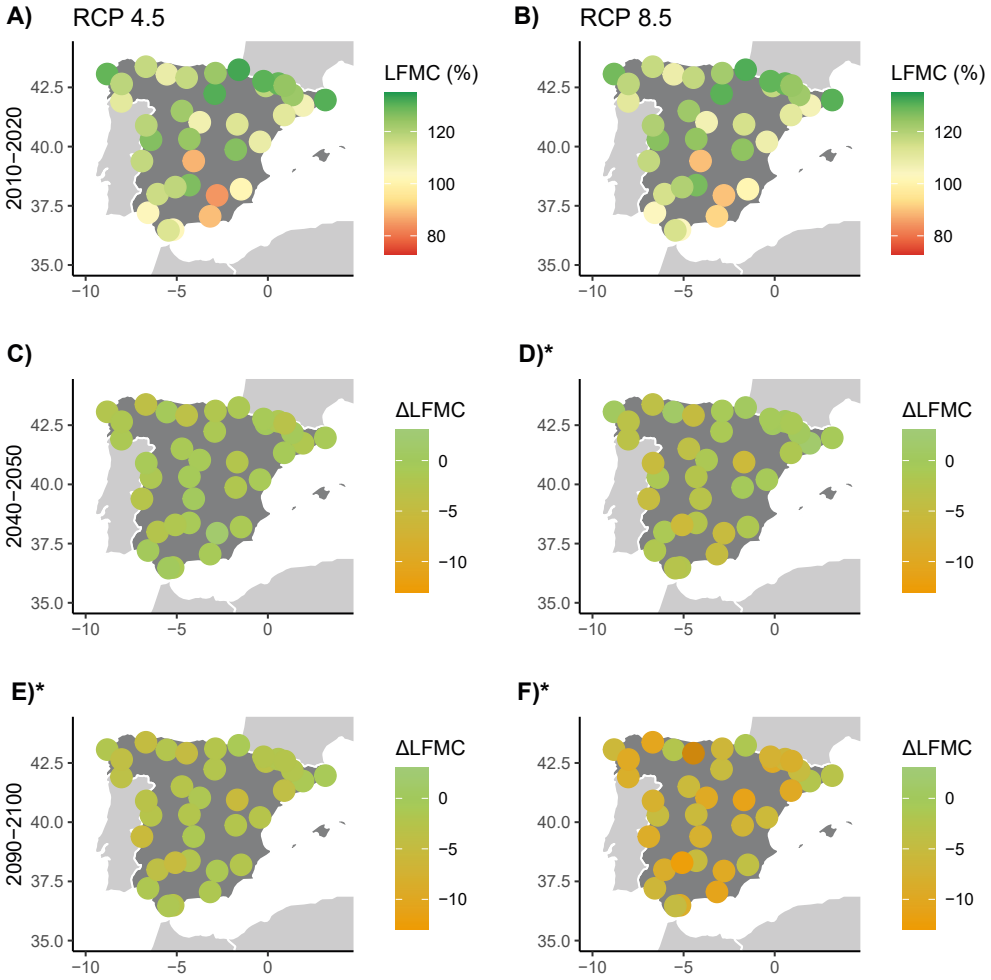

Figure V.2: LFMC projections. Projected changes in LFMC across Spain for three decadal time periods under RCP4.5 and RCP8.5. Summer mean LFMC values of each study site for the period 2010-2020 for both RCP 4.5 (A) and 8.5 (B). Differences in summer mean LFMC between 2040-2050 and 2010-2020 for RCP 4.5 (C) and 8.5 (D). Differences in summer mean LFMC between 2090-2100 and 2010-2020 for RCP 4.5 (E) and 8.5 (F). Asterisks after the subplot letter indicate significant LFMC differences between 2010-2020 and future periods.

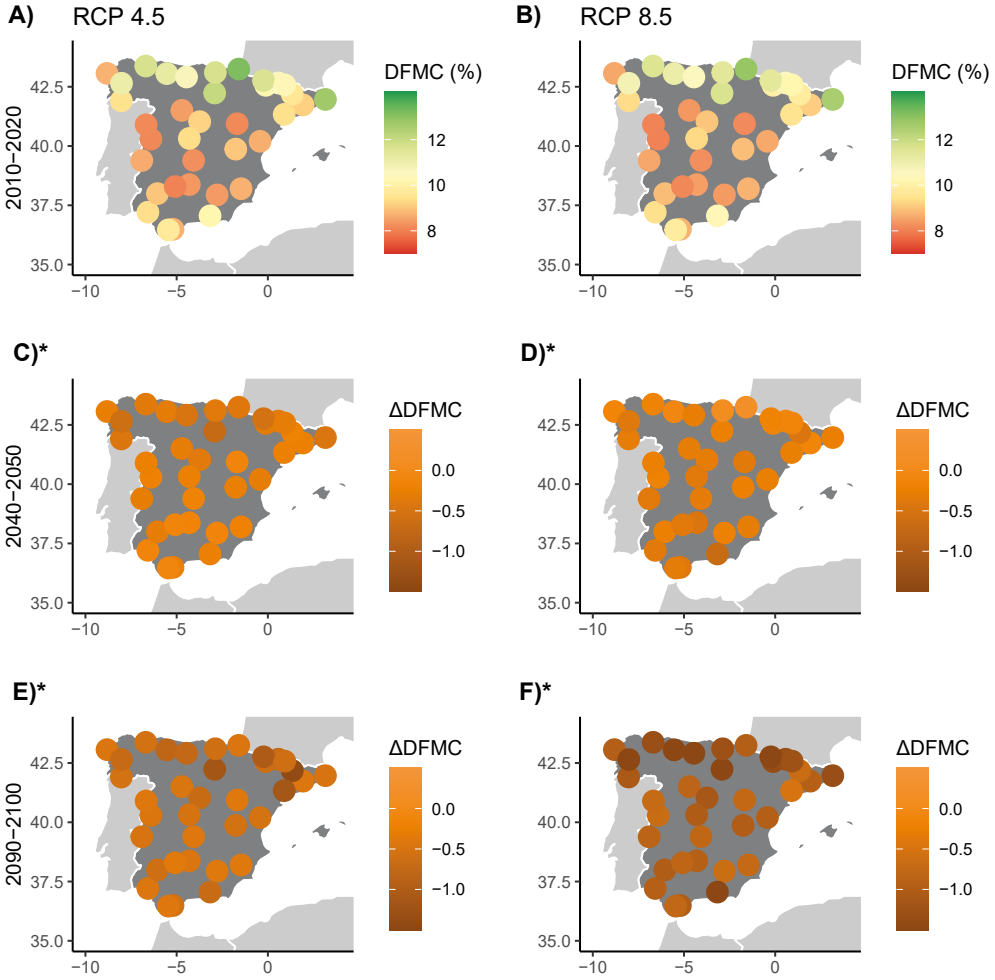

Figure V.3: DFMC projections. Projected changes in DFMC across Spain for three decadal time periods under RCP4.5 and RCP8.5. Summer mean DFMC values of each study site for the period 2010-2020 for both RCP 4.5 (A) and 8.5 (B). Differences in summer mean DFMC between 2040-2050 and 2010-2020 for RCP 4.5 (C) and 8.5 (D). Differences in summer mean DFMC between 2090-2100 and 2010-2020 for RCP 4.5 (E) and 8.5 (F). Asterisks after the subplot letter indicate significant DFMC differences between 2010-2020 and future periods.

V.3.2 Fire season length

Fire season length was calculated from the total number of days per year (d yr^{-1}) with predicted LFMC and DFMC values below empirical wildfire occurrence thresholds. For 2010-2020, it was recorded a mean fire season length of 112, 32 and 2 days with LFMC values below the minimum (120 % LFMC), the critical (100 % LFMC) and the extreme (80 % LFMC) thresholds, respectively. Regarding DFMC, mean fire season length varied between 112, 70 and 16 days depending on whether the fire season was defined from values below the minimum (12 % DFMC), the critical (10 % DFMC) or the extreme (8 % DFMC) thresholds. Predicted fire season lengths as defined by live and dead moisture content thresholds showed an increasing trend for the 21st century in all study sites for both emission scenarios RCP4.5 and RCP8.5 (Fig. V.4, Table V.1). There was a significant effect of *RCP, Period*, and their interaction on LFMC variation for minimum and critical thresholds (Table S.V.7 and S.V.8) and on DFMC variation for all three thresholds (Table S.V.9-11). From 2010-2020 to 2090-2100 fire season length regarding minimum and critical LFMC thresholds was predicted to increase on average by 15 and 8 d yr^{-1} under RCP4.5 and by 50 and 30 d yr^{-1} under RCP8.5. Across the same periods, fire season length regarding minimum, critical and extreme DFMC thresholds was predicted to increase by 20, 17, 15 d yr^{-1} under RCP4.5 and by 46, 40, 33 d yr^{-1} under RCP8.5.

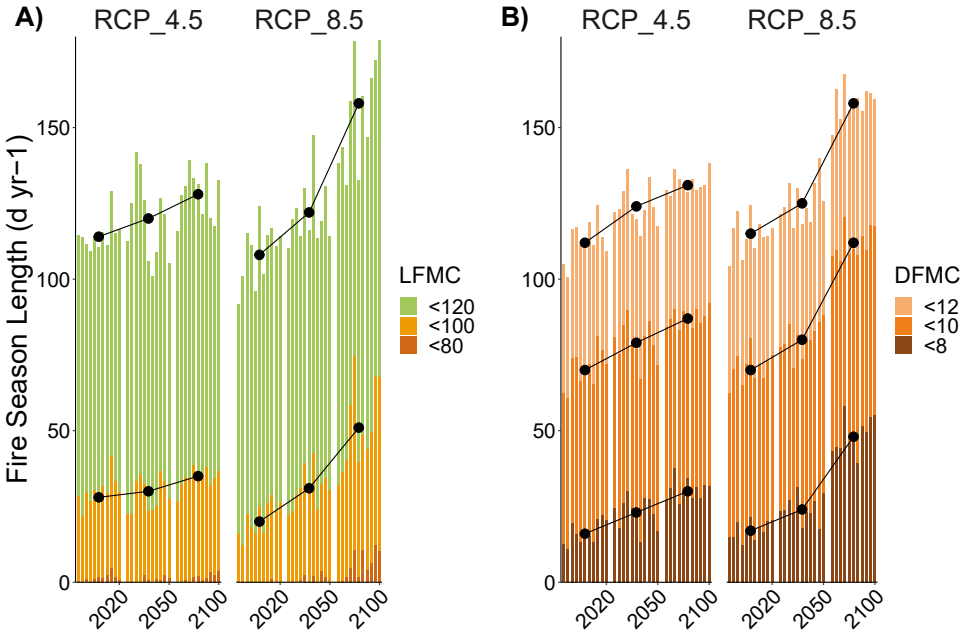

Figure V.4: Fire season length. Fire season length represented by the number of days per year (d yr^{-1}) with LFMC (a) and DFMC (b) values below wildfire occurrence thresholds (minimum: 120-12 %, critical: 100-10 % and extreme: 80-8 % for LFMC-DFMC, respectively) under scenarios RCP4.5 and RCP8.5. Each bar represents a year within each period (2010-2020, 2040-2050 and 2090-2100). Black dots represent mean values for each period. Mean values for the extreme LFMC threshold of 80 % were not represented as the fitted model does not meet normality assumptions.

Table V.1: Fire season length. Fire season length represented by the number of days per year (d yr^{-1}) with LFMC and DFMC values below wildfire occurrence thresholds (minimum: 120-12 % | critical: 100-10 % | extreme: 80-8 % for LFMC-DFMC, respectively) under scenarios RCP4.5 and RCP8.5. Values for the extreme LFMC threshold of 80 % were not represented as the fitted model does not meet normality assumptions.

	LFMC		DFMC	
Period	RCP4.5	RCP8.5	RCP4.5	RCP8.5
2010-2020	112 | 32 | 2	110 | 27 | 2	112 | 70 | 16	112 | 70 | 16
2040-2050	117 | 35 | -	123 | 39 | -	124 | 79 | 23	124 | 79 | 23
2090-2100	127 | 40 | -	160 | 57 | -	132 | 87 | 31	158 | 110 | 49

V.3.3 Changes across productivity gradients

The effects of climate change on LFMC depended on site productivity, with the decline in summer mean LFMC being more marked at the least productive sites. A negative relationship ($p = 0.007$, $R^2 = 0.2$) was recorded comparing current summer mean LFMC with predicted levels at the end of the 21st century (ΔLFMC, Fig. V.5.A,C), as ΔLFMC changed from -10 to -2 % from the least to the most productive site under RCP8.5. The slope of the relationship was significantly higher ($p = 0.001$) in conifer forests, meaning that the future decrease in summer mean LFMC could be less marked at broadleaf forests locations. Under RCP4.5, the change in summer mean LFMC with productivity was only marginally significant ($p = 0.057$) for conifer forests, where the ΔLFMC change across the productivity gradient was from -3 to -1 %. Predicted fire season lengthening was also significantly less in places with higher productivity (Fig. V.5.B,D). The increase in fire season length (defined from days under the minimum LFMC threshold of 120 %) with productivity under RCP8.5 ranged from 100 to 7 d yr^{-1} from the least to the most productive site, and the slope of the relationship was more negative in broadleaf forests (from 80 to 7 d yr^{-1}) than in conifer forests (ranging from 95 to 38 d yr^{-1}). The same trends were observed under RCP4.5, but less pronounced. The change in fire season length with productivity ranged to 22 to 0 d yr^{-1}, again only significant in conifer forests and with lower slope estimates. Finally, correlations between variation in mean summer DFMC and productivity were not significant.

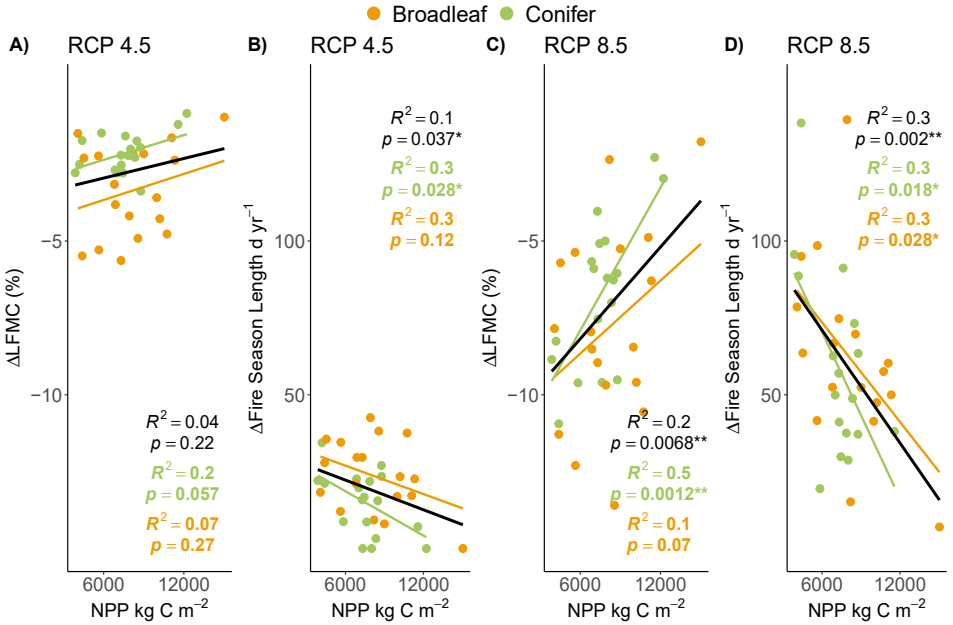

Figure V.5 Productivity gradients. The effects of climate change on fuel moisture depend on site productivity (2010-2020 mean annual net primary productivity in Kg C m^{-2}). Correlations between changes in LFMC (ΔLFMC) between 2090-2100 and 2010-2020 and changes in fire season length (minimum threshold of LFMC < 120 %) as a function of mean annual net primary productivity under RCP4.5 (A, B) and RCP8.5 (C, D). R^2 and *p-values* represent the results of linear fitting for all species and separately for conifer forests (blue) and broadleaf forests (orange).

V.3.4 CO_2 effects

Results of the dependent samples sign test showed that median LFMC values predicted under an increasing atmospheric CO_2 concentration were significantly greater ($p < 0.001$) than median LFMC values predicted under a constant [CO_2]. Comparing summer median LFMC, it was observed that predicted values were higher under increasing atmospheric [CO_2] (114 %) than under a constant atmospheric [CO_2] (113 %). Median values differences between constant and increasing atmospheric [CO_2] predictions were greater for RCP8.5 (1.5 %) than for RCP4.5 (0.75 %). LFMC levels under RCP4.5, from 2010-2020 to 2090-2100, were predicted to decline about 4 % under increasing atmospheric [CO_2], and by about 5 % under stable atmospheric [CO_2]. Under RCP8.5, predicted declines in summer mean LFMC were larger for the same periods, with a LFMC decline of 10 % under increasing atmospheric [CO_2], and a decline of 13 % under constant atmospheric [CO_2] conditions. Predicted fire seasons lengthening was approximately 10 d yr^{-1} lower in simulations conducted under increasing atmospheric [CO_2]. Thus, predicted lengthening under RCP8.5 between 2020 to 2100, was 55 and 39 d yr^{-1} for

minimum and critical fuel moisture thresholds under increasing atmospheric [CO_2], while under constant [CO_2] conditions lengthening was 66 and 47 d yr^{-1} for the same RCP, period, and thresholds (Table S.V.12).

V.4 Discussion

In this chapter LFMC and DFMC dynamics were estimated throughout the 21st century by applying semi-mechanistic models for medium and high greenhouse gas emission scenarios (RCPs 4.5 and 8.5). I found that seasonal mean LFMC and DFMC are projected to experience generalized declining trends in the coming decades, with increasing annual frequencies of fuel moisture content dropping below wildfire occurrence thresholds and consequently a lengthening of the fire season. Under middle of the road emission scenarios (RCP4.5), summer mean LFMC and DFMC values are expected to decrease by 3 % and 1 % respectively, extending annual fire season length by 20 days per year between 2020-2100. Under high emissions scenario (RCP8.5), summer mean LFMC and DFMC values are expected to decrease by 10 % and 1.5 % respectively, causing the annual fire season length to increase by 50 days at the end of the 21st century compared with current fire season.

Despite predicted declines in summer mean LFMC and DFMC (-10 and -1.5 % respectively) are relatively small, it is important to consider that relationships between fuel moisture and burned area are exponential. Longer periods with low fuel moisture values increase the connectivity of available fuels at landscape scales by affecting wet local areas, as valley bottoms, that could act as natural fire breaks (Resco de Dios *et al.*, 2022). Thus, considering that current fuel moisture values in large European areas are already close to the limit of wildfire occurrence thresholds (Carnicer *et al.*, 2022; Resco de Dios *et al.*, 2021), even minimum decreases in fuel moisture can lead to large wildfire events that exponentially increase the burned area (Nolan *et al.*, 2016).

DFMC showed proportionally steeper declining trends during the remainder of the 21st century than LFMC. More study sites were found with fuel moisture values below wildfire occurrence thresholds for DFMC (Fig. V.3) than for LFMC (Fig. V.2) and DFMC projections showed more days per year with values below critical and extreme threshold (70 and 16 d yr^{-1} respectively) than LFMC (32 and 2 d yr^{-1}). Furthermore, CO_2 mitigation effects did not impact DFMC, as it only affects physiological plant regulation (Wullschleger *et al.*, 2002). This misalignment between live and dead fuels moisture declines could modify fire regimes by affecting fire behavior and fire spread. DFMC mostly affects the spread of low intensity surface fires and LFMC affect the onset and propagation of high intensity crown fires (Scott & Reinhardt, 2001). Thus, while generalized

DFMC declines may increase surface fires activity, relatively higher LFMC values may restrict the transition to crown fires acting as switch for the occurrence of large wildfire events (Krawchuk & Moritz, 2011).

We can observe a productivity gradient effect over the predicted fuel moisture trends with the largest declines at the least productive sites (Fig. V.5). But, despite low productivity southern study sites recorded the minimum moisture content values (Fig. V.3, V.4), high productivity northern sites of Spain, where fire is currently rare due to high fuel moisture (Resco de Dios *et al.*, 2021), showed significant increases in the fire season length. Furthermore, it is in northern study sites where the greater DFMC declines were recorded (Fig. V.3E, F). Northern Spain climatic conditions favor the development of forests dominated by temperate deciduous broad-leaf species (Fig. V.1C). These ecosystems are highly productive and hold high amounts of biomass (Fig. V.1D) resulting in vast amounts of fuel loads accumulated in forests, being the major Spain's forest carbon sinks (Alberdi *et al.*, 2016). Several decades of land abandonment have promoted the encroachment of forest into former pastures and croplands increasing fuel accumulation and forest continuity at the expense of the traditional managed landscapes mosaics (Gelabert *et al.*, 2022). These vast amounts of forest fuels have formed fuel arrays of high vertical and horizontal continuity in relatively humid environments, where fire activity is currently limited by high fuel moisture content. In these regions, declines in fuel moisture are predicted to develop in the coming decades, setting the stage for high intensity/severity crown fires with potential to escalate to megafires that go well beyond extinction capacities (Linley *et al.*, 2022; Resco de Dios, 2020), threatening the major Spain's carbon sinks (Anderegg *et al.*, 2020).

We can observe that simulations conducted with increasing atmospheric CO_2 concentrations showed significantly higher LFMC values compared to estimations conducted with stable CO_2 concentrations. Under RCP 8.5, the CO_2 mitigation effect causes an average increase of 3 % in summer mean LFMC values, which is not enough to compensate for a net LFMC decline of 10 % expected by the end of the century as a result of increasing temperature and decreasing precipitation. Also, fire season lengthening was 10 d yr^{-1} lower under increasing CO_2 concentration scenarios, but again not enough to overcome a net increase of 50 d yr^{-1} predicted as a result of climate change alone. Our model of CO_2 effects over LFMC only accounted for water savings through stomatal conductance, and it did not include negative LFMC feedbacks through, for instance, increasing leaf area index which would increase transpiration and, hence, soil water depletion (McDowell *et al.*, 2022). Thus, results present a "best-case scenario" on CO_2 ameliorating projected decline of summer mean LFMC.

This is the first study to apply semi-mechanistic process-based models to quantify future trends in fuel moisture under climate change considering

productivity gradients. Although the fire season lengthening trends found in this study are consistent with previous studies for the Mediterranean region (Abatzoglou *et al.*, 2019; Dupuy *et al.*, 2020; Ellis *et al.*, 2022; Jones *et al.*, 2022; Rigo *et al.*, 2017), it is important to consider that these studies are based on weather indices such as the Canadian Fire Weather Index (FWI; Van Wagner, 1987). Weather indices ignore species-level physiological capabilities to adjust the moisture status of live fuels, which would explain the less pronounced fire season lengthening here reported compared to previous studies (*i.e.*, Jones *et al.*, 2022 predicted a fire season lengthening of 60 d yr^{-1} from 2020 to 2100 under RCP8.5 conditions while this research report a lengthening of 50 d yr^{-1}). Further studies should assess how physiological plant responses to climate change conditions (e.g., vulnerability to cavitation) will increase the proportion of dead particles in tree canopies, which will increase crown fire risk because of the lower moisture of standing material that may serve as ladder fuels (Van Wagner, 1977).

Overall, this analyses projects generalized declines in fuel moisture through Spanin's forests which are going to lengthen fire seasons from the present through to the end of the century. Although the most pronounced declines in fuel moisture are projected to occur in the least productive environments, significant increases in the fire season length were also projected in the most productive environments that are currently largely fire-free, where an increase in fire activity would pose a threat to major Spain's carbon sinks. Finally, results indicate that the CO_2 mitigations effect on plant water relations and LFMC (via increases in water-use-efficiency) is not enough to offset climate change driven declines in seasonal LFMC levels.

V.5 Conclusions

• Fuel moisture is projected to experience generalized declining trends in the coming decades, leading to longer fire seasons.

• The use of semi-mechanistic approaches to infer future live fuel moisture dynamics allows the consideration of physiological traits that enhance plant species resilience over climate change impacts.

• Possible mitigation effects derived from plant physiological traits are not enough to offset climate change driven LFMC declines.

• Significant increases in the fire season length in the most productive environments that are currently fire-free would pose a threat to major Spain's carbon sinks.

V.6 References

Abatzoglou, J. T., Williams, A. P., & Barbero, R. (2019). Global Emergence of Anthropogenic Climate Change in Fire Weather Indices. Geophysical Research Letters, 46(1), 326–336. https://doi.org/10.1029/2018GL080959

Alberdi, I., Sandoval, V., Condes, S., Cañellas, I., & Vallejo, R. (2016). The Spanish National Forest Inventory, a tool for the knowledge, management and conservation of forest ecosystems. Ecosistemas, 25(3), 88–97. https://doi.org/10.7818/ecos.2016.25-3.10

An, H., Gan, J., & Cho, S. J. (2015). Assessing climate change impacts on wildfire risk in the United States. Forests, 6(9), 3197–3211. https://doi.org/10.3390/f6093197

Anderegg, W. R. L., Trugman, A. T., Badgley, G., Anderson, C. M., Bartuska, A., Ciais, P., Cullenward, D., Field, C. B., Freeman, J., Goetz, S. J., Hicke, J. A., Huntzinger, D., Jackson, R. B., Nickerson, J., Pacala, S., & Randerson, J. T. (2020). Climate-driven risks to the climate mitigation potential of forests. Science 368(6497). https://doi.org/10.1126/science.aaz7005

Arnholt A, E. B. (2022). BSDA: Basic Statistics and Data Analysis. R package version 1.2.0.

Balaguer-Romano, R., Díaz-Sierra, R., De Cáceres, M., Cunill-Camprubí, À., Nolan, R. H., Boer, M. M., Voltas, J. & Resco de Dios, V. (2022). A semi-mechanistic model for predicting daily variations in species-level live fuel moisture content. Agricultural and Forest Meteorology, 323, 109022. https://doi.org/10.1016/j.agrformet.2022.109022

Bates, D., Mächler, M., Bolker, B. M., & Walker, S. C. (2015). Fitting linear mixed-effects models using lme4. Journal of Statistical Software, 67(1), 1-48. https://doi.org/10.18637/jss.v067.i01

Boer, M. M., Resco de Dios, V., Stefaniak, E. Z., & Bradstock, R. A. (2021). A hydroclimatic model for the distribution of fire on earth. Environmental Research Communications, 3(3). https://doi.org/10.1088/2515-7620/abec1f

Boer, M. M., Nolan, R. H., Resco de Dios, V., Clarke, H., Owen, F., & Bradstock, R. A. (2017). Changing Weather Extremes Call for Early Warning of Potential for Catastrophic Fire. Earth's Future, 5:1196–1202. https://doi.org/10.1002/eft2.274

Carnicer, J., Alegria, A., Giannakopoulos, C., Di Giuseppe, F., Karali, A., Koutsias, N., Lionello, P., Parrington, M., & Vitolo, C. (2022). Global warming is shifting the relationships between fire weather and realized fire-induced CO2 emissions in Europe. Scientific Reports, 12(1), 8–13. https://doi.org/10.1038/s41598-022-14480-8

Chazarra-Bernabé, A., Flórez García, E., Peraza Sánchez, B., Tohá Rebull, T., Lorenzo Mariño, B., Criado Pinto, E., Moreno García, J. V., Romero Fresneda, R., & Botey Fullat, R. (2018). Mapas climáticos de España (1981-2010) y ETo (1996-2016). Agencia Estatal de Meteorología. https://doi.org/10.31978/014-18-004-2

De Cáceres, M., Martin-StPaul, N., Turco, M., Cabon, A., & Granda, V. (2018). Estimating daily meteorological data and downscaling climate models over landscapes. Environmental Modelling and Software, 108, 186–196. https://doi.org/10.1016/j.envsoft.2018.08.003

De Cáceres, M., Mencuccini, M., Martin-StPaul, N., Limousin, J. M., Coll, L., Poyatos, R., Cabon, A., Granda, V., Forner, A., Valladares, F., & Martínez-Vilalta, J. (2021). Unravelling the effect of species mixing on water use and drought stress in Mediterranean forests: A modelling approach. Agricultural and Forest Meteorology, 296, 108233. https://doi.org/10.1016/j.agrformet.2020.108233

Dinerstein, E., Olson, D., Joshi, A., Vynne, C., Burgess, N. D., Wikramanayake, E., Hahn, N., Palminteri, S., Hedao, P., Noss, R., Hansen, M., Locke, H., Ellis, E. C., Jones, B., Barber, C. V., Hayes, R., Kormos, C., Martin, V., Crist, E., Saleem, M. (2017). An Ecoregion-Based Approach to Protecting Half the Terrestrial Realm. BioScience, 67(6), 534–545. https://doi.org/10.1093/biosci/bix014

Dupuy, J. luc, Fargeon, H., Martin-StPaul, N., Pimont, F., Ruffault, J., Guijarro, M., Hernando, C., Madrigal, J., & Fernandes, P. (2020). Climate change impact on future wildfire danger and activity in southern Europe: a review. Annals of Forest Science, 77(2). https://doi.org/10.1007/s13595-020-00933-5

Duursma, R. A. (2015). Plantecophys - An R package for analysing and modelling leaf gas exchange data. PLoS ONE, 10(11), 1–13. https://doi.org/10.1371/journal.pone.0143346

Ellis, T. M., Bowman, D. M. J. S., Jain, P., Flannigan, M. D., & Williamson, G. J. (2022). Global increase in wildfire risk due to climate-driven declines in fuel moisture. Global Change Biology, 28(4), 1544–1559. https://doi.org/10.1111/gcb.16006

Fargeon, H., Pimont, F., Martin-StPaul, N., De Caceres, M., Ruffault, J., Barbero, R., & Dupuy, J. L. (2020). Projections of fire danger under climate change over France: where do the greatest uncertainties lie? Climatic Change, 160(3), 479–493. https://doi.org/10.1007/s10584-019-02629-w

Gannon, C. S., & Steinberg, N. C. (2021). A global assessment of wildfire potential under climate change utilizing keetch-byram drought index and land cover classifications. Environmental Research Communications, 3(3), 035002. https://doi.org/10.1088/2515-7620/abd836

Gao, P., Terando, A. J., Kupfer, J. A., Morgan Varner, J., Stambaugh, M. C., Lei, T. L., & Kevin Hiers, J. (2021). Robust projections of future fire probability for the conterminous United States. Science of the Total Environment, 789, 147872. https://doi.org/10.1016/j.scitotenv.2021.147872

Gelabert, P. J., Rodrigues, M., Vidal-Macua, J. J., Ameztegui, A., & Vega-Garcia, C. (2022). Spatially explicit modeling of the probability of land abandonment in the Spanish Pyrenees. Landscape and Urban Planning, 226, 104487. https://doi.org/10.1016/j.landurbplan.2022.104487

Hantson, S., Arneth, A., Harrison, S. P., Kelley, D. I., Colin Prentice, I., Rabin, S. S., Archibald, S., Mouillot, F., Arnold, S. R., Artaxo, P., Bachelet, D., Ciais, P., Forrest, M., Friedlingstein, P., Hickler, T., Kaplan, J. O., Kloster, S., Knorr, W., Lasslop, G., Yue, C. (2016). The status and challenge of global fire modelling. Biogeosciences, 13(11), 3359–3375. https://doi.org/10.5194/bg-13-3359-2016

Hengl, T., Jesus, J. M. De, Heuvelink, G. B. M., Ruiperez, M., Kilibarda, M., Blagoti, A., Shangguan, W., Wright, M. N., Geng, X., Bauer-marschallinger, B., Guevara, M. A., Vargas, R., Macmillan, R. A., Batjes, N. H., Leenaars, J. G. B., Ribeiro, E., Wheeler, I., Mantel, S., & Kempen, B. (2017). SoilGrids250m : Global gridded soil information based on machine learning. PLoS ONE 12(2): e0169748. https://doi.org/10.1371/journal.pone.0169748

IPCC. (2021). Climate Change 2021: The Physical Science Basis. Contribution of Working Group I to the Sixth Assessment Report of the Intergovernmental Panel on Climate Change. Cambridge University Press, United Kingdom.

Jolly, W. M., Cochrane, M. A., Freeborn, P. H., Holden, Z. A., Brown, T. J., Williamson, G. J., & Bowman, D. M. J. S. (2015). Climate-induced variations in global wildfire danger from 1979 to 2013. Nature Communications, 6, 1–11. https://doi.org/10.1038/ncomms8537

Jones, M. W., Abatzoglou, J. T., Veraverbeke, S., Andela, N., Lasslop, G., Forkel, M., Smith, A. J. P., Burton, C., Betts, R. A., van der Werf, G. R., Sitch, S., Canadell, J. G., Santín, C., Kolden, C., Doerr, S. H., & Le Quéré, C. (2022). Global and Regional Trends and Drivers of Fire Under Climate Change. Reviews of Geophysics, 60(3), 1–76. https://doi.org/10.1029/2020rg000726

Kotlarski, S., Keuler, K., Christensen, O. B., Colette, A., Déqué, M., Gobiet, A., Goergen, K., Jacob, D., Lüthi, D., Van Meijgaard, E., Nikulin, G., Schär, C., Teichmann, C., Vautard, R., Warrach-Sagi, K., & Wulfmeyer, V. (2014). Regional climate modeling on European scales: A joint standard evaluation of the EURO-CORDEX RCM ensemble. Geoscientific Model Development, 7(4), 1297–1333. https://doi.org/10.5194/gmd-7-1297-2014

Krawchuk, M. A., & Moritz, M. A. (2011). Constraints on global fire activity vary across a resource gradient. Ecology, 92(1), 121–132. https://doi.org/10.1890/09-1843.1

Linley, G. D., Jolly, C. J., Doherty, T. S., Geary, W. L., Armenteras, D., Belcher, C. M., Bliege, R., Andrea, B., Fletcher, M.-S., Giorgis, M. A., Haslem, A., Jones, G. M., Kelly, L. T., Lee, C. K. F., Nolan, R. H., Parr, C. L., Pausas, J. G., Price, J. N., Regos, A., Nimmo, D. G. (2022). What do you mean, ' megafire '? Global Ecology and Biogeography, February, 1–17. https://doi.org/10.1111/geb.13499

Ma, W., Zhai, L., Pivovaroff, A., Shuman, J., Buotte, P., Ding, J., Christoffersen, B., Knox, R., Moritz, M., Fisher, R. A., Koven, C. D., Kueppers, L., & Xu, C. (2021). Assessing climate change impacts on live fuel moisture and wildfire risk using a hydrodynamic vegetation model. Biogeosciences, 18(13), 4005–4020. https://doi.org/10.5194/bg-18-4005-2021

Matthews, S. (2014). Dead fuel moisture research: 1991-2012. International Journal of Wildland Fire, 23(1), 78–92. https://doi.org/10.1071/WF13005

Matthews, S., Nguyen, K., & McGregor, J. L. (2011). Modelling fuel moisture under climate change. International Journal of Climate Change Strategies and Management, 3(1), 6–15. https://doi.org/10.1108/17568691111107916

McDowell, N. G., Sapes, G., Pivovaroff, A., Adams, H. D., Allen, C. D., Anderegg, W. R. L., Arend, M., Breshears, D. D., Brodribb, T., Choat, B., Cochard, H., De Cáceres, M., De Kauwe, M. G., Grossiord, C., Hammond, W. M., Hartmann, H., Hoch, G., Kahmen, A., Klein, T., Xu, C. (2022). Mechanisms of woody-plant mortality under rising drought, CO2 and vapour pressure deficit. Nature Reviews Earth and Environment, 3(5), 294–308. https://doi.org/10.1038/s43017-022-00272-1

McSweeney, C. F., Jones, R. G., Lee, R. W., & Rowell, D. P. (2015). Selecting CMIP5 GCMs for downscaling over multiple regions. Climate Dynamics, 44(11–12), 3237–3260. https://doi.org/10.1007/s00382-014-2418-8

Meinshausen, M., Smith, S. J., Calvin, K., Daniel, J. S., Kainuma, M. L. T., Lamarque, J., Matsumoto, K., Montzka, S. A., Raper, S. C. B., Riahi, K., Thomson, A., Velders, G. J. M., & van Vuuren, D. P. P. (2011). The RCP greenhouse gas concentrations and their extensions from 1765 to 2300. Climatic Change, 109(1), 213–241. https://doi.org/10.1007/s10584-011-0156-z

Moss, R. H., Edmonds, J. A., Hibbard, K. A., Manning, M. R., Rose, S. K., Van Vuuren, D. P., Carter, T. R., Emori, S., Kainuma, M., Kram, T., Meehl, G. A., Mitchell, J. F. B., Nakicenovic, N., Riahi, K., Smith, S. J., Stouffer, R. J., Thomson, A. M., Weyant, J. P., & Wilbanks, T. J. (2010). The next generation of scenarios for climate change research and assessment. Nature, 463(7282), 747–756. https://doi.org/10.1038/nature08823

Nolan, R. H., Boer, M. M., Resco De Dios, V., Caccamo, G., & Bradstock, R. A. (2016a). Large-scale, dynamic transformations in fuel moisture drive wildfire activity across southeastern Australia. Geophysical Research Letters, 43(9), 4229–4238. https://doi.org/10.1002/2016GL068614

Nolan, R. H, Resco de Dios, V., Boer, M. M., Caccamo, G., Goulden, M. L., & Bradstock, R. A. (2016b). Predicting dead fine fuel moisture at regional scales using vapour pressure deficit from MODIS and gridded weather data. Remote Sensing of Environment, 174, 100–108. https://doi.org/10.1016/j.rse.2015.12.010

Nolan, R. H., Hedo, J., Arteaga, C., Sugai, T., & Resco de Dios, V. (2018). Physiological drought responses improve predictions of live fuel moisture dynamics in a Mediterranean forest. Agricultural and Forest Meteorology, 263, 417–427. https://doi.org/10.1016/j.agrformet.2018.09.011

Pausas, J. G., & Ribeiro, E. (2013). The global fire-productivity relationship. Global Ecology and Biogeography, 22(6), 728–736. https://doi.org/10.1111/geb.12043

Rabin, S. S., Melton, J. R., Lasslop, G., Bachelet, D., Forrest, M., Hantson, S., Kaplan, J. O., Li, F., Mangeon, S., Ward, D. S., Yue, C., Arora, V. K., Hickler, T., Kloster, S., Knorr, W., Nieradzik, L., Spessa, A., Folberth, G. A., Sheehan, T., Arneth, A. (2017). The Fire Modeling Intercomparison Project (FireMIP), phase 1: Experimental and analytical protocols with detailed model descriptions. Geoscientific Model Development, 10(3), 1175–1197. https://doi.org/10.5194/gmd-10-1175-2017

Resco de Dios, V. (2020). Plant-Fire Interactions. Applying Ecophysiology to Wildfire Management. Vol 36. Springer, Switzerland.

Resco de Dios, V., Cunill Camprubí, À., Pérez-Zanón, N., Peña, J. C., Martínez del Castillo, E., Rodrigues, M., Yao, Y., Yebra, M., Vega-García, C., & Boer, M. M. (2022). Convergence in critical fuel moisture and fire weather thresholds associated with fire activity in the pyroregions of Mediterranean Europe. Science of the Total Environment, 806(4), 151462. https://doi.org/10.1016/j.scitotenv.2021.151462

Resco de Dios, V., Fellows, A. W., Nolan, R. H., Boer, M. M., Bradstock, R. A., Domingo, F., & Goulden, M. L. (2015). A semi-mechanistic model for predicting the moisture content of fine litter. Agricultural and Forest Meteorology, 203, 64–73. https://doi.org/10.1016/j.agrformet.2015.01.002

Resco de Dios, V., Hedo, J., Cunill, À., Thapa, P., Martínez, E., Martínez, J., Aragón, D., Antonio, J., Balaguer-Romano, R., Díaz-sierra, R., Yebra, M., & Boer, M. M. (2021). Climate change induced declines in fuel moisture may turn currently fi re-free Pyrenean mountain forests into fi re-prone ecosystems. Science of the Total Environment, 797, 149104. https://doi.org/10.1016/j.scitotenv.2021.149104

Rigo, D. de, Libertà, G., Durrant, T. H., Vivancos, T. A., & San-Miguel-Ayanz, J. (2017). Forest fire danger extremes in Europe under climate change: variability and uncertainty. In Publication Office of the European Union.

Rodríguez, E., & Gutiérrez, J. M. (2018). Escenarios PNACC 2017: Nueva colección de escenarios de cambio climático regionalizados del Plan Nacional de Adaptación al Cambio Climático (PNACC). Aemet, 0, 1–17.

Ruffault, J., Martin-StPaul, N. K., Duffet, C., Goge, F., & Mouillot, F. (2014). Projecting future drought in Mediterranean forests: Bias correction of climate models matters! Theoretical and Applied Climatology, 117(1), 113–122. https://doi.org/10.1007/s00704-013-0992-z

Ruffault, J., Martin-StPaul, N., Pimont, F., & Dupuy, J. L. (2018). How well do meteorological drought indices predict live fuel moisture content (LFMC)? An assessment for wildfire research and operations in Mediterranean ecosystems. Agricultural and Forest Meteorology, 262, 391–401. https://doi.org/10.1016/j.agrformet.2018.07.031

Running, S., & Zhao, M. (2019). MOD17A3HGF MODIS/Terra Net Primary Production Gap-Filled Yearly L4 Global 500 m SIN Grid V006. NASA EOSDIS Land Processes DAAC.

Scott, J. H., & Reinhardt, E. D. (2001). Assessing crown fire potential by linking models of surface and crown fire behavior. USDA Forest Service - Research Paper RMRS-RP, 29 RMRS-RP, 1–62. https://doi.org/10.2737/RMRS-RP-29

Sperry, J. S., Venturas, M. D., Anderegg, W. R. L., Mencuccini, M., Mackay, D. S., Wang, Y., & Love, D. M. (2017). Predicting stomatal responses to the environment from the optimization of photosynthetic gain and hydraulic cost. Plant Cell and Environment, 40(6), 816–830. https://doi.org/10.1111/pce.12852

Taylor, K. E., Stouffer, R. J., & Meehl, G. A. (2012). An overview of CMIP5 and the experiment design. Bulletin of the American Meteorological Society, 93(4), 485–498. https://doi.org/10.1175/BAMS-D-11-00094.1

Teckentrup, L., Harrison, S. P., Hantson, S., Heil, A., Melton, J. R., Forrest, M., Li, F., Yue, C., Arneth, A., Hickler, T., Sitch, S., & Lasslop, G. (2019). Response of simulated burned area to historical changes in environmental and anthropogenic factors: A comparison of seven fire models. Biogeosciences, 16(19), 3883–3910. https://doi.org/10.5194/bg-16-3883-2019

Thornton, P. E., & Running, S. W. (1999). An improved algorithm for estimating incident daily solar radiation from measurements of temperature , humidity , and precipitation. Agricultural and Forest Meteorology, 93(4), 211-228. https://doi.org/10.1016/S0168-1923(98)00126-9.

Van Wagner, C. E. (1977). Conditions for the start and spread of crown fire. Canadian Journal of Forest Research, 7(1), 23–34. https://doi.org/10.1139/x77-004

Van Wagner, C. E. (1987). Development and structure of the Canadian forest fire weather index system. Canadian Forest Service, Information Report 35.

Varela, V., Vlachogiannis, D., Sfetsos, A., Karozis, S., Politi, N., & Giroud, F. (2019). Projection of forest fire danger due to climate change in the French Mediterranean region. Sustainability, 11(16), 4284 . https://doi.org/10.3390/su11164284

Vilar, L., Herrera, S., Tafur-García, E., Yebra, M., Martínez-Vega, J., Echavarría, P., & Martín, M. P. (2021). Modelling wildfire occurrence at regional scale from land use/cover and climate change scenarios. Environmental Modelling and Software, 145, 105200. https://doi.org/10.1016/j.envsoft.2021.105200

Wullschleger, S. D., Gunderson, C. A., Hanson, P. J., Wilson, K. B., & Norby, R. J. (2002). Sensitivity of stomatal and canopy conductance to elevated CO2 concentration - Interacting variables and perspectives of scale. New Phytologist, 153(3), 485–496. https://doi.org/10.1046/j.0028-646X.2001.00333.x

CHAPTER VI:
CLIMATE CHANGE MITIGATION & WILDFIRES

CLIMATE CHANGE MITIGATION AND WILDFIRES

ABSTRACT

In this Chapter I estimate to which extent projected future wildfire activity would compromise the capacity of large-scale reforestation strategies to offset anthropogenic carbon emissions. First, I introduce why forest restoration is considered a strategy with potential to mitigate climate change and what its limitations are. Then, I describe how the net carbon sequestration resulting from a potential reforestation is simulated and how future wildfire activity is inferred through climate change projections. Results show that there is room to reforest 311.5 Mha for which simulations predict climate-benefits that would reach a cumulative carbon stock of 22.4 Gt C until 2100. However, the estimated carbon sequestration potential of this reforestation effort is less than 3 % of the accumulated anthropogenic CO_2 emissions. Furthermore, projected generalized wildfire activity increases threaten the 40 % of potential carbon stocks. This suggests that the climatic benefits of forest restoration have been largely exaggerated because of lack of consideration of indirect effects, as changes in surface albedo or fire danger.

VI.1. Introduction

Large scale reforestation has been proposed to mitigate global warming as photosynthetic carbon sequestration produces a cooling effect by lowering atmospheric CO_2 concentration (IPCC, 2021). Bastin *et al.* (2019) modeled the global tree restoration potential and claimed that reforestation and afforestation provide one of the most effective strategies for climate change mitigation, estimating that a global area of 1700 Mha could be restored sequestering 205 Gt C over the forest's lifetime. The claim by Bastin *et al.* prompted others to point out significant limitations of large-scale tree plantings that reduce potential mitigation effects (Friedlingstein *et al.*, 2019; Lewis *et al.*, 2019; Skidmore *et al.*, 2019; Veldman *et al.*, 2019). First, afforestation in naturally low tree cover ecosystems such as grasslands, savannahs, and tundra should not be considered, as it is likely to result in detrimental effects derived from water cycle alterations and biodiversity losses with no clear carbon sequestration gains (Friedlingstein *et al.*, 2019; Veldman *et al.*, 2019). Second, reforestation of areas that were once covered by forests may increase carbon uptake and reduce atmospheric CO_2 concentrations with a climate cooling effect, but this climate change mitigation potential could be reduced by biogeophysical effects derived from changes in surface albedo (Rohatyn *et al.*, 2022). Reforested land surfaces are less reflective than most other land cover types and thus absorb more solar energy, creating local warming effects that, in some cases, can offset the cooling effects of enhanced carbon sequestration (Betts, 2000; Li *et al.*, 2015). Lastly, climate-driven risks to reforested lands should also be quantified, as future drought or wildfire disturbances could cause reforested areas to potentially switch from carbon sinks to carbon sources (Anderegg *et al.*, 2020). However, the climatic impacts of decreasing surface albedo and increasing wildfire risk have not yet been quantified at a global scale.

Tree plantations are one of the most flammable vegetation types nowadays. Increasing tree cover in areas where trees are currently sparse inherently increases fuel loads and, consequently, the likelihood of high intensity fires. Additionally, global warming is projected to increase the frequency and intensity of droughts in many forest regions worldwide (IPCC, 2021). Droughts cause live and dead plant biomass (fuel) to dry out and increasing forest flammability (Nolan *et al.*, 2020). Consequently, climate change is expected to increase fire activity and the duration of fire seasons as the moisture content of wildfire fuels declines below critical thresholds more frequently and for longer periods (Jones *et al.*, 2022). Even forested ecosystems that are currently fire-free due to prevailing high fuel moisture contents may dry out periodically and start experiencing large wildfire events in the coming decades (Resco de Dios *et al.*, 2021). Large scale reforestation projects should, therefore, consider feedbacks between increasing fuel loads and decreasing fuel moisture dynamics in a warming world, in order to assess potential wildfire risks associated with carbon sinks in the near future.

The magnitude of climate change mitigation achievable through forest restoration remains uncertain, as related benefits depend on the balance between the climate effects of enhanced carbon sequestration and the climate effects of changes in surface albedo (Rohatyn *et al.*, 2023). Furthermore, since forest restoration is a long-term approach, projections of future fire risks should also be considered to avoid reforestation in areas that are expected to be prone to large wildfire events in the coming decades. In this chapter, I sought to re-assess the net climate change mitigation potential of forest restoration by (i) simulating global net carbon sequestration, including effects of changes in albedo, derived from potential reforestation actions, and (ii) quantifying wildfire incidence in these reforested areas, assessing the extent to which future wildfire danger could compromise net carbon sequestration and the climate change mitigation potential of reforested lands.

VI.2 Materials and Methods

VI.2.1 Potential reforestation areas identification

Target reforestation area selection englobed all potential tree restoration locations mapped as 1-km grid cells by Bastin *et al.* (2019) occurring within forest biomes and projected to have the potential to support a tree cover equal to or higher than 30 %. Target locations were limited to forest biomes (Dinerstein *et al.*, 2017) in order to avoid negative effects derived from reforestation actions in non-forested ecosystems (Friedlingstein *et al.*, 2019; Veldman *et al.*, 2019). Reforestation area selection was limited to grid cells projected to have the potential to support a tree cover equal to or higher than 30 % in order to ensure the selection of realistic targets regarding tree restoration programs that seek to increase carbon sequestration. All layers used in this study were re-sampled at a resolution of 0.01º (~1 km^2). All data analysis and preparation were performed using the *R* packages *terra* and *sf* (Pebesma, 2018; R Development Core Team, 2021). Layers, products, and datasets used in this study are described and referenced in Table S.VI.1.

VI.2.2 Carbon balance estimation

Following Rohatyn *et al.* (2021, 2022), the overall carbon balance that would result from reforestation of each selected potential forest restoration area was simulated taking into account cooling effects derived from carbon sequestration and climatic effects derived from changes in surface albedo. Thus, the net equivalent carbon stock change (NESC, t C ha^{-1}) derived from potential reforestation actions was estimated as the difference between net sequestration potential (ΔSP) and the emissions equivalent of shortwave forcing (EESF):

$$NESC = \Delta SP - EESF \quad \text{(VI.1)}$$

Net sequestration potential (ΔSP, t C ha^{-1}) refers to forest carbon stock changes that would result from reforestation actions. ΔSP was simulated over a forest lifetime period of 80 years (from 2020 to 2100) in order to assess potential contributions to offset anthropogenic CO_2 emissions accumulated over the same period. ΔSP was simulated in each target location grid cell as the difference between the cumulative annual net ecosystem productivity (NEP) of the potential post-reforestation ecosystem and the current pre-reforestation ecosystem as follows:

$$\Delta SP = \sum_{t=1}^{t=80} NEP_{t,post} - \sum_{t=1}^{t=80} NEP_{t,pre} \quad \text{(VI.2)}$$

Global multiyear average gridded NEP values were obtained from the Fluxcom database (Jung *et al.*, 2020). NEP values of potential post-reforestation ecosystems were predicted through an inverse distance weighted (IDW) interpolation of the existing nearest forest NEP values. Nearest forests were identified by selecting locations that, in 2020, showed a tree cover of at least 30 % in the MODIS product MOD44B (Dimiceli *et al.*, 2015). Then, it was applied the approach defined in Besnard *et al.* (2018), which considers forest age effects over cumulative NEP in post-reforestation ecosystems. Regarding the current pre-reforestation ecosystem, it was assumed that carbon gain was equal to that in the current vegetation NEP and that it remained constant throughout the 80 years simulated period. Finally, target locations where current pre-reforestation ecosystems sequester more carbon than potential post-reforestation ecosystems (ΔSP < 0) were excluded.

The emission equivalent of shortwave forcing (EESF) refers to the carbon emissions that would be needed to equal radiative forcing climatic effects derived from changes in surface albedo after reforestation actions. EESF (t C ha^{-1}) was simulated in each target location grid cell using the radiative forcing of the carbon equation (3):

$$EESF = C_0 \frac{RF_{\Delta\alpha_S}^{ToA}}{RE \cdot A_E} \cdot \frac{k}{\zeta} \quad \text{(VI.3)}$$

where C_0 is a reference atmospheric CO_2 concentration (410 ppm), *RE* represents the net change in Earth's radiative forcing due to changes in greenhouse gases concentration (5.35 W m^{-2}), A_E is the Earth surface area ($5.1 \cdot 10^{14}$ m^2), k is a factor to convert ppm to kg C ($2.13 \cdot 10^{12}$) and ζ is the airborne fraction of total anthropogenic CO_2 emissions (0.44). $RF_{\Delta\alpha_S}^{ToA}$ (W m^{-2}) refers to the annual average change in radiative forcing at the top of the atmosphere as a result of the change in surface albedo. Following Rohatyn *et al.* (2021, 2022), $RF_{\Delta\alpha_S}^{ToA}$ was calculated as in Bright *et al.* (2015):

$$RF_{\Delta\alpha_S}^{ToA} = \sum_{m=1}^{m=12} -\frac{R_{SW}^{\downarrow}(t,m,i)\,\Delta\alpha_S(t,m,i)T_{SW}^{\uparrow}}{12} \quad \text{(VI.4)}$$

where $R^{\downarrow}_{SW}$ is surface shortwave radiation in W m^{-2}, $\Delta\alpha_S$ represents changes in surface albedo after reforestation actions ($\Delta\alpha_S = \alpha_{S,post} - \alpha_{S,pre}$) and $T^{\uparrow}_{SW}$ is an upward atmospheric parameter (0.85). Thus $RF^{ToA}_{\Delta\alpha_S}$ was calculated from monthly (m) values and then summed over the year (t) to provide an annual mean value for each target location grid cell (i). $R^{\downarrow}_{SW}$ multiyear average monthly mean layers were obtained from EUMETSAT CLARA-A products (Karlsson *et al.*, 2017). Current pre-reforestation surface albedo values were obtained from MODIS albedo look-up maps (LUMs) multiyear average monthly mean layers (Gao *et al.*, 2014). Finally, potential post-reforestation surface albedo values were estimated using a moving window method applying a 100x100 km search window to the albedo values of the previously identified existing nearest forest.

VI.2.3 Wildfire risk estimation

Wildfire danger was estimated in each target location grid cell based on the annual frequency of days exceeding vapor pressure deficit (VPD) thresholds associated with a 50 % probability of fire incidence (fire-days). Each subcontinental forest biome type's VPD thresholds (Table S.VI.2) were obtained from Clarke *et al.* (2022), as they showed a probability of 73 % to correctly predict a wildfire event on a fire-day. Current (2001-2020) daily maximum VPD values were computed from daily maximum temperature and dew point temperature data obtained from the ERA5 dataset (Hersbach *et al.*, 2020). Future (2081-2100) daily maximum VPD values were computed from daily maximum air temperature and relative humidity data obtained from the CMIP5 dataset (Taylor *et al.*, 2012) selecting three global climate models (Table S.VI.3) under greenhouse gas emission scenarios RCP4.5 and RCP8.5. Global climate models were selected through an objectively designed ensemble following McSweeney *et al.* (2015) global evaluation of CMIP5 models. Therefore, the three global climate models were selected: i) considering data availability for RCP 4.5 and 8.5 scenarios and for the specific humidity, air temperature and surface pressure variables required to calculate VPD; ii) ensuring the ability to span projected future seasonal and regional changes in climate; and iii) avoiding models of the same model family to ensure projections independence and prevent projections biases duplications. These selected models capture a wide range in the variability of humidity and temperature across the different GCMs, as justified in Clarke *et al.* (2022). Current VPD data was used to bias correct future VPD data following a quantile mapping approach (Cannon *et al.*, 2015). Then, average annual frequency of days exceeding VPD thresholds was estimated in both periods to finally account for the annual fire-days frequency increases from 2020 (Fig. S.VI.1) to 2100 (Fig. S.VI.2 and S.VI.3) in potential forest restoration areas, projected by each global climate model under RCP4.5 and RCP8.5 greenhouse gas emission scenarios.

VI.2.4 Climate change mitigation

To assess the climate change mitigation potential of reforestation, it was quantified the proportion of the cumulative anthropogenic CO_2 emissions that could be offset by the associated carbon sequestration after accounting for biogeophysical and wildfire feedbacks. CO_2 emissions data from 2020 to 2100 under RCP4.5 (stabilization scenario) and RCP8.5 (rising scenario) were obtained from the RCP Database (Version 2.0).

VI.2.5 Data analysis

Results description regarding fire-days incidence and fire-days increasing factor distribution over reforestation areas and potential carbon stocks across forest biome types was focused on the global climate model CNRM-CM5 projections under the high emission scenario (RCP8.5). This is because CNRM-CM5 showed a more moderate level of fire-days frequency increases (Clarke *et al.*, 2022) and, consequently, our results represent a "best-case" scenario. RCP8.5 was chosen as it represents a "business as usual" scenario. Analyses were focused on future wildfire threats over potential carbon stocks by considering the mitigation potential of carbon sinks in where future fire-days frequency is going to increase less than 50 %. This is because increases greater than a 50 % would imply a significant increase of fire occurrence, with potential implications for global burned area (Resco de Dios *et al.*, 2022).

VI.3 Results

VI.3.1 Reforestation climatic effects

In total, 470.6 Mha previously identified by Bastin *et al.* (2019) as having reforestation potential were selected within current global forest biomes. Simulations estimations showed that reforestation of these areas results in a cumulative net carbon sequestration potential (ΔSP) of 28.3 Gt C from 2020 to 2100 (Fig. S.VI.1.A). But warming effects derived from changes in surface albedo were estimated to reduce potential climate change mitigation due to an emission equivalent of 10.4 Gt C resulting from shortwave forcing (EESF; Fig. S.VI.1.B). Thus, the net equivalent carbon stock change (NESC) derived from reforesting selected locations would result in a cooling effect equivalent to the sequestration of 17.9 Gt C (Table VI.1). Major concentrations of potential reforestation areas where simulations estimated a cooling effect (NESC > 0; blue colors) are located in North-East United States and North-East Asia along with significant concentrations in Madagascar, Scandinavia, and Iceland (Fig. VI.1). By excluding reforestation actions in areas where the simulations estimated net warming effects (NESC < 0), it was identified a "smart reforestation" scenario comprising 311.5 Mha that increases global carbon sequestration efficiency to 22.4 Gt C, nearly doubling climate change mitigation potential as measured by average NESC per hectare (Table VI.1).

Table VI.1: Reforestation climatic effects. The first column indicates the accumulated surface (Mha) of the selected forest restoration areas located within current forest biomes. Next columns indicate the summed carbon sequestration potential (ΔSP), the emissions equivalent of shortwave forcing (EESF), and the net equivalent carbon stock change (NESC = ΔSP – EESF, Gt C) simulated from the reforestation of target locations during a period of 80 years. The last column represents average NESC values in tons of carbon per hectare. Simulation results are presented for two cases: i) considering all reforestation opportunities (Total) and ii) only considering reforestation areas where simulations estimated a cooling effect (Smart, NESC > 0).

Reforestation	Surface (Mha)	ΔSP (Gt C)	EESF (Gt C)	NESC (Gt C)	Average NESC (t C ha^{-1})
Total	470.6	28.3	10.4	17.9	38.1
Smart	311.5	27.7	5.3	22.4	71.9

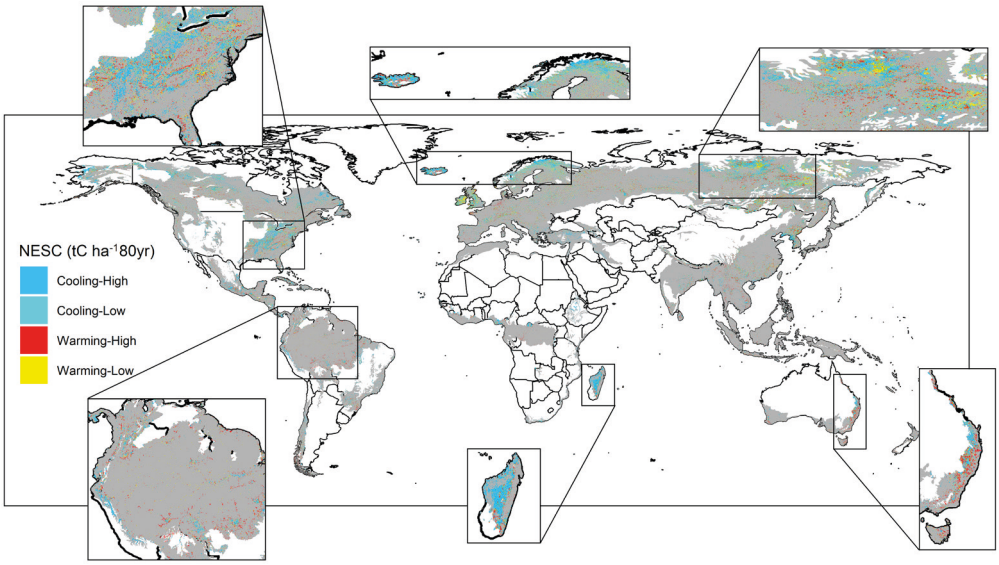

Figure VI.1: Reforestation climatic effects. Net equivalent carbon stock change (NESC) simulated from potential reforestation actions. NESC (t C ha^{-1}) was estimated as the difference between net sequestration potential (ΔSP) and the emissions equivalent of shortwave forcing (EESF) derived from changes in surface albedo over an 80-year period. Gray background represents the current extension of forest biomes (Dinerstein *et al.*, 2017). Blue colors represent potential reforestation areas where simulations estimated a cooling effect (low: 0 > NESC < 50; high: NESC > 50). Yellow and red colors represent potential reforestation areas where simulations estimated a warming effect (low: 0 < NESC > -50; high: NESC < -50).

VI.3.2 Wildfire danger projections

Modeling of current wildfire incidence over smart reforestation areas (NESC > 0) resulted in a global mean frequency of 60 fire-days per year (Fig. S.VI.1 and S.VI.5). All global climate models projected generalized fire-days frequency increases across target locations under both emission scenarios (Table VI.2). Projections showed that, by the end of the century, annual fire-days frequency incidence would increase more than a 50 % in one third of total smart reforestation areas (Fig. VI.2. A), which contain 40 % of global potential carbon stocks (8.9 Gt C, Fig. S.VI.4). However, wildfire projections showed large spatial differences across forest biome types. Maximum and minimum values in the annual number of fire-days were observed over smart reforestation areas within temperate forests and boreal forests, respectively (Fig. VI.2. B). Meanwhile, the largest increases in wildfire activity were projected in the smart reforestation areas located within tropical and mediterranean forests (Fig. VI.2.A, Fig.S.VI.6).

Table VI.2: Fire-Days. Mean annual fire-days frequency in 2100, mean fire-days increases from 2020 to 2100 (ΔFire-Days) and mean Fire-Days increasing factor (Fire-Days IF) projected in each global climate model (GCM) under both representative concentration pathway scenario (RCPs) 4.5 and 8.5.

GCM	RCP	2100 Fire-Days (d yr^{-1})	ΔFire-Days (d yr^{-1})	Fire-Days IF
CNRM-CM5	4.5	72	12	1.4
	8.5	82	22	1.7
ACCESS1-0	4.5	86	26	2.1
	8.5	110	50	2.9
GFDL-CM3	4.5	75	15	1.9
	8.5	92	32	2.5

VI.3.3 Climate change mitigation potential

Quantifications of the anthropogenic CO_2 emissions accumulated until 2100 that could be offset by the associated carbon sequestration derived from reforestation actions are detailed in Table VI.3. CO_2 emissions from 2020 to 2100 under RCP4.5 (stabilization scenario) and RCP8.5 (rising scenario) lead to a projected accumulation of 737 and 2008 Gt C by 2100, respectively. The carbon sequestration from 2020 to 2100 over all reforestation areas could compensate between 2.5 % of CO_2 emissions under RCP4.5, and less than 1 % under RCP8.5. When considering only potential carbon stocks derived from reforestation areas where simulations estimated a net cooling effect (NESC > 0; smart reforestation areas), the climate change mitigation potential increases slightly to 3 % under RCP4.5, and to 1.1 % under RCP8.5. But projections of future wildfire risks reduce the percentage of

accumulated CO_2 emissions potentially mitigable by a smart reforestation scenario to an interval between 2.3-1.5 % under RCP4.5 and to 0.6-0.3 % under RCP 8.5.

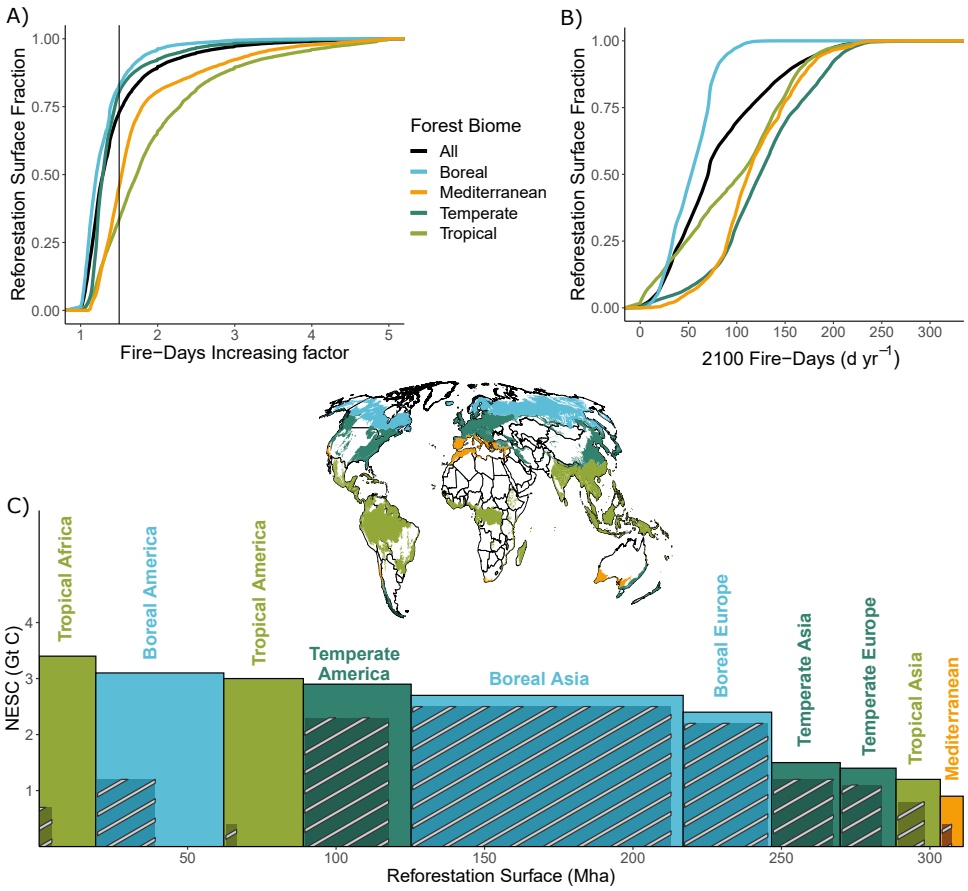

Figure VI.2: Fire-days projections. Projected fire-days incidence over smart reforestation areas across forest biome types. Distribution of global forest biome types (Dinerstein *et al.*, 2017): all forest biome types in black, boreal forests in blue, temperate forests in dark-green, tropical forests in light-green and mediterranean forests in orange. (A) Empirical distribution function of the 2020-2100 increasing factor in the annual frequency of fire-days over the surface fraction of smart reforestation areas (311.5 Mha). Vertical black line shows an increasing factor of 1.5, representing a 50 % increase in the annual frequency of fire-days. (B) Empirical distribution function of the fire-days incidence (d yr^{-1}) in 2100. (C) Distribution of the smart reforestation surface area (Mha), and net equivalent carbon stock change (NESC; Gt C), over each continent and forest biomes type. The shaded space within each column represents the summed surface area and carbon uptake of the target locations where projected fire-days frequency increases are less than 50 %.

Table VI.3: Climate change mitigation potential. Accumulated CO_2 emissions from 2020 to 2100 under RCP4.5 (stabilization scenario) and RCP8.5 (rising scenario) and the proportion (%) of accumulated emissions that could be potentially mitigated by reforesting target locations. Five reforestation scenarios are shown: i) considering all tree restoration opportunities (Total); ii) only considering reforestation areas where simulations predicted a cooling effect (Smart, NESC > 0); and only considering smart reforestation locations where fire-days incidence increase less than a 50 % under different global climate model projections: iii) CNRM-CM5, iv) ACCESS1-0 and v) GFDL-CM3 (surface and carbon stocks data in Table S.VI.4).

Emissions scenario	Accumulated CO_2 emissions 2020-2100 (Gt C)	Proportion (%) of accumulated CO_2 emissions potentially mitigable by reforestation				
		Total	Smart	CNRM-CM5	ACESS1-0	GFDL-CM3
RCP 4.5	737	2.5	3	2.3	1.5	1.9
RCP 8.5	2008	0.9	1.1	0.6	0.3	0.5

VI.4 Discussion

In this chapter, I have provided an accurate global spatial distribution and quantification of potential carbon sinks derived from reforestation actions where simulations predicted cooling effects through carbon sequestration. I identified 311.5 Mha where simulations predict climate-benefits that would reach a cumulative carbon stock of 22.4 Gt C until 2100. However, proportional potential contribution to offset anthropogenic CO_2 emissions during the same time does not exceed 3 % under any combination of reforestation and greenhouse gas emission scenarios. Furthermore, despite we can observe spatial differences across forests biome types, generalized increases in wildfire activity threaten 40 % of the potential global carbon stock, halving a limited potential to mitigate climate change by reforestation. The results revealed continental-scale differences in the spatial distribution of smart reforestation areas, the associated carbon uptake, and the projected increases in wildfire activity (Fig. VI.2.C). While there are many potential reasons to justify forest restoration, this study focused on current programs that seek to increase carbon sequestration. In this sense, African and American tropical forests showed the highest carbon sequestration efficiency, concentrating large potential carbon stocks in relatively few smart reforestation areas (Fig. VI.2.C), probably due to the elevated productivity rates observed in tropical ecosystems (Huston & Wolverton, 2009). But projected wildfire risks showed the highest fire-days frequency increases in the tropical forests (Fig. VI.2.A), indicating the need to consider that reforested areas within this biome can potentially switch from carbon sinks to carbon sources reversing climatic-benefits effects in the near future. The boreal and temperate forests of America also concentrate great potential carbon stocks. However, while wildfire risk increases are less pronounced in temperate reforestation areas, reforestation in the boreal region of North American may become largely threatened by wildfire activity by the end of the century. In contrast, boreal

Asian and European forests showed few reforestation areas recording fire danger increases. But the large restoration surface with relatively low associated potential carbon stocks within Asian boreal forests suggests a limited carbon sequestration efficiency in these reforestation areas. The temperate Asian and European forests as well as the tropical Asian forests contain relatively lower reforestation areas and associated carbon stocks amounts, but also recorded lower wildfire activity increases, suggesting that reforestation actions would result in long-term climate benefits effects within this continental forest biomes. Finally, global mediterranean forests showed the lowest concentration of smart reforestation areas along with high fire-days frequency increases (Fig. VI.2.A) indicating that future wildfire danger would largely compromise reforestation actions within this biome globally. Although projections of future fire incidence showed high fire-days increasing factor values in both, mediterranean and tropical forest biomes (Fig. S.VI.6), future wildfire risk increases in tropical forests is of particular concern (Clarke *et al.*, 2022). This is because tropical forests store vast amounts of biomass, and the current constrain over fire activity imposed by high fuel moisture values may ease under global warming (Boer *et al.*, 2021). Therefore, projected increases in the frequency of fire-days over tropical forests would raise the likelihood of large wildfire events that would threaten major potential carbon stocks compared to the other forest biomes. Overall, we can observe a limited proportional contribution to offset anthropogenic CO_2 emissions by reforestation. Result analyses showed that the amount of CO_2 offset by tree restoration (22.4 Gt C) would delay climate change impacts by two years, under current emission rates of 11 Gt C per year. This suggests that the climatic benefits of forest restoration have been largely exaggerated because of lack of consideration of indirect effects as changes in surface albedo or fire danger increases. After accounting for these detrimental effects, results indicate that reforestation is thus not an effective solution to curb CO_2 emissions, stressing the need to consider greenhouse gas emissions reduction at the forefront of global warming mitigation strategies.

VI.5 Conclusions

• The consideration of indirect effects derived from reforestation actions allowed to identify 311.5 Mha where simulations predict climate-benefits that would reach a cumulative carbon stock of 22.4 Gt C until 2100.

• Proportional potential contribution to offset anthropogenic CO_2 emissions until 2100 does not exceed 3 % under any combination of reforestation and greenhouse gas emission scenarios.

• Projected generalized increases in wildfire activity threaten 40 % of the potential global carbon stock, halving the limited potential to mitigate climate change by reforestation.

• Results indicate that reforestation is not an effective solution to curb CO_2 emissions.

VI.6. References

Anderegg, W. R. L., Trugman, A. T., Badgley, G., Anderson, C. M., Bartuska, A., Ciais, P., Cullenward, D., Field, C. B., Freeman, J., Goetz, S. J., Hicke, J. A., Huntzinger, D., Jackson, R. B., Nickerson, J., Pacala, S., & Randerson, J. T. (2020). Climate-driven risks to the climate mitigation potential of forests. Science 368(6497). https://doi.org/10.1126/science.aaz7005

Bastin, J. F., Finegold, Y., Garcia, C., Mollicone, D., Rezende, M., Routh, D., Zohner, C. M., & Crowther, T. W. (2019). The global tree restoration potential. Science, 364(6448), 76–79. https://doi.org/10.1126/science.aax0848

Besnard, S., Carvalhais, N., Arain, M. A., Black, A., De Bruin, S., Buchmann, N., Cescatti, A., Chen, J., Clevers, J. G. P. W., Desai, A. R., Gough, C. M., Havrankova, K., Herold, M., Hörtnagl, L., Jung, M., Knohl, A., Kruijt, B., Krupkova, L., Law, B. E., Reichstein, M. (2018). Quantifying the effect of forest age in annual net forest carbon balance. Environmental Research Letters, 13(12), 124018. https://doi.org/10.1088/1748-9326/aaeaeb

Betts, R. A. (2000). Offset of the potential carbon sink from boreal forestation by decreases in surface albedo. Nature, 408(6809), 187–190. https://doi.org/10.1038/35041545

Boer, M. M., Resco de Dios, V., Stefaniak, E. Z., & Bradstock, R. A. (2021). A hydroclimatic model for the distribution of fire on earth. Environmental Research Communications, 3(3). https://doi.org/10.1088/2515-7620/abec1f

Bright, R. M., Zhao, K., Jackson, R. B., & Cherubini, F. (2015). Quantifying surface albedo and other direct biogeophysical climate forcings of forestry activities. Global Change Biology, 21(9), 3246–3266. https://doi.org/10.1111/gcb.12951

Cannon, A. J., Sobie, S. R., & Murdock, T. Q. (2015). Bias correction of GCM precipitation by quantile mapping: How well do methods preserve changes in quantiles and extremes? Journal of Climate, 28(17), 6938–6959. https://doi.org/10.1175/JCLI-D-14-00754.1

Clarke, H., Nolan, R. H., Resco de Dios, V., Bradstock, R., Griebel, A., Khanal, S., & Boer, M. M. (2022). Forest fire threatens global carbon sinks and population centres under rising atmospheric water demand. Nature Communications, 13(1), 1–10. https://doi.org/10.1038/s41467-022-34966-3

Dimiceli, C., Carroll, M., Sohlberg, R., Kim, D. H., Kelly, M., & Townshend, J. R. G. (2015). MOD44B MODIS/Terra vegetation continuous fields yearly L3 global 250 m SIN grid V006. NASA EOSDIS Land Processes Distributed Active Archive Center.

Dinerstein, E., Olson, D., Joshi, A., Vynne, C., Burgess, N. D., Wikramanayake, E., Hahn, N., Palminteri, S., Hedao, P., Noss, R., Hansen, M., Locke, H., Ellis, E. C., Jones, B., Barber, C. V., Hayes, R., Kormos, C., Martin, V., Crist, E., Saleem, M. (2017). An Ecoregion-Based Approach to Protecting Half the Terrestrial Realm. BioScience, 67(6), 534–545. https://doi.org/10.1093/biosci/bix014

Friedlingstein, P., Allen, M., Canadell, J. G., Peters, G. P., & Seneviratne, S. I. (2019). Comment on "The global tree restoration potential." Science, 366(6463). https://doi.org/10.1126/science.aay8060

Gao, F., He, T., Wang, Z., Ghimire, B., Shuai, Y., Masek, J., Schaaf, C., & Williams, C. (2014). Multiscale climatological albedo look-up maps derived from moderate resolution imaging spectroradiometer BRDF/albedo products. Journal of Applied Remote Sensing, 8(1), 083532. https://doi.org/10.1117/1.jrs.8.083532

Hersbach, H., Bell, B., Berrisford, P., Hirahara, S., Horányi, A., Muñoz-Sabater, J., Nicolas, J., Peubey, C., Radu, R., Schepers, D., Simmons, A., Soci, C., Abdalla, S., Abellan, X., Balsamo, G., Bechtold, P., Biavati, G., Bidlot, J., Bonavita, M., Thépaut, J. N. (2020). The ERA5 global reanalysis. Quarterly Journal of the Royal Meteorological Society, 146(730), 1999–2049. https://doi.org/10.1002/qj.3803

Huston, M. A., & Wolverton, S. (2009). The global distribution of net primary production: Resolving the paradox. Ecological Monographs, 79(3). https://doi.org/10.1890/08-0588.1

IPCC. (2021). Climate Change 2021: The Physical Science Basis. Contribution of Working Group I to the Sixth Assessment Report of the Intergovernmental Panel on Climate Change. Cambridge University Press, United Kingdom.

Jones, M. W., Abatzoglou, J. T., Veraverbeke, S., Andela, N., Lasslop, G., Forkel, M., Smith, A. J. P., Burton, C., Betts, R. A., van der Werf, G. R., Sitch, S., Canadell, J. G., Santín, C., Kolden, C., Doerr, S. H., & Le Quéré, C. (2022). Global and Regional Trends and Drivers of Fire Under Climate Change. Reviews of Geophysics, 60(3), 1–76. https://doi.org/10.1029/2020rg000726

Jung, M., Schwalm, C., Migliavacca, M., Walther, S., Camps-Valls, G., Koirala, S., Anthoni, P., Besnard, S., Bodesheim, P., Carvalhais, N., Chevallier, F., Gans, F., S Goll, D., Haverd, V., Köhler, P., Ichii, K., K Jain, A., Liu, J., Lombardozzi, D., Reichstein, M. (2020). Scaling carbon fluxes from eddy covariance sites to globe: Synthesis and evaluation of the FLUXCOM approach. Biogeosciences, 17(5), 1343–1365. https://doi.org/10.5194/bg-17-1343-2020

Karlsson, K. G., Anttila, K., Trentmann, J., Stengel, M., Fokke Meirink, J., Devasthale, A., Hanschmann, T., Kothe, S., Jaäskelaïnen, E., Sedlar, J., Benas, N., Van Zadelhoff, G. J., Schlundt, C., Stein, Di., Finkensieper, S., Häkansson, N., & Hollmann, R. (2017). CLARA-A2: The second edition of the CM SAF cloud and radiation data record from 34 years of global AVHRR data. Atmospheric Chemistry and Physics, 17(9), 17, 5809–5828. https://doi.org/10.5194/acp-17-5809-2017

Lewis, S. L., Mitchard, E. T. A., Prentice, C., Maslin, M., & Poulter, B. (2019). Comment on "The global tree restoration potential." Science, 366(6469). https://doi.org/10.1126/science.aaz0111

Li, Y., Zhao, M., Motesharrei, S., Mu, Q., Kalnay, E., & Li, S. (2015). Local cooling and warming effects of forests based on satellite observations. Nature Communications, 6. https://doi.org/10.1038/ncomms7603

McSweeney, C. F., Jones, R. G., Lee, R. W., & Rowell, D. P. (2015). Selecting CMIP5 GCMs for downscaling over multiple regions. Climate Dynamics, 44(11–12), 3237–3260. https://doi.org/10.1007/s00382-014-2418-8

Nolan, R. H, Blackman, C. J., Resco de Dios, V., Choat, B., Medlyn, B. E., Li, X., Bradstock, R. A., & Boer, M. M. (2020). Linking Forest Flammability and Plant Vulnerability to Drought. Forests, 11(7), 779. https://doi.org/10.3390/f11070779

Pebesma, E. (2018). Simple features for R: Standardized support for spatial vector data. R Journal, 10(1), 439-446.. https://doi.org/10.32614/rj-2018-009

R Development Core Team. (2021). R: A language and environment for statistical computing. R Foundation for Statistical Computing. Austria. https://www.r-project.org/.

RCP Database Version 2.0.

Resco de Dios, V., Hedo, J., Cunill, À., Thapa, P., Martínez, E., Martínez, J., Aragón, D., Antonio, J., Balaguer-Romano, R., Díaz-sierra, R., Yebra, M., & Boer, M. M. (2021). Climate change induced declines in fuel moisture may turn currently fi re-free Pyrenean mountain forests into fi re-prone ecosystems. Science of the Total Environment, 797, 149104. https://doi.org/10.1016/j.scitotenv.2021.149104

Resco de Dios, V., Cunill Camprubí, À., Pérez-Zanón, N., Peña, J. C., Martínez del Castillo, E., Rodrigues, M., Yao, Y., Yebra, M., Vega-García, C., & Boer, M. M. (2022). Convergence in critical fuel moisture and fire weather thresholds associated with fire activity in the pyroregions of Mediterranean Europe. Science of the Total Environment, 806(4), 151462. https://doi.org/10.1016/j.scitotenv.2021.151462

Rohatyn, S., Rotenberg, E., Tatarinov, F., Carmel, Y., & Yakir, D. (2023). Large variations in afforestation-related climate cooling and warming effects across short distances. Communications Earth and Environment, 4(1), 1–10. https://doi.org/10.1038/s43247-023-00678-9

Rohatyn, S., Rotenberg, E., Yakir, D., & Carmel, Y. (2021). Assessing climatic benefits from forestation potential in semi-arid lands. Environmental Research Letters, 16(10), 104039. https://doi.org/10.1088/1748-9326/ac29e9

Rohatyn, S., Yakir, D., Rotenberg, E., & Carmel, Y. (2022). Limited climate change mitigation potential through forestation of the vast dryland regions. Science, 377(6613), 1436–1439. https://doi.org/10.1126/science.abm9684

Skidmore, A. K., Wang, T., de Bie, K., & Pilesjö, P. (2019). Comment on "The global tree restoration potential." Science, 366(6469). https://doi.org/10.1126/science.aaz0111

Taylor, K. E., Stouffer, R. J., & Meehl, G. A. (2012). An overview of CMIP5 and the experiment design. Bulletin of the American Meteorological Society, 93(4), 485–498. https://doi.org/10.1175/BAMS-D-11-00094.1

Veldman, J. W., Aleman, J. C., Alvarado, S. T., Anderson, T. M., Sally, A., Bond, W. J., Boutton, T., Buchmann, N., Buisson, E., Canadell, J. G., Michele de Sá, D., Diaz-Toribio, M. H., Durigan, G., Ewel, J. J., Fernandes, G. W., Fidelis, A., Fleischman, F., Good, S. P., Griffith, D. M., Zaloumis, N. P. (2019). Comment on "The global tree restoration potential." Science, 366(6469). https://doi.org/10.1126/science.aaz0111

CHAPTER VII:
GENERAL DISCUSSION

GENERAL DISCUSSION

VII.1 Discussion

In this PhD Thesis, I have: i) simulated the interactions between seasonal LFMC variations and wildfire activity; ii) developed a semi-mechanistic model to infer species-specific LFMC dynamics; iii) projected future fuel moisture content and wildfire danger under climate change conditions; and iv) assessed future wildfire danger effects on large-scale reforestation potential to mitigate climate change. In Chapter III, simulation studies showed that LFMC variations driven by *Pinus halepensis* needle senescence enhanced the development of more intense and severe crown fires. Thus, I assessed the role of LFMC variation as a contributing factor that promotes extreme fire behavior under different environmental conditions. In Chapter IV, in order to overcome the limitations of current LFMC estimates, I developed, calibrated, and validated a semi-mechanistic model that provides species-specific estimations. By considering crucial physiological traits across the soil-plant-atmosphere continuum, the developed model provided estimations that showed better agreement with observed data than estimations from widely used approaches. In Chapter V, I applied the developed model under different global climate projections to quantify the effects of global warming on fuel dry-down and its impacts on future fire danger in Spain's forests. The results showed a widespread fire season lengthening, indicating that projected fuel dry-down processes would enable large wildfire events at landscape scales in the coming decades. In Chapter VI, I simulated global net carbon sequestration derived from potential reforestation actions quantifying future wildfire incidence in these reforested areas. The results suggest that the climatic benefits of large-scale forest restoration strategies have been largely exaggerated because of a lack of consideration of indirect effects as changes in surface albedo or fire danger increases.

Fuel moisture effects on wildfire activity has been extensively analyzed since the onset of fire modeling, proving its role as a major driver of critical fire behavior aspects such as fire rate of spread, flame dimensions and fuel consumption (McArthur, 1966; Anderson, 1970; Rothermel, 1983). However, traditional fire behavior models only consider the effect of DFMC or do not distinguish between live and dead fuels, as the specific LFMC influence over fire behavior has been more controversial (Pimont *et al.*, 2019). Alexander & Cruz (2013) state that, despite laboratory experiments showing significant relationships, there is limited field evidence linking fire rate of spread and LFMC, indicating that the effect of LFMC might be inconsequential under high-intensity fire conditions. However, Rossa & Fernandez (2018) suggest that the lack of field evidence supporting the effect of LFMC on fire rate of spread was due to statistical analysis difficulties. Furthermore, Pimont *et al.* (2019) reanalyzed the mismatch between laboratory and field experiments, concluding that the effect of LFMC on fire rate of spread

in field studies was stronger than previously reported. Nevertheless, despite these discussions on how LFMC affects fire propagation, its interaction with wildfire activity has been largely recognized, associating LFMC declining trends with increases in burned area (Nolan *et al.*, 2016, Resco de Dios *et al.*, 2022) and with the occurrence of large wildfire events (Martin-StPaul *et al.*, 2018). The simulation study conducted in this PhD Thesis indicates that the physiological changes associated with needle senescence increase the probability of more intense and severe crown fire development (Figs. III.2-III.4). Therefore, the results support the consideration of LFMC as a contributing factor that, along with other environmental conditions, significantly affects wildfire danger and thus, disregarding LFMC in fire modeling attempts would lead to underpredictions of fire behavior. In this sense, estimating and forecasting temporal and spatial LFMC variations is crucial to anticipate future wildfire risks and to achieve fuel and fire management strategies.

The lack of consideration of LFMC in traditional fire behavior models can also be attributed to the difficulties in obtaining accurate spatial and temporal estimations (Jolly & Jhonson, 2018). While the use of meteorological drought indices fails to estimate spatial LFMC variations, as these approaches cannot consider species-specific dynamics, remote sensing approaches fail to estimate temporal LFMC variations, as these proxies cannot forecast future conditions. The semi-mechanistic model developed in this PhD Thesis allowed to overcome the limitations of these commonly used approaches by providing more accurate LFMC variation estimations (Fig. IV.2, IV.3). The use of the water balance model MEDFATE (De Caceres *et al.*, 2015, 2021) allowed to incorporate species-specific plant physiological traits, along to site-specific vegetation, meteorological and edaphic data, providing a precise estimation of temporal and spatial predawn leaf water potential (Ψ_{pd}) variations. It is important to highlight that by estimating LFMC as a function of Ψ_{pd}, I incorporated drought-related plant traits into a fuel moisture modeling approach, bridging the gap between drought and fire research literature (Nolan *et al.*, 2020). The inclusion of physiological traits in fuel moisture modeling usually entails the development of complex mechanistic models that are seldom applied within operational contexts due to the difficulties of obtaining all input variable data or to computation times needed (Resco de Dios, 2020). However, the new approach has been developed using a relatively simple parametrization, and much of the complexities of state variables and parameters can be hidden from the user in practical operational tools within fire prevention scenarios. The results support that the inclusion of crucial plant physiological traits in LFMC modeling approaches increases the biological realism of the estimations, enhancing temporal and spatial predictive capabilities.

A main advantage of using semi-mechanistic approaches to infer the dynamics of LFMC is the capacity to estimate future values, which depends on the physiological adjustments that live plants can face against climate change conditions. The future values projected in this PhD Thesis showed widespread fuel moisture decreases

that would lengthen fire seasons and enhance wildfire activity throughout the 21st century. However, the use of semi-mechanistic approaches allowed to observe proportionally steeper moisture content declining trends in dead fuels than in live fuels (Fig. V.2-V4). These observed differences would not arise if future moisture content dynamics of both fuel types were projected by applying commonly used meteorological drought indices. Therefore, the results support the use of semi-mechanistic approaches to forecast fuel moisture dynamics, as it improves predictive capabilities and allows a better anticipation of future wildfire risks derived from climate change. The projected misalignment between live and dead fuels moisture declines highlights the potential role of LFMC as a switch for large wildfire events in the near future, as it would enable ecosystems flammability through available fuels connectivity from local to landscape scales. The projected fire danger increases in high-productive ecosystems (Fig. V.5) would entail huge carbon emissions into the atmosphere, potentially resulting in positive feedbacks with global warming.

In this sense, large-scale reforestation has been proposed to mitigate climate change through carbon sequestration (Bastin *et al.*, 2019). However, the proportional contribution to offset anthropogenic CO_2 emissions through tree planting strategies remains uncertain as adverse effects are less considered. The carbon offset quantifications assessed in this PhD Thesis suggest that the climatic benefits of large-scale forest restoration strategies have been largely exaggerated because of a lack of consideration of indirect effects as changes in surface albedo or fire danger increases (Tables VI.1-VI.3). By considering biogeophysical effects derived from changes in surface albedo, I was able to assess adverse climate-warming effects that reduce climate-cooling benefits derived from carbon sequestration in reforestation (Table VI.1). I also limited potential reforestation areas to forest ecosystems in order to avoid detrimental effects associated with the afforestation of naturally low tree cover ecosystems. Thus, the consideration of large-scale tree planting limitations previously highlighted by several authors (Friedlingstein *et al.*, 2019; Lewis *et al.*, 2019; Skidmore *et al.*, 2019; Veldman *et al.*, 2019), allowed to estimate reforestation net climate-benefits in a more accurate way that largely reduces the potential global carbon stock amount and the associated anthropogenic CO_2 emissions mitigation (Table VI.3). Projected generalized wildfire activity increases over this potential carbon stocks reduced even more the limited potential to mitigate climate change by reforestation (Table VI.3). Therefore, the results support that it is crucial to consider future changes in fuel moisture and fire danger to correctly evaluate large-scale reforestation programs that seek to increase carbon sequestration in order to avoid adverse effects, such as the switch of reforested areas from carbon sinks to carbon sources in the near future (Anderegg *et al.*, 2020).

Overall, this PhD Thesis research, together with fire research literature, indicate that we may be on the brink of a dramatically increase in the incidence of large wildfire events. In the last decades, rural land abandonment (Gelabert *et al.*, 2022)

together with fire suppression strategies (Stephens *et al.*, 2018) have promoted the increase of forest lands, that accumulate huge fuel loads with large vertical and horizontal spatial connectivity (Resco de Dios *et al.*, 2021). As drought events become more frequent and intense due to climate change conditions (IPCC, 2021), competition for water resources would increase in these densely forested areas, resulting in widespread fuel moisture content declines. Therefore, even forested ecosystems that are currently fire-free due to prevailing high fuel moisture contents may dry out periodically and start experiencing large wildfire events at landscape scales in the coming decades (Resco de Dios *et al.*, 2021). The development of large wildfire events implies widespread consequences, beyond ecosystem effects. Projected increases in fire activity near major population centers would have substantial impacts on human health, as these populations would experience increased exposure to wildfire smoke (Clarke *et al.*, 2022). Furthermore, large wildfire events in high-productivity ecosystems entail the emission of huge carbon stocks into the atmosphere with unknown effects on the global carbon cycle (Anderegg *et al.*, 2020).

Future research efforts should focus on the inclusion of plant phenology effects over physiological and anatomical traits, such as specific leaf area (SLA), to continue improving the biological realism of process-based models (Griebel al., 2023). The combination of biophysical and satellite-based models, along with short time-scale forecasts of environmental variables, shows great potential to obtain near-real-time LFMC estimations, paving the way for the development of an early fire warning system. Moreover, these near-real-time LFMC estimations could be coupled to fine-scale fire behavior models to enable mechanistic evaluations of the interactions between physiological and heat transfer processes (Dickman *et al.*, 2023). Wildfire danger projections should continue to provide future wildfire risk assessments to anticipate ecosystem effects, threats to human populations and carbon sink losses. Large-scale reforestation programs that seek to increase carbon sequestration to mitigate climate change should consider future changes in fuel moisture and fire danger that may compromise the stated objectives. Finally, the extent to which fuel management can mitigate the growing impacts of large wildfire events driven by increases in water scarcity should be analyzed.

VII.2 References

Alexander, M. E., & Cruz, M. G. (2013). Assessing the effect of foliar moisture on the spread rate of crown fires. International Journal of Wildland Fire, 22(6), 415–427. https://doi.org/10.1071/WF12008-CO

Anderegg, W. R. L., Trugman, A. T., Badgley, G., Anderson, C. M., Bartuska, A., Ciais, P., Cullenward, D., Field, C. B., Freeman, J., Goetz, S. J., Hicke, J. A., Huntzinger, D., Jackson, R. B., Nickerson, J., Pacala, S., & Randerson, J. T. (2020). Climate-driven risks to the climate mitigation potential of forests. Science 368(6497). https://doi.org/10.1126/science.aaz7005

Bastin, J. F., Finegold, Y., Garcia, C., Mollicone, D., Rezende, M., Routh, D., Zohner, C. M., & Crowther, T. W. (2019). The global tree restoration potential. Science, 364(6448), 76–79. https://doi.org/10.1126/science.aax0848

Anderson, H. E. (1970). Forest fuel ignitibility. Fire Technology, 6(4), 312–319. https://doi.org/10.1007/BF02588932

Clarke, H., Nolan, R. H., Resco de Dios, V., Bradstock, R., Griebel, A., Khanal, S., & Boer, M. M. (2022). Forest fire threatens global carbon sinks and population centres under rising atmospheric water demand. Nature Communications, 13(1), 1–10. https://doi.org/10.1038/s41467-022-34966-3

De Cáceres, M., Martínez-Vilalta, J., Coll, L., Llorens, P., Casals, P., Poyatos, R., Pausas, J. G., & Brotons, L. (2015). Coupling a water balance model with forest inventory data to predict drought stress: The role of forest structural changes vs. climate changes. Agricultural and Forest Meteorology, 213, 77–90. https://doi.org/10.1016/j.agrformet.2015.06.012

De Cáceres, M., Mencuccini, M., Martin-StPaul, N., Limousin, J. M., Coll, L., Poyatos, R., Cabon, A., Granda, V., Forner, A., Valladares, F., & Martínez-Vilalta, J. (2021). Unravelling the effect of species mixing on water use and drought stress in Mediterranean forests: A modelling approach. Agricultural and Forest Meteorology, 296, 108233. https://doi.org/10.1016/j.agrformet.2020.108233

Dickman, L. T., Jonko, A. K., Linn, R. R., Altintas, I., Atchley, A. L., Bär, A., Collins, A. D., Dupuy, J., Gallagher, M. R., Hiers, J. K., Hoffman, C. M., Hood, S. M., Hurteau, M. D., Jolly, W. M., Josephson, A., Loudermilk, E. L., Ma, W., Michaletz, S. T., Nolan, R. H., Younes, N. (2023). Integrating plant physiology into simulation of fire behavior and effects. New Phytologist, 238(3), 952-970. https://doi.org/10.1111/nph.18770

Friedlingstein, P., Allen, M., Canadell, J. G., Peters, G. P., & Seneviratne, S. I. (2019). Comment on "The global tree restoration potential." Science, 366(6463), 76–79. https://doi.org/10.1126/science.aay8060

Gelabert, P. J., Rodrigues, M., Vidal-Macua, J. J., Ameztegui, A., & Vega-Garcia, C. (2022). Spatially explicit modeling of the probability of land abandonment in the Spanish Pyrenees. Landscape and Urban Planning, 226, 104487. https://doi.org/10.1016/j.landurbplan.2022.104487

Griebel, A., Boer, M. M., Blackman, C., Choat, B., Ellsworth, D. S., Madden, P., Medlyn, B., Resco de Dios, V., Wujeska-Klause, A., Yebra, M., Younes Cardenas, N., & Nolan, R. H. (2023). Specific leaf area and vapour pressure deficit control live fuel moisture content. Functional Ecology, 37(3), 719–731. https://doi.org/10.1111/1365-2435.14271

IPCC. (2021). Climate Change 2021: The Physical Science Basis. Contribution of Working Group I to the Sixth Assessment Report of the Intergovernmental Panel on Climate Change. Cambridge University Press, United Kingdom.

Jolly, W. M., & Johnson, D. M. (2018). Pyro-ecophysiology: Shifting the paradigm of live wildland fuel research. Fire, 1(1), 1–5. https://doi.org/10.3390/fire1010008

Lewis, S. L., Mitchard, E. T. A., Prentice, C., Maslin, M., & Poulter, B. (2019). Comment on "The global tree restoration potential." Science, 366(6469), 5–8. https://doi.org/10.1126/science.aaz0111

Martin-StPaul N, Ruffault J, Pimont F, Dupuy J-L., & et. al. (2018). Live fuel moisture content: variability, predictability and impact on fire behavior and activity. Advances in forest fire research 2018 (pp. 246–253). Imprensa da Universidade de Coimbra. Portugal.

McArthur, A. G. (1966). Weather and grassland fire behaviour. Australian Forestry and Timber Bureau., Leaflet 10, 23pp.

Nolan, R. H., Boer, M. M., Resco De Dios, V., Caccamo, G., & Bradstock, R. A. (2016). Large-scale, dynamic transformations in fuel moisture drive wildfire activity across southeastern Australia. Geophysical Research Letters, 43(9), 4229–4238. https://doi.org/10.1002/2016GL068614

Nolan, R. H, Blackman, C. J., Resco de Dios, V., Choat, B., Medlyn, B. E., Li, X., Bradstock, R. A., & Boer, M. M. (2020). Linking Forest Flammability and Plant Vulnerability to Drought. Forests, 11(7), 779. https://doi.org/10.3390/f11070779

Pimont, F., Ruffault, J., Martin-StPaul, N. K., & Dupuy, J. L. (2019). Why is the effect of live fuel moisture content on fire rate of spread underestimated in field experiments in shrublands? International Journal of Wildland Fire, 28(2), 127–137. https://doi.org/10.1071/WF18091

Resco de Dios, V. (2020). Plant-Fire Interactions. Applying Ecophysiology to Wildfire Management. Vol 36. Springer, Switzerland.

Resco de Dios, V., Hedo, J., Cunill, À., Thapa, P., Martínez, E., Martínez, J., Aragón, D., Antonio, J., Balaguer-Romano, R., Díaz-sierra, R., Yebra, M., & Boer, M. M. (2021). Climate change induced declines in fuel moisture may turn currently fi re-free Pyrenean mountain forests into fi re-prone ecosystems. Science of the Total Environment, 797, 149104. https://doi.org/10.1016/j.scitotenv.2021.149104

Resco de Dios, V., Cunill Camprubí, À., Pérez-Zanón, N., Peña, J. C., Martínez del Castillo, E., Rodrigues, M., Yao, Y., Yebra, M., Vega-García, C., & Boer, M. M. (2022). Convergence in critical fuel moisture and fire weather thresholds associated with fire activity in the pyroregions of Mediterranean Europe. Science of the Total Environment, 806(4), 151462. https://doi.org/10.1016/j.scitotenv.2021.151462

Rossa, C. G., & Fernandes, P. M. (2018). On the effect of live fuel moisture content on fire rate of spread. Forest Systems, 26(3), eSC08.. https://doi.org/10.5424/fs/2017263-12019

Rothermel, R. C. (1983). How to predict the spread and intensity of forest and range fires. US Department of Agriculture, Forest Service, General Technical Report, INT-143. https://doi.org/10.2737/INT-GTR-143

Skidmore, A. K., Wang, T., de Bie, K., & Pilesjö, P. (2019). Comment on "The global tree restoration potential." Science, 366(6469). https://doi.org/10.1126/science.aaz0111

Stephens, S. L., Collins, B. M., Fettig, C. J., Finney, M. A., Hoffman, C. M., Knapp, E. E.,

North, M. P., Safford, H., & Wayman, R. B. (2018). Drought, Tree Mortality, and Wildfire in Forests Adapted to Frequent Fire. BioScience, 68(2), 77–88. https://doi.org/10.1093/biosci/bix146

Veldman, J. W., Aleman, J. C., Alvarado, S. T., Anderson, T. M., Archibald, S., William J. Bond, Thomas W. Boutton1, Nina Buchmann, E. B., , Josep G. Canadell, M. de S. D., , Milton H. Diaz-Toribio, G. D., John J. Ewel, G. Wilson Fernandes, A. F., Fleischman, F., Good, S. P., Daniel M. Griffith, J.-M. H., , William A. Hoffmann, S. L. S., Caroline E. R. Lehmann, Gregory Mahy, Ashish N. Nerlekar, J. B. N., Noss, R. F., Colin P. Osborne, Gerhard E. Overbeck, Catherine L. Parr, Pausas, J. G., R. Toby Pennington, Michael P. Perring, Francis E. Putz, J. R., Mahesh Sankaran, J. Morgan Varner, N. P. Z. (2019). Comment on "The global tree restoration potential." Science, 366(6469), 1–5. https://doi.org/10.1126/science.aaz0111

CHAPTER VIII:
CONCLUSIONS

CONCLUSIONS

• LFMC is a contributing factor that, along with other environmental conditions, significantly affects fire behavior. Thus, disregarding LFMC in fire modeling attempts would lead to underpredictions of wildfire danger.

• Including crucial plant physiological traits in LFMC modeling strategies increases the biological realism of its estimations, enhancing the prediction of temporal and spatial variations.

• Estimated fuel moisture declines are projected to length fire seasons, enhancing wildfire danger throughout the 21st century. The use of semi-mechanistic approaches to forecast LFMC dynamics allows the consideration of plant species capabilities to buffer climate change impacts, providing more accurate future wildfire risk assessments.

• The climatic benefits of forest restoration have been largely exaggerated because of a lack of consideration of indirect effects as changes in surface albedo or fire danger increases. Thus, reforestation is not an effective solution to curb CO_2 emissions.

SUPPLEMENTARY MATERIALS

Supplementary materials IV
Supplementary materials V
Supplementary materials VI

SUPPLEMENTARY MATERIALS IV

Table S.IV.1. Location and climate of sampling sites: Latitude and Longitude (º), Altitude (m), Mean Annual Temperature (ºC), Mean Annual Precipitation (mm), Number of observations (n) and Sampling period.

Site	LAT (º)	LON (º)	ALT (m)	MAT (ºC)	MAP (mm)	n	Period
AlbAlb5	38.30524105	-2.150574725	1025	12.6	359	7	2006
AlbAlb6	38.20498837	-2.308259286	1160	13.3	344	6	2006
AnCad7	36.75485307	-5.435622944	870	16.8	873	20	2001
AndCad8	36.76005833	-5.384229902	1050	16.6	1099	20	2001-2002
AraCin10	42.29367395	-0.907665838	720	12.9	788	28	2001-2002
AraCin11	42.28440656	-0.895820428	700	13.1	566	54	2001-2002
AraCin12	42.27758322	-1.017229674	620	13	824	48	2001-2002
AraCin9	42.40210458	-0.928257159	920	13.3	726	28	2001-2002
Aralbe13	41.25410987	-1.215673378	860	13.6	460	81	2001-2002
Aralbe14	41.19952912	-1.181320918	845	13.8	421	60	2001-2002
Aralbe15	41.25539174	-1.299152734	1050	13.6	567	40	2001-2002
Aralbe16	41.31144454	-1.44104871	1060	13.1	482	20	2001-2002
AraPre17	42.24581101	-0.339556662	810	11.1	1045	36	2001-2002
AraPre18	42.35121142	-0.225813742	1260	10.9	971	20	2001-2002
AraPre19	42.46231921	-0.354653363	900	11.2	955	42	2001-2002
AraPre20	42.42986001	-0.514043092	840	10.5	1003	22	2001-2002
CacMaj99	39.940332	-5.7746	265	16.2	751	49	2009-2016
CamPat29	40.87587603	-3.49668028	940	12.8	561	48	2001-2002
CamVil32	40.29218175	-4.317216074	610	15	486	48	2001-2002
CasAvi37	40.55690121	-4.665993166	1355	11	587	10	2001
CorCor40	38.09512436	-4.278865396	322	17.8	243	6	2006
GuaAlt44	40.89595683	-2.248819638	1210	12.7	584	9	2006
GuaAlt47	40.87070923	-2.223341931	995	11.8	477	6	2006
GuaGua54	41.04477795	-3.208403414	1105	12.8	397	4	2006
HuePar56	37.00830798	-6.468929879	15	18.9	733	3	2006
JaeJae59	37.73283292	-3.498868004	1660	14.3	336	6	2006
JaeJae60	37.75135031	-3.502057181	1320	15	560	6	2006
LugCas62	43.1995203	-7.476268092	400	11.7	1113	6	2006
LugCau63	42.60799748	-7.18125571	775	12.2	1345	6	2006
LugCau66	42.6483873	-7.223811437	1200	10.9	820	6	2006
LugMou68	43.39828193	-7.559647945	900	11.2	1180	6	2006
MurMor72	38.25827059	-1.782337964	400	17.3	384	6	2006
Poblet	41.343935	1.058036	720	15.3	545	42	2017
SevSev82	37.96375049	-5.60949183	660	16.8	247	7	2006
TolCab96	39.34049298	-4.44628958	670	15.6	479	743	1996-2006
TolCab97	39.34680141	-4.479155713	710	15.3	531	775	1996-2007
TolCab98	39.3393891	-4.500035995	705	14.9	549	165	1997-2007
ValAyo89	39.05332782	-0.953629752	765	15.6	485	6	2006
ValTer90	39.12094481	-0.966352054	1030	14.3	343	8	2006
ValTer91	39.11702302	-0.946687206	980	14.9	480	8	2006

Methods S.IV.1. Species list

Acer monspessulanum (L.), Arbutus unedo (L.), Buxus sempervirens (L.), Calluna vulgaris (L.), Cistus albidus (L.), Cistus clusii (Dunal.), Cistus ladanifer (L.), Cistus salviifolius (L.), Crataegus monogyna (Jacq.), Erica arborea (L.), Erica australis (L.), Erica ciliaris (Loefl.), Erica mackaiana (Bab.), Erinacea anthyllis (Link.), Genista scorpius (L.), Genista tridentata (L.), Juniperus communis (L.), Juniperus oxycedrus (L.), Juniperus phoenicea (L.), Juniperus thurifera (L.), Lavandula angustifolia (Mill), Lavandula latifolia (Medik), Lavandula stoechas (Lam.), Olea europea (L.), Phillyrea angustifolia (L.), Pinus halepensis (Mill.), Pinus nigra (Arnold.) , Pinus pinaster (Ait.), Pinus sylvestris (L.), Pistacia lentiscus (L.), Quercus coccifera (L.), Quercus faginea (Lam.), Quercus ilex (L.), Salvia rosmarinus (L.), Thymus mastichina (L.), Thymus vulgaris (L.), Ulex gallii (Planch.), Ulex parviflorus (Pourr.).

Table S.IV.2. MEDFATE data inputs and sources

INPUT	Variable	Source	Reference
Soil	• Clay (%) • Sand (%) • Organic matter (%) • Bulk density (g/cm^3) • Rock fragment content (%)	SoilGrids250 2.0	Hengl *et al.* , 2017
Vegetation	• Species identity (Code) • Shrub cover (%) • Tree density (N) • Height (cm) • DBH (cm)	Third National Forest Inventory of Spain	Alberdi *et al.* , 2016
Meteorology	• Temperature (ºC) • Precipitation (mm) • Wind speed (Km/h at 10m)	ERA5-Land	Hersbach *et al* ., 2020
Meteorology	• Relative humidity (%) • Incoming solar radiation (MJ/m^2) • Potential evapotranspiration (mm)	Meteoland	De Cáceres *et al.* , 2018

Alberdi, I., Sandoval, V., Condes, S., Cañellas, I., & Vallejo, R. (2016). The Spanish National Forest Inventory, a tool for the knowledge, management and conservation of forest ecosystems. Ecosistemas, 25(3), 88–97.

De Cáceres, M., Martin-StPaul, N., Turco, M., Cabon, A., & Granda, V. (2018). Estimating daily meteorological data and downscaling climate models over landscapes. Environmental Modelling and Software, 108, 186–196.

Hengl, T., Jesus, J. M. De, Heuvelink, G. B. M., Ruiperez, M., Kilibarda, M., Blagoti, A., Shangguan, W., Wright, M. N., Geng, X., Bauer-marschallinger, B., Guevara, M. A., Vargas, R., Macmillan, R. A., Batjes, N. H., Leenaars, J. G. B., Ribeiro, E., Wheeler, I., Mantel, S., & Kempen, B. (2017). SoilGrids250m : Global gridded soil information based on machine learning. PLoS ONE 12(2): e0169748.

Hersbach, H., Bell, B., Berrisford, P., Hirahara, S., Horányi, A., Muñoz-Sabater, J., Nicolas, J., Peubey, C., Radu, R., Schepers, D., Simmons, A., Soci, C., Abdalla, S., Abellan, X., Balsamo, G., Bechtold, P., Biavati, G., Bidlot, J., Bonavita, M. Thépaut, J. N. (2020). The ERA5 global reanalysis. Quarterly Journal of the Royal Meteorological Society, 146(730), 1999–2049.

Table S.IV.3. Spectral indices obtained from MODIS MCD43A4 data. *Px* is the reflectance in band x; NIR, near-infrared; SWIR, short wave infrared. Adapted from Merino *et al.* 2020.

Index	Equation	Bands	Reference
Normalized Difference Vegetation Index	$NDVI = \frac{\rho_{NIR} - \rho_{red}}{\rho_{NIR} + \rho_{red}}$	$\rho_{NIR} = \rho_2$ $\rho_{red} = \rho_1$	Rouse *et al.*, 1974
Global Vegetation Moisture Index	$GVMI = \frac{(\rho_{NIR} + 0.1) - (\rho_{SWIR} + 0.02)}{(\rho_{NIR} + 0.1) + (\rho_{SWIR} + 0.02)}$	$\rho_{NIR} = \rho_2$ $\rho_{SWIR} = \rho_6$	Ceccato *et al.*, 2002
Normalized Difference Infrared Index	$NDII = \frac{\rho_{NIR} - \rho_{SWIR}}{\rho_{NIR} + \rho_{SWIR}}$	$\rho_{NIR} = \rho_2$ $\rho_{SWIR} = \rho_6 (NDII6)$ $\rho_{SWIR} = \rho_7 (NDII7)$	Hardisky *et al.*, 1983
Normalized Difference Water Index	$NDWI = \frac{\rho_{NIR2} - \rho_{NIR1}}{\rho_{NIR2} + \rho_{NIR1}}$	$\rho_{NIR2} = \rho_2$ $\rho_{NIR1} = \rho_5$	Gao, 1996
Soil Adjusted Vegetation Index	$SAVI = (1 + 0.5)\frac{\rho_{NIR} - \rho_{red}}{\rho_{NIR} + \rho_{red} + 0.5}$	$\rho_{NIR} = \rho_2$ $\rho_{red} = \rho_1$	Huete, 1988
Visible Atmospherically Resistant Index	$VARI = \frac{\rho_{green} - \rho_{red}}{\rho_{green} + \rho_{red} - \rho_{blue}}$	$\rho_{green} = \rho_4$ $\rho_{red} = \rho_1$ $\rho_{blue} = \rho_3$	Gitelson *et al.*, 2002
Enhanced Vegetation Index	$EVI = \frac{2.5(\rho_{NIR} - \rho_{red})}{\rho_{NIR} + 6(\rho_{red}) - 7.5(\rho_{blue}) + 1}$	$\rho_{NIR} = \rho_2$ $\rho_{red} = \rho_1$ $\rho_{blue} = \rho_3$	Huete *et al.*, 2002
Vegetation Index - Green	$VI_{green} = \frac{\rho_{green} - \rho_{red}}{\rho_{green} + \rho_{red}}$	$\rho_{green} = \rho_4$ $\rho_{red} = \rho_1$	Tucker, 1979

Ceccato P, Flasse S, Gregoire JM. Designing a spectral index to estimate vegetation water content from remote sensing data: Part 2. Validation and applications. . Remote Sens. Environ. 2002; 82: 198–207.

Gao BC. NDWI. A normalized difference water index for remote sensing of vegetation liquid water from space. . Remote Sens. Environ. 1996; 58: 257–266.

Gitelson A, Kaufmam JY, Stark R, Rundquist D. Novel algorithms for remote estimation of vegetation fraction. Remote Sens. Environ. 2002; 80: 76–87.

Hardisky MA, Klemas V, Smart RM. The influence of soil salinity, growth form, and leaf moisture on the spectral radiance of Spartina alterniflora canopies. . Photogramm. Eng. Remote Sens. 1983; 49: 77–83.

Huete A, Didan K, Miura T, Rodriguez EP, Gao X, Ferreira LG. Overview of the radiometric and biophysical performance of the MODIS vegetation indices. Remote Sens. Environ. 2002; 83: 195–213.

Huete AR. A soil-adjusted vegetation index (SAVI). Remote Sens. Environ. 1988; 25: 295–309.

Rouse JW, Jr., Haas RW, Schell JA, Deering DH, Harlan JC. Monitoring the Vernal Advancement and Retrogradation (Greenwave Effect) of Natural Vegetation; Type III Final Report; NASA/GSFC: Greenbelt, MD, USA, , 1974.

Tucker CJ. Red and photographic infrared linear combinations for monitoring vegetation. Remote Sens. Environ. 1979; 8: 127–150.

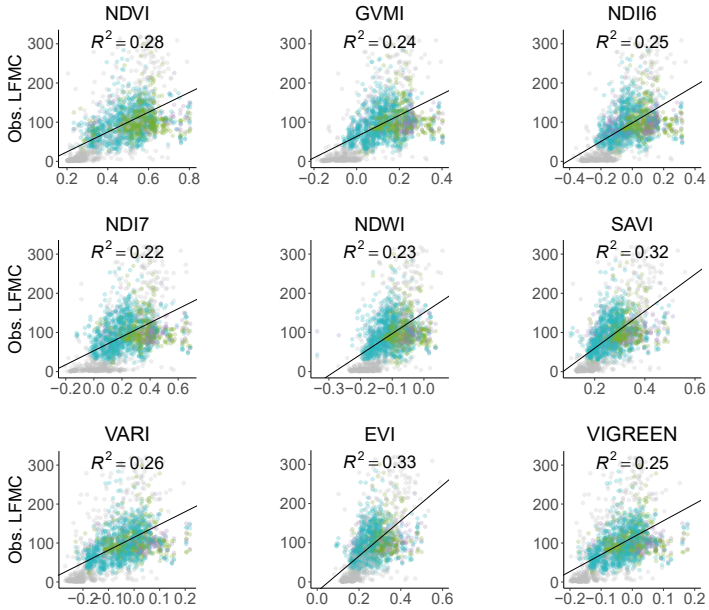

Figure S.IV.1. Relationship between observed LFMC and nine spectral vegetation indices. Colours represent species functional types: seeding shrubs (R-) in blue, resprouting shrubs (R+) in purple, trees (Tr) in green and unknown species in grey. The line and R^2 are the results of linear fitting.

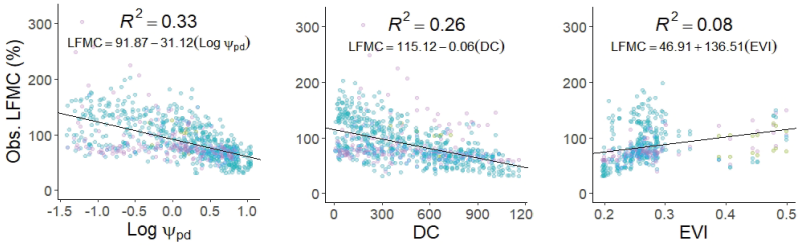

Figure S.IV.2. Model calibration relationships between observed LFMC (%) and logarithmically transformed predawn leaf water potential (Ψ_{pd}) and drought code. Relationship between equivalent water thickness (EWT, g.cm^{-2}) and logarithmically transformed enhanced vegetation index (EVI).

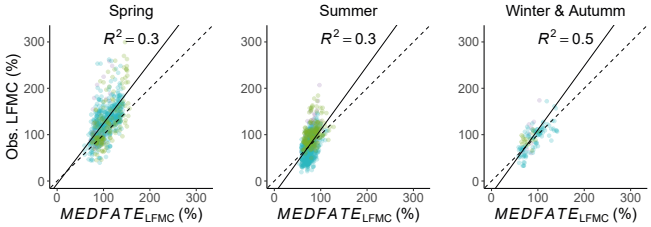

Figure S.IV.3. Relationship between observed LFMC and predicted values from $MEDFATE_{LFMC}$ across the different seasons.

SUPPLEMENTARY MATERIALS V

Table SV.1. Location, IFN3 plot selection and target species for each sampling site. Latitude and Longitude (º), Altitude (m), Spanish region, plot ID, target species, mean annual temperature, mean annual precipitation, and net primary productivity. Sites followed by an asterisk (*) were used for a second simulation round considering stable CO_2 atmospheric concentration across the century.

Site	Lat (º)	Long (º)	Alt (m)	Plot ID	Species	MAT (ºC)	MAP (mm)	NPP (Kg C/m2)
Fs01	43.05448	-5.54181	935	33.2006	*Fagus sylvatica*	10.5	1370	8190
Fs02*	43.24519	-1.59578	440	31.0051	*Fagus sylvatica*	14.1	2200	15031
Fs03	42.23615	-2.91516	1525	26.0339	*Fagus sylvatica*	10.3	861	8999
Ph01	41.73583	1.929772	370	8.1868	*Pinus halepensis*	13.5	659	7867
Ph02*	40.19882	-0.42705	720	12.0965	*Pinus halepensis*	14.5	853	8340
Ph03	38.19899	-1.46966	840	30.063	*Pinus halepensis*	17.9	374	5837
Pn01	42.17916	1.341125	660	25.1559	*Pinus nigra*	13.3	654	8764
Pn02	39.86943	-1.76057	1440	16.1831	*Pinus nigra*	12.4	536	7447
Pn03*	37.93838	-2.78377	1620	23.1713	*Pinus nigra*	11.7	654	3870
Pp01	43.06455	-8.81578	370	15.1673	*Pinus pinaster*	14.9	1652	12225
Pp02	40.28856	-6.41189	525	10.0534	*Pinus pinaster*	15.7	1072	6853
Pp03*	36.48957	-5.1993	1240	29.4033	*Pinus pinaster*	17.7	771	8483
Pa01	41.96588	3.156888	70	17.2492	*Pinus pinea*	15.1	660	11570
Pa02	41.50287	-4.71338	700	47.0366	*Pinus pinea*	12.3	523	7015
Pa03*	37.20728	-6.57598	40	21.2208	*Pinus pinea*	18.4	530	7289
Ps01	42.56004	-0.11294	1060	22.0614	*Pinus sylvestris*	11.2	1517	8778
Ps02*	41.02685	-3.7375	1800	28.0085	*Pinus sylvestris*	11.5	656	7627
Ps03	37.05512	-3.16871	2417	18.2431	*Pinus sylvestris*	12.9	428	4393
Pu01	42.66074	0.571909	1875	22.0833	*Pinus uncinata*	10.9	1143	8010
Pu02	42.76123	-0.23803	1660	22.3024	*Pinus uncinata*	10.3	1707	7317
Pu03*	42.57769	0.928493	2200	25.0308	*Pinus uncinata*	11.1	1082	4192
Qf01	37.9917	-6.05067	600	41.0133	*Quercus faginea*	11.6	402	6876
Qf02*	39.39359	-4.06839	800	45.1358	*Quercus faginea*	15.1	465	4071
Qf03	40.9406	-1.68137	1150	19.1085	*Quercus faginea*	16.3	646	4399
Qi01	41.33428	0.89669	680	43.056	*Quercus ilex*	15.8	447	4071
Qi02*	40.31915	-4.30646	700	28.1857	*Quercus ilex*	12.1	459	4399
Qi03	38.37293	-4.30506	605	13.1541	*Quercus ilex*	15.7	499	7919
Qp01*	42.91134	-4.45787	1300	34.0154	*Quercus pyrenaica*	10.2	1032	4524
Qp02	41.9079	-8.03542	615	32.1777	*Quercus pyrenaica*	13.4	997	5612
Qp03	40.89763	-6.67317	700	37.288	*Quercus pyrenaica*	14.6	646	8566
Qr01	42.6463	-8.02409	645	36.0697	*Quercus robur*	12.6	1161	9970
Qr02*	43.37458	-6.69172	550	33.0344	*Quercus robur*	12.8	1011	6803
Qr03	43.10066	-2.87711	310	48.2135	*Quercus robur*	13.8	1434	10201
Qs01	39.38873	-6.90989	430	6.0007	*Quercus suber*	15.9	493	10739
Qs02	38.28964	-5.08106	790	14.0367	*Quercus suber*	16.6	480	7299
Qs03*	36.46204	-5.45516	270	11.0786	*Quercus suber*	17.8	864	5642

Table SV.2. Global Climate Models (GCM) and Regional Climate Models (RCM) couples selection and corresponding projected climatic changes in summer precipitation and temperature for Europe according to McSweeney *et al.* (2015).

GCM	RCM	Projected climatic changes for Europe
CNRM-CM5	CCLM4-8-17	Moderate summer temperature increase, slight summer precipitation increase
EC-EARTH	RACMO22E	Moderate summer temperature increase, medium summer precipitation increase
CM5A-MR	WRF331F	High summer temperature increase, high summer precipitation decrease
MPI-ESM-LR	RCA4	High summer temperature increase, medium summer precipitation decrease

Table SV.3. Analysis of variance table for fixed effects in the linear mixed-effects model fitted with annual summer mean LFMC as response variable. Significant effects (*P values*) are represented with asterisks (*<0.05, **<0.01, ***<0.001).

Fixed effects	Sum sq.	Mean sq.	Num *df*	Den *df*	*F* value	*P* value
Period	598.24	299.12	2	30	43.85	***
RCP	1455.18	1455.18	1	2305	213.33	***
Period x RCP	2286.32	1143.16	2	2305	167.59	***

Table SV.4-1. Pairwise differences between different *Period* (1: 2010-2020; 2: 2040-2050 and 3: 2090-2100) and *RCP* (4.5 and 8.5) fixed factors combinations from the linear mixed-effects model fitted with annual summer mean LFMC as response variable. Significant effects (*P values*) are represented with asterisks (*<0.05, **<0.01, ***<0.001).

Period x RCP	Estimate	SE	*df*	*t* ratio	*P* value
Period1 RCP4.5 - Period2 RCP4.5	1.29	0.56	33.6	2.31	0.4
Period1 RCP4.5 - Period3 RCP4.5	2.75	0.56	33.6	4.92	***
Period1 RCP4.5 - Period1 RCP8.5	-0.19	0.18	2305	-1.05	1
Period1 RCP4.5 - Period2 RCP8.5	1.88	0.56	33.6	3.36	*
Period1 RCP4.5 - Period3 RCP8.5	7.05	0.56	33.6	12.61	***
Period2 RCP4.5 - Period3 RCP4.5	1.46	0.56	33.6	2.61	*
Period2 RCP4.5 - Period1 RCP8.5	-1.49	0.56	33.6	-2.66	*
Period2 RCP4.5 - Period2 RCP8.5	0.58	0.18	2305	3.1	*
Period2 RCP4.5 - Period3 RCP8.5	5.76	0.56	33.6	10.3	***
Period3 RCP4.5 - Period1 RCP8.5	-2.95	0.56	33.6	-5.27	***
Period3 RCP4.5 - Period2 RCP8.5	-0.87	0.56	33.6	-1.56	1
Period3 RCP4.5 - Period3 RCP8.5	4.3	0.18	2305	23.18	***
Period1 RCP8.5 - Period2 RCP8.5	2.07	0.56	33.6	3.71	**
Period1 RCP8.5 - Period3 RCP8.5	7.25	0.56	33.6	12.96	***

Table S.V.4-2. ANOVA-like table for *Site* and *Year* (as a replicate of *Period*) random-effects from the linear mixed-effects model fitted with annual summer mean LFMC as response variable. Significant effects (*P values*) are represented with asterisks (*<0.05, **<0.01, ***<0.001).

	N	logLik	AIC	LRT	*df*	*P* value
none	9	-5825.6	11669			
Site	8	-9318.2	18652	6985.2	1	***
Year x Period	8	-6003.4	12023	355.6	1	***

Table S.V.5 Analysis of variance table for fixed effects in the linear mixed-effects model fitted with annual summer mean DFMC as response variable. Significant effects (*P values*) are represented with asterisks (*<0.05, **<0.01, ***<0.001).

Fixed effects	Sum sq.	Mean sq.	Num *df*	Den *df*	F value	*P* value
Period	18.61	9.3	2	30	112.13	***
RCP	29.93	29.93	1	2305	360.73	***
Period x RCP	32.42	16.21	2	2305	195.35	***

Table S.V.6.1. Pairwise differences between *Period* (1: 2010-2020; 2: 2040-2050 and 3: 2090-2100) and *RCP* (4.5 and 8.5) from the linear mixed-effects model fitted with annual summer mean DFMC as response variable. Significant effects (*P values*) are represented with asterisks (*<0.05, **<0.01, ***<0.001).

Period x RCP	Estimate	SE	*df*	*t* ratio	*P* value
Period1 RCP4.5 - Period2 RCP4.5	0.32	0.06	33.9	5.34	***
Period1 RCP4.5 - Period3 RCP4.5	0.61	0.06	33.9	10.32	***
Period1 RCP4.5 - Period1 RCP8.5	0.08	0.02	2305	3.94	***
Period1 RCP4.5 - Period2 RCP8.5	0.36	0.06	33.9	6	***
Period1 RCP4.5 - Period3 RCP8.5	1.17	0.06	33.9	19.65	***
Period2 RCP4.5 - Period3 RCP4.5	0.3	0.06	33.9	4.98	***
Period2 RCP4.5 - Period1 RCP8.5	-0.24	0.06	33.9	-3.99	**
Period2 RCP4.5 - Period2 RCP8.5	0.04	0.02	2305	1.9	0.87
Period2 RCP4.5 - Period3 RCP8.5	0.85	0.06	33.9	14.31	***
Period3 RCP4.5 - Period1 RCP8.5	-0.53	0.06	33.9	-8.97	***
Period3 RCP4.5 - Period2 RCP8.5	-0.26	0.06	33.9	-4.33	***
Period3 RCP4.5 - Period3 RCP8.5	0.55	0.02	2305	27.06	***
Period1 RCP8.5 - Period2 RCP8.5	0.28	0.06	33.9	4.64	***
Period1 RCP8.5 - Period3 RCP8.5	1.09	0.06	33.9	18.29	***

Table S.V.6.2. ANOVA-like table for *Site* and *Year* random-effects from the linear mixed-effects model fitted with annual summer mean DFMC as response variable. Significant effects (*P values*) are represented with asterisks (*<0.05, **<0.01, ***<0.001).

	N	logLik	AIC	LRT	*df*	*P* value
none	9	-599.1	1216.2			
Site	8	-4060.3	8136.7	6922.5	1	***
Year:Period	8	-761.3	1538.6	324.5	1	***

Table S.V.7. Analysis of variance table for fixed effects in the linear mixed-effects model fitted with the number of days per year when LFMC < 120 % as response variable. Significant effects (*P values*) are represented with asterisks (*<0.05, **<0.01, ***<0.001).

Fixed effects	Sum sq.	Mean sq.	Num *df*	Den *df*	F value
Period	65503	32752	2	57.4	***
RCP	72057	72057	1	126.3	***
Period x RCP	176413	88206	2	154.6	***

Table S.V.8. Analysis of variance table for fixed effects in the linear mixed-effects model fitted with the number of days per year when LFMC < 100 % (square root transformed) as response variable. Significant effects (*P values*) are represented with asterisks (*<0.05, **<0.01, ***<0.001).

Fixed effects	Sum sq.	Mean sq.	Num *df*	Den *df*	F value
Period	247.1	123.5	2	40.9	***
RCP	124.3	124.3	1	41.2	***
Period x RCP	441.7	220.9	2	73.1	***

Table S.V.9. Analysis of variance table for fixed effects in the linear mixed-effects model fitted with the number of days per year when DFMC < 12 % as response variable. Significant effects (*P values*) are represented with asterisks (*<0.05, **<0.01, ***<0.001).

Fixed effects	Sum sq.	Mean sq.	Num *df*	Den *df*	F value
Period	29827	14914	2	161.9	***
RCP	60445	60445	1	656.4	***
Period x RCP	81852	40926	2	444.4	***

Table S.V.10. Analysis of variance table for fixed effects in the linear mixed-effects model fitted with the number of days per year when DFMC < 10 % as response variable. Significant effects (*P values*) are represented with asterisks (*<0.05, **<0.01, ***<0.001).

Fixed effects	Sum sq.	Mean sq.	Num *df*	Den *df*	F value
Period	36891	18445	2	203.5	***
RCP	45513	45513	1	502.2	***
Period x RCP	73092	36546	2	403.2	***

Table S.V.11. Analysis of variance table for fixed effects in the linear mixed-effects model fitted with the number of days per year when DFMC < 8 % as response variable. Significant effects (*P values*) are represented with asterisks (*<0.05, **<0.01, ***<0.001).

Fixed effects	Sum sq.	Mean sq.	Num *df*	Den *df*	F value
Period	32631	16316	2	158.5	***
RCP	27111	27111	1	263.4	***
Period x RCP	37669	18835	2	182.9	***

Table S.V.12. Fire season lengthening median values (d yr^{-1}) regarding minimum (<120%) and critical (<100%) LFMC thresholds for wildfire occurrence under increasing and constant atmospheric [CO_2] conditions for both RCPs (4.5 and 8.5) and in all periods (2010-2020, 2040-2050, 2090-2100).

RCP	Period	Increasing atmospheric [CO_2]		Constant atmospheric [CO_2]	
		Minimum	Critical	Minimum	Critical
4.5	2010-2020	119	31	117	34
4.5	2040-2050	122	32	127	36
4.5	2090-2100	133	40	136	45
8.5	2010-2020	115	27	116	27
8.5	2040-2050	127	35	127	38
8.5	2090-2100	170	66	182	74

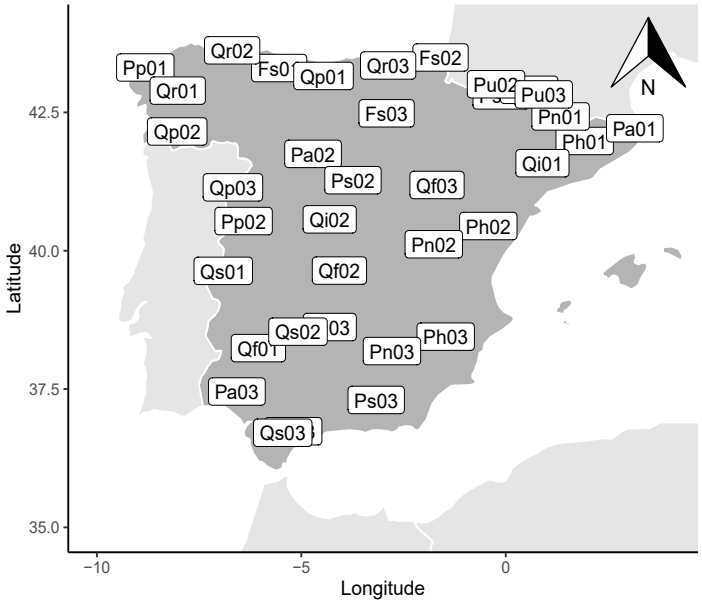

Figure S.V.1. Study sites location. Northern sites overlap: Pu01 and Ps01. Southern sites overlap: Pp03

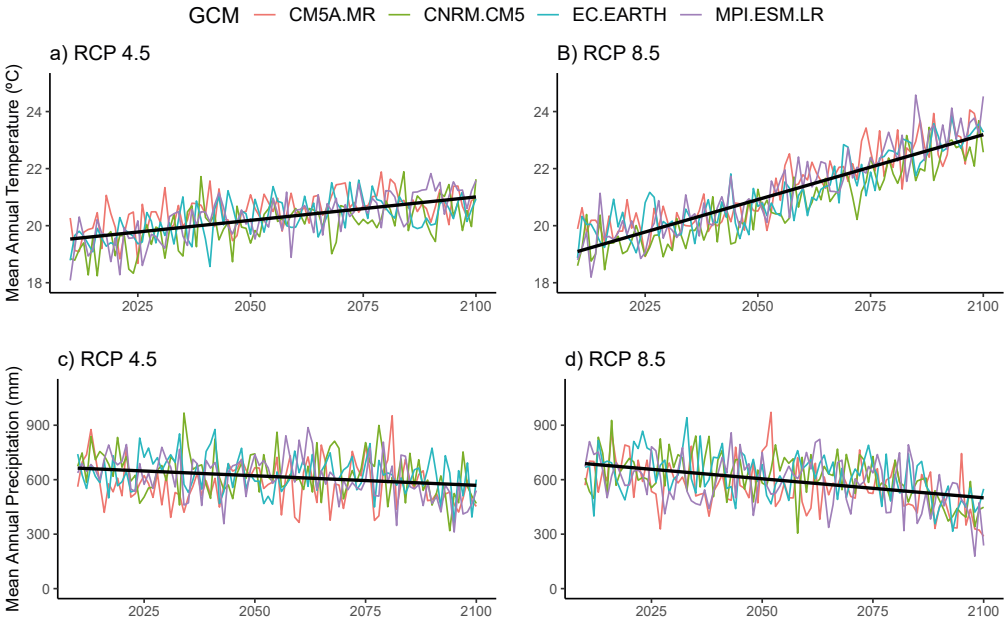

Figure S.V.2. Mean annual temperature (ºC) and mean annual precipitation (mm) projections of each Global Climate Model (GCM) for each greenhouse gas emission scenario (RCP4.5 and RCP8.5).

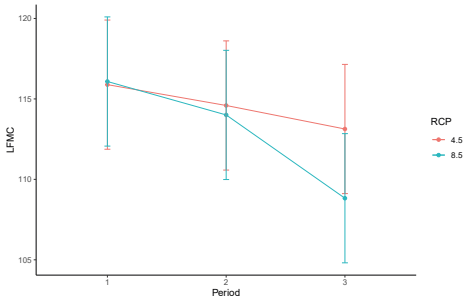

Figure S.V.3. LFMC mean values across the three decadal periods (1: 2010-2020; 2: 2040-2050 and 3: 2090-2100) in both RCP scenarios (4.5 in red and 8.5 in blue). Bars represent standard deviation (SD).

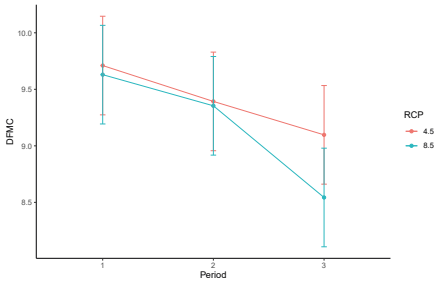

Figure S.V.4. DFMC mean values across the three decadal periods (1: 2010-2020; 2: 2040-2050 and 3: 2090-2100) in both RCP scenarios (4.5 in red and 8.5 in blue). Bars represent standard deviation (SD).

SUPPLEMENTARY MATERIALS VI

Table S.VI.1. Description and sources of the layers, products and datasets used in this study.

Data description	Use in this study	Source
Tree restoration potential	Potential reforestation areas identification	Bastin *et al.,* 2019
Global biomes distribution	Potential reforestation areas identification	Dinerstein *et al.,* 2017
Net ecosystem productivity (NEP)	Net sequestration potential simulation	Jung *et al.,* 2020
Tree cover distribution	Future NEP estimation	Dimiceli *et al.,* 2015
Incoming solar radiation	Emission equivalent of shortwave forcing simulation	Karlsson *et al.,* 2017
Surface albedo	Emission equivalent of shortwave forcing simulation	Gao *et al.,* 2014
Forest biomes VPD thresholds	Fire-days incidence estimation	Clarke *et al.,* 2022
Daily current VPD (2020)	Current fire-days incidence	Hersbach *et al.,* 2020
Daily future VPD (2100)	Future fire-days incidence	Taylor *et al.,* 2012

Bastin, J. F., Finegold, Y., Garcia, C., Mollicone, D., Rezende, M., Routh, D., Zohner, C. M., & Crowther, T. W. (2019). The global tree restoration potential. Science, 364(6448), 76–79.

Clarke, H., Nolan, R. H., De Dios, V. R., Bradstock, R., Griebel, A., Khanal, S., & Boer, M. M. (2022). Forest fire threatens global carbon sinks and population centres under rising atmospheric water demand. Nature Communications, 13(1), 1–10.

Dimiceli, C., Carroll, M., Sohlberg, R., Kim, D. H., Kelly, M., & Townshend, J. R. G. (2015). MOD44B MODIS/Terra vegetation continuous fields yearly L3 global 250 m SIN grid V006. NASA EOSDIS Land Processes Distributed Active Archive Center.

Dinerstein, E., Olson, D., Joshi, A., Vynne, C., Burgess, N. D., Wikramanayake, E., Hahn, N., Palminteri, S., Hedao, P., Noss, R., Hansen, M., Locke, H., Ellis, E. C., Jones, B., Barber, C. V., Hayes, R., Kormos, C., Martin, V., Crist, E., Saleem, M. (2017). An Ecoregion-Based Approach to Protecting Half the Terrestrial Realm. BioScience, 67(6), 534–545.

Gao, F., He, T., Wang, Z., Ghimire, B., Shuai, Y., Masek, J., Schaaf, C., & Williams, C. (2014). Multiscale climatological albedo look-up maps derived from moderate resolution imaging spectroradiometer BRDF/albedo products. Journal of Applied Remote Sensing, 8(1), 083532.

Hersbach, H., Bell, B., Berrisford, P., Hirahara, S., Horányi, A., Muñoz-Sabater, J., Nicolas, J., Peubey, C., Radu, R., Schepers, D., Simmons, A., Soci, C., Abdalla, S., Abellan, X., Balsamo, G., Bechtold, P., Biavati, G., Bidlot, J., Bonavita, M., Thépaut, J. N. (2020). The ERA5 global reanalysis. Quarterly Journal of the Royal Meteorological Society, 146(730), 1999–2049.

Jung, M., Schwalm, C., Migliavacca, M., Walther, S., Camps-Valls, G., Koirala, S., Anthoni, P., Besnard, S., Bodesheim, P., Carvalhais, N., Chevallier, F., Gans, F., S Goll, D., Haverd, V., Köhler, P., Ichii, K., K Jain, A., Liu, J., Lombardozzi, D., Reichstein, M. (2020). Scaling carbon fluxes from eddy covariance sites to globe: Synthesis and evaluation of the FLUXCOM approach. Biogeosciences, 17(5), 1343–1365.

Karlsson, K. G., Anttila, K., Trentmann, J., Stengel, M., Fokke Meirink, J., Devasthale, A., Hanschmann, T., Kothe, S., Jaäskelaïnen, E., Sedlar, J., Benas, N., Van Zadelhoff, G. J., Schlundt, C., Stein, Di., Finkensieper, S., Häkansson, N., & Hollmann, R. (2017). CLARA-A2: The second edition of the CM SAF cloud and radiation data record from 34 years of global AVHRR data. Atmospheric Chemistry and Physics, 17(9).

Taylor, K. E., Stouffer, R. J., & Meehl, G. A. (2012). An overview of CMIP5 and the experiment design. Bulletin of the American Meteorological Society, 93(4), 485–498.

Table S.VI.2. Forest biomes VPD thresholds. Median (minimum-maximum) VPD threshold at which the probability of fire is 50% ($VPD_{P=50}$) for each forest biome type (Dinerstein *et al.,* 2017). Adapted from Clarke *et al.* (2022).

Biome	$VPD_{P=50}$ (kPa)
Tropical and Subtropical Moist Broadleaf Forests	2.46 (1.58 – 3.49)
Tropical and Subtropical Dry Broadleaf Forests	3.05 (2.70 – 4.04)
Tropical and Subtropical Coniferous Forests	2.54 (1.46 – 3.65)
Mediterranean Forests, Woodlands, and Scrub	2.31 (1.44 – 4.35)
Temperate Broadleaf and Mixed Forests	1.30 (0.91 – 2.55)
Temperate Coniferous Forests	1.54 (0.90 – 2.04)
Boreal	1.11 (0.72 – 1.37)

Table S.VI.3. Global Climate Models. CMIP5 dataset (Taylor *et al.*, 2012) Global Climate Models (GCM) selection, references and corresponding projected changes in annual precipitation and temperature according to McSweeney *et al.,* 2015.

GCM	Reference	Projected climatic changes
CNRM-CM5	Voldoire *et al.,* 2013	Moderate annual temperature increases, slight annual precipitation increases
ACCESS1-0	Ackerley & Dommenget, 2016	High annual temperature increases, slight annual precipitation decreases
GFDL-CM3	Griffies *et al.,* 2011	Extreme annual temperature increases, slight annual precipitation increases

Ackerley, D. & Dommenget, D. Atmosphere-only GCM (ACCESS1.0) simulations with prescribed land surface temperatures. (2016). Geoscientific Model Development 9(6), 2077-2098.

Griffies, S. M., Winton, M., Donner, L. J., Horowitz, L. W., Downes, S. M., Farneti, R., Gnanadesikan, A., Hurlin, W. J., Lee, H. C., Liang, Z., Palter, J. B., Samuels, B. L., Wittenberg, A. T., Wyman, B. L., Yin, J. J., & Zadeh, N. The GFDL CM3 Coupled Climate Model: Characteristics of the Ocean and Sea Ice Simulations. (2011). Journal of Climate 24(13), 3520-3544

Voldoire, A., Sanchez-Gomez, E., Melia, D. S. Y., Decharme, B., Cassou, C., Senesi, S., Valcke, S., Beau, I., Alias, A., Chevallier, M., Deque, M., Deshayes, J., Douville, H., Fernandez, E., Madec, G., Maisonnave, E., Moine, M. P., Planton, S., Saint-Martin, D., Szopa, S., Tyteca, S., Alkama, R., Belamari, S., Braun, A., Coquart, L., & Chauvin, F. The CNRM-CM5.1 global climate model: description and basic evaluation. (2013). Climate Dynamics 40(9-10), 2091-2121

Table S5. ΔFire-Days impacts over carbon balances. Relationship between reforestation surface (Mha) and the associated Net Equivalent Carbon Stock Change (NESC, Gt C) of the smart reforestation areas (NESC > 0) that recorded less than a 50 % increase in the annual fire-days frequency from 2020 to 2100, projected by each global climate model (GCM) under both representative concentration pathway scenarios (RCPs) 4.5 and 8.5.

GCM	RCP	Surface (Mha)	NESC (Gt C)
CNRM-CM5	4.5	261.2	16.8
	8.5	216.4	12.9
ACCESS1-0	4.5	182.4	11.1
	8.5	91	5.7
GFDL-CM3	4.5	215.3	13.9
	8.5	147.5	9.4

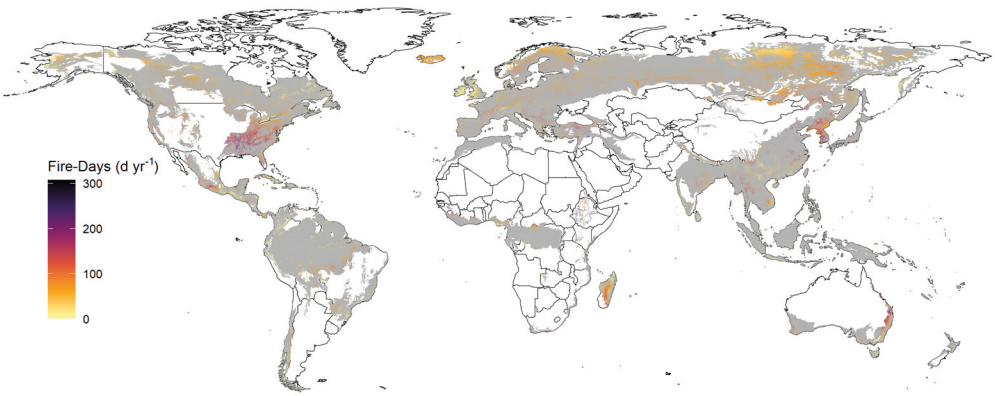

Figure SVI.2. Spatial distribution of current (2020) annual fire-days frequency (d yr^{-1}). Fire-days indicate days exceeding vapor pressure deficit (VPD) thresholds associated with a 50 % probability of fire incidence.

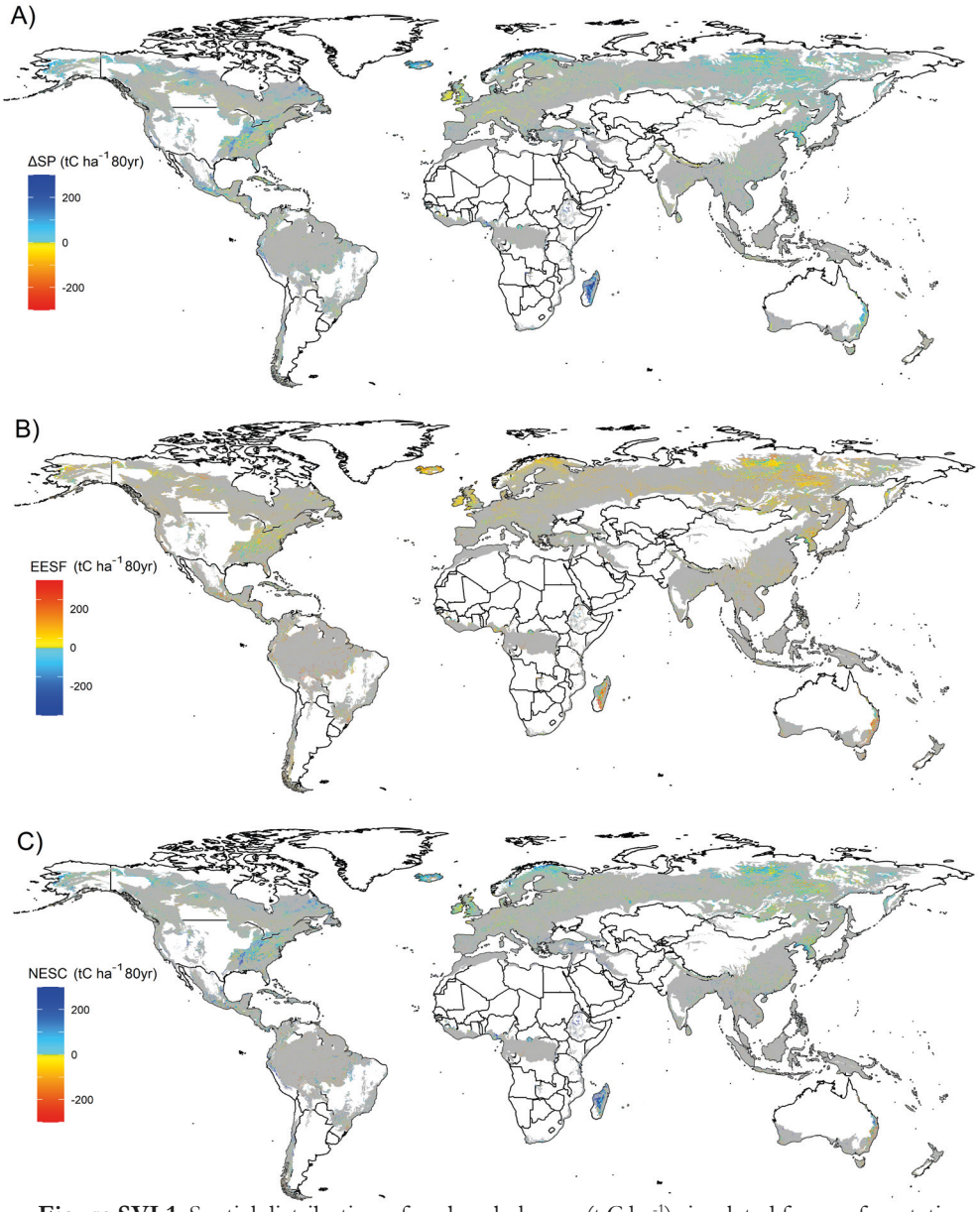

Figure SVI.1. Spatial distribution of carbon balances (t C ha^{-1}) simulated from reforestation actions over an 80-year period: (A) Net sequestration potential (ΔSP). (B) Emissions equivalent of shortwave forcing (EESF). (C) Net equivalent carbon stock change (NESC = ΔSP – EESF). Gray background represents forest biomes extension (Dinerstein *et al.*, 2017). While ΔSP and NESC represents carbon uptake, EESF represent carbon emissions and gradient colors are consequently inverted.

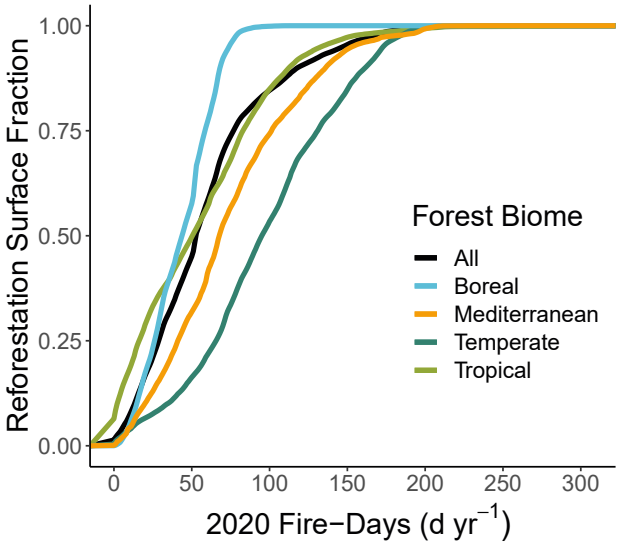

Figure SVI.3. Empirical distribution function of the fire-days incidence (d yr^{-1}) in 2020 over reforestation surface fraction. Colors represent global forest biome types (Dinerstein *et al.*, 2017): all forest biome types in black, boreal forests in blue, temperate forests in dark-green, tropical forests in light-green and mediterranean forests in orange.

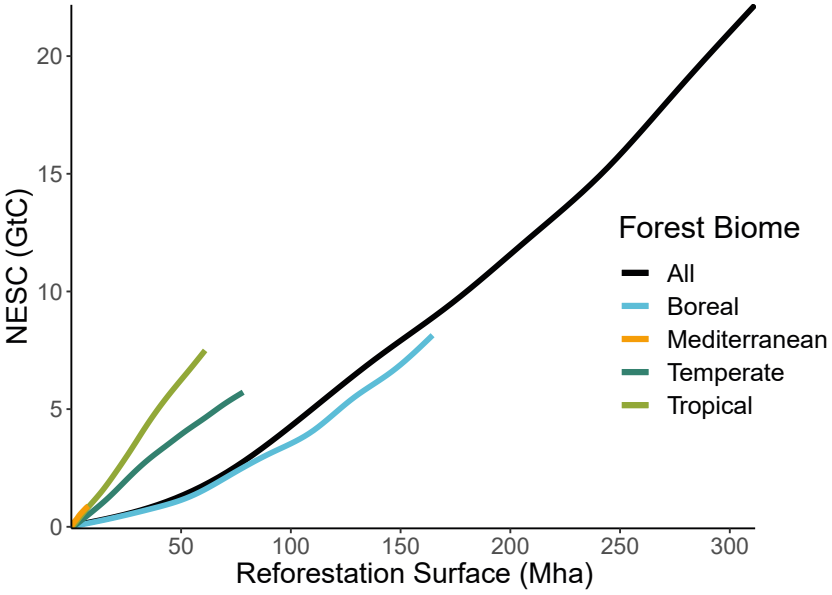

Figure SVI.4. Net equivalent carbon stock change (NESC, Gt C) distribution over smart reforestation surface (Mha). Colors represent global forest biome types (Dinerstein *et al.,* 2017): all forest biome types in black, boreal forests in blue, temperate forests in dark-green, tropical forests in light-green and mediterranean forests in orange.

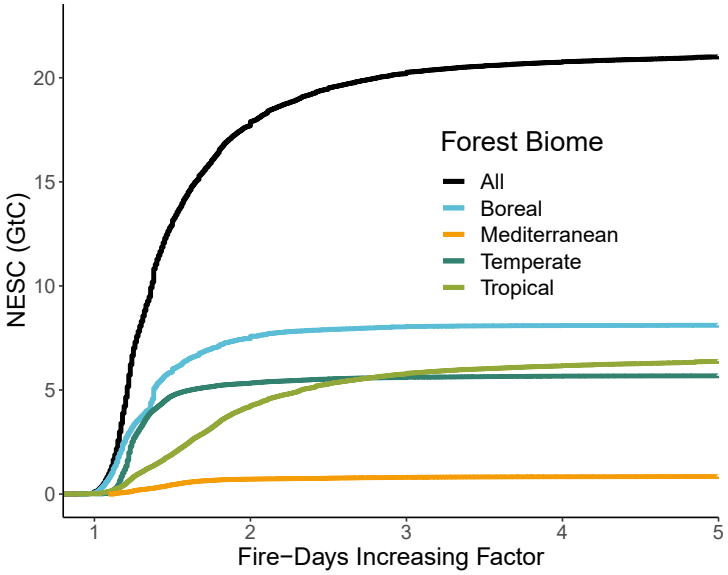

Figure SVI.5. Fire-Days Increasing Factor distribution over net equivalent carbon stock change (NESC, Gt C). Colors represent global forest biome types (Dinerstein *et al.*, 2017): all forest biome types in black, boreal forests in blue, temperate forests in dark-green, tropical forests in light-green and mediterranean forests in orange.

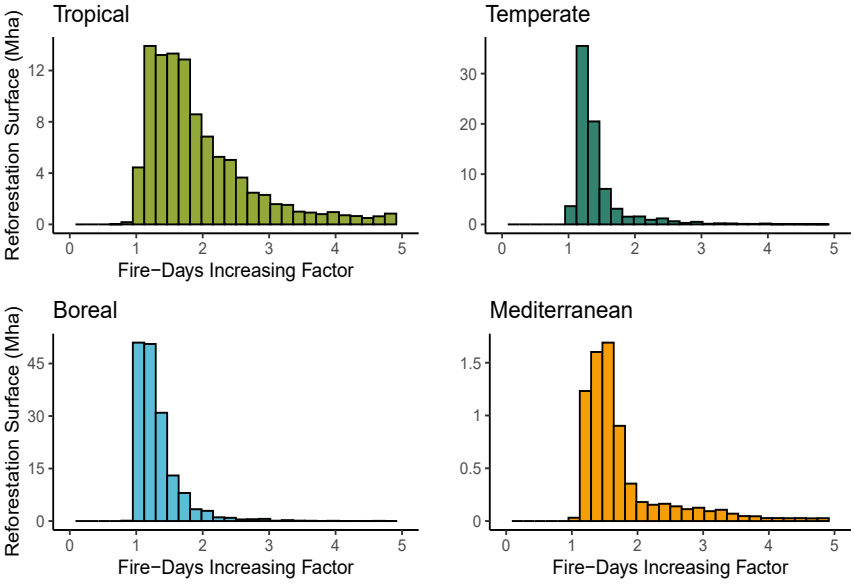

Figure SVI.6. Fire-Days Increasing Factors distribution across forest biome types.

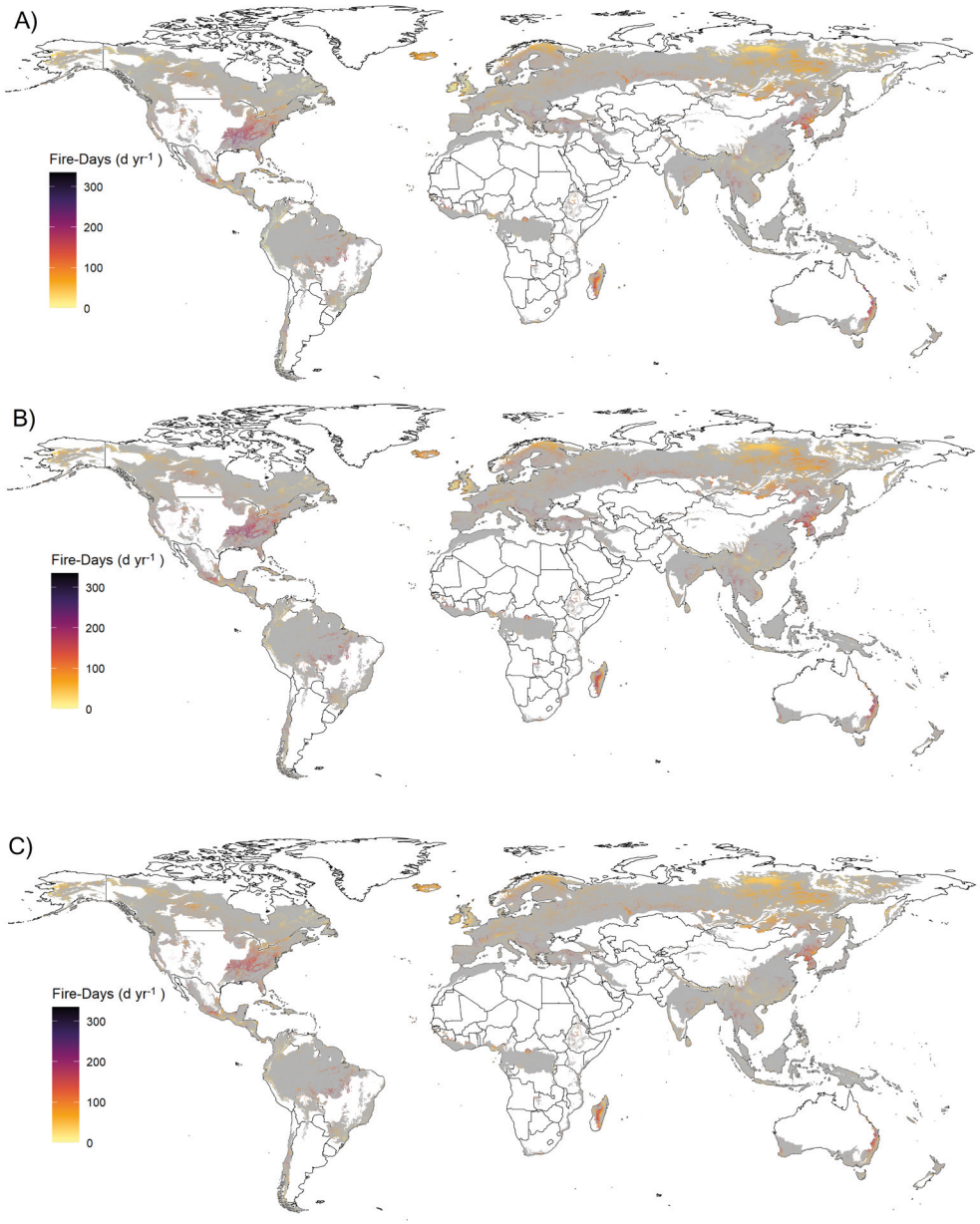

Figure SVI.7. Spatial distribution of future (2100) annual fire-days frequency (d yr^{-1}) projected under greenhouse gas emissions scenario RCP 4.5 considering the global climate models: (A) CNRM-CM5; (B) ACCESS1-0; and (C) GFDL-CM3. Fire-days indicate days exceeding vapor pressure deficit (VPD) thresholds associated with a 50 % probability of fire incidence.

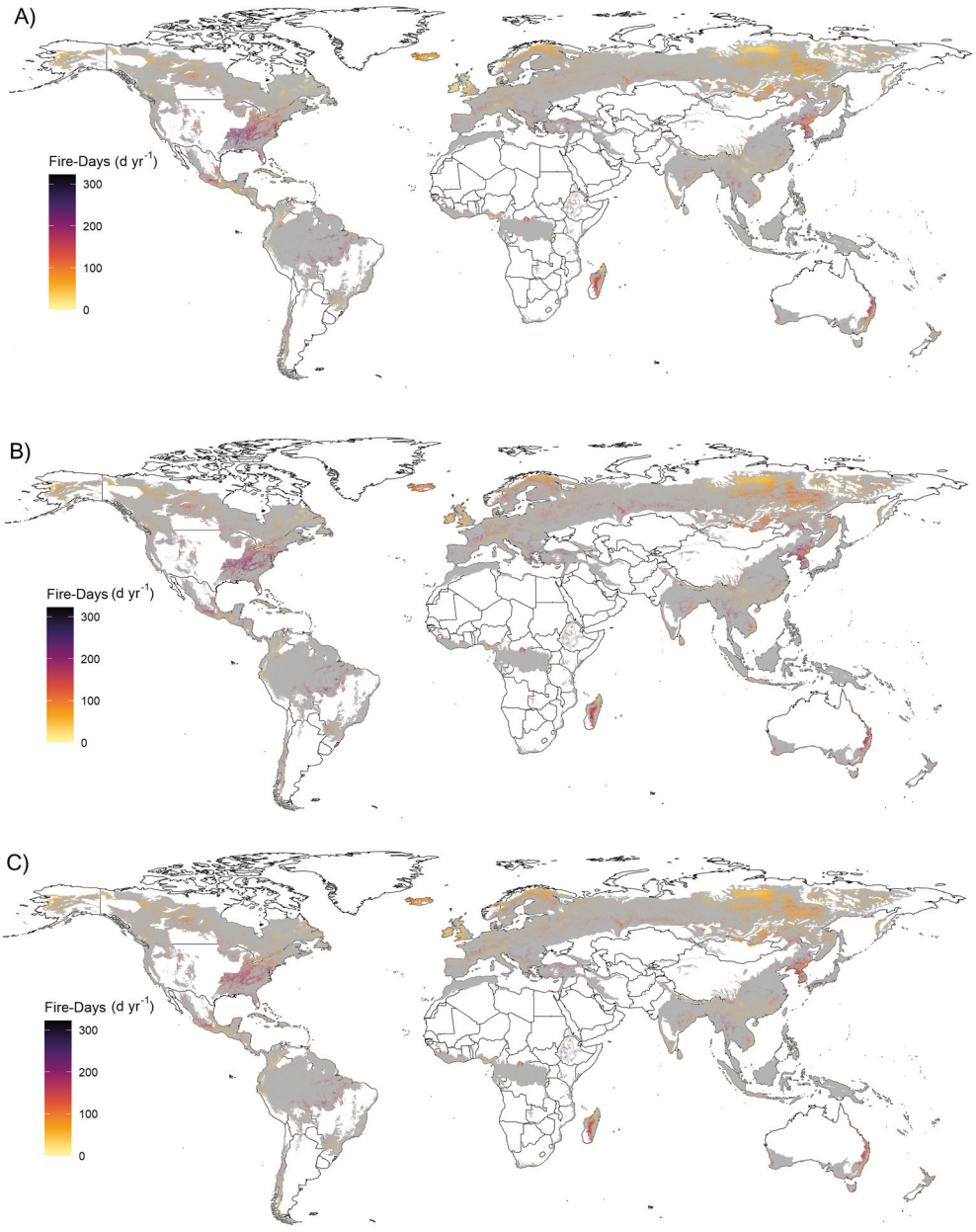

Figure SVI.8. Spatial distribution of future (2100) annual fire-days frequency (d yr^{-1}) projected under greenhouse gas emissions scenario RCP 8.5 considering the global climate models: (A) CNRM-CM5; (B) ACCESS1-0; and (C) GFDL-CM3. Fire-days indicate days exceeding vapor pressure deficit (VPD) thresholds associated with a 50 % probability of fire incidence.

APPENDIX

forests

MDPI

Article

Needle Senescence Affects Fire Behavior in Aleppo Pine (*Pinus halepensis* Mill.) Stands: A Simulation Study

Rodrigo Balaguer-Romano [1,*], Rubén Díaz-Sierra [1], Javier Madrigal [2,3], Jordi Voltas [4,5] and Víctor Resco de Dios [4,5,6,*]

1 Mathematical and Fluid Physics Department, Faculty of Sciences, Universidad Nacional de Educación a Distancia (UNED), 28040 Madrid, Spain; sierra@ccia.uned.es
2 Department of Forest Dynamics and Management, INIA–CIFOR, Ctra. A Coruña Km 7.5, 28040 Madrid, Spain; incendio@inia.es
3 ETSI Montes, Forestal y del Medio Natural, Universidad Politécnica de Madrid (UPM), Ramiro de Maeztu, 28040 Madrid, Spain
4 Department of Crop and Forest Sciences, Universitat Lleida, 25198 Lleida, Spain; jordi.voltas@udl.cat
5 Oint Research Unit CTFC-AGROTECNIO, Universitat de Lleida, 25198 Lleida, Spain
6 School of Life Science and Engineering, Southwest University of Science and Technology, Mianyang 621010, China
* Correspondence: rodrigo.balaguer.romano@gmail.com (R.B.-R.); v.rescodedios@gmail.com (V.R.d.D.)

Received: 21 August 2020; Accepted: 28 September 2020; Published: 29 September 2020

Abstract: *Research Highlights:* Pre-programmed cell death in old Aleppo pine needles leads to low moisture contents in the forest canopy in July, the time when fire activity nears its peak in the Western Mediterranean Basin. Here, we show, for the first time, that such needle senescence may increase fire behavior and thus is a potential mechanism explaining why the bulk of the annual burned area in the region occurs in early summer. *Background and Objectives:* The brunt of the fire season in the Western Mediterranean Basin occurs at the beginning of July, when live fuel moisture content is near its maximum. Here, we test whether a potential explanation to this conundrum lies in Aleppo pine needle senescence, a result of pre-programmed cell death in 3-years-old needles, which typically occurs in the weeks preceding the peak in the burned area. Our objective was to simulate the effects of needle senescence on fire behavior. *Materials and Methods:* We simulated the effects of needle senescence on canopy moisture and structure. Fire behavior was simulated across different phenological scenarios and for two highly contrasting Aleppo pine stand structures, a forest, and a shrubland. Wildfire behavior simulations were done with BehavePlus6 across a wide range of wind speeds and of dead fine surface fuel moistures. *Results:* The transition from surface to passive crown fire occurred at lower wind speeds under simulated needle senescence in the forest and in the shrubland. Transitions to active crown fire only occurred in the shrubland under needle senescence. Maximum fire intensity and severity were always recorded in the needle senescence scenario. *Conclusions:* Aleppo pine needle senescence may enhance the probability of crown fire development at the onset of the fire season, and it could partly explain the concentration of fire activity in early July in the Western Mediterranean Basin.

Keywords: fire behavior; crown fire; fire modeling; senescence; foliar moisture content; canopy bulk density

A1. Publication of the research activities detailed in Chapter III.

Agricultural and Forest Meteorology 323 (2022) 109022

Contents lists available at ScienceDirect

Agricultural and Forest Meteorology

journal homepage: www.elsevier.com/locate/agrformet

A semi-mechanistic model for predicting daily variations in species-level live fuel moisture content

Rodrigo Balaguer-Romano [a,b,*], Rubén Díaz-Sierra [a], Miquel De Cáceres [c], Àngel Cunill-Camprubí [d], Rachael H. Nolan [e], Matthias M. Boer [e], Jordi Voltas [d,f], Víctor Resco de Dios [d,f,g]

[a] Mathematical and Fluid Physics Department, Faculty of Sciences, Universidad Nacional de Educación a Distancia (UNED), Madrid 28040, Spain
[b] EIUNED, Escuela Internacional de Doctorado. PhD Program in Sciences, Universidad Nacional de Educación a Distancia (UNED), Madrid 28040, Spain
[c] CREAF, E08193 Bellaterra (Cerdanyola del Vall`es), Catalonia, Spain
[d] Joint Research Unit CTFC – AGROTECNIO – CERCA, Av. Alcalde Rovira Roure 191, Lleida 25198, Spain
[e] Hawkesbury Institute for the Environment, Western Sydney University, Locked Bag 1797, Penrith, NSW 2751, Australia
[f] Department of Crop and Forest Sciences, Universitat de Lleida, Lleida 25198, Spain
[g] School of Life Science and Engineering, Southwest University of Science and Technology, Mianyang 621010, China

ARTICLE INFO

Key words:
Wildfire
Fire behaviour
Drought stress
Drought Code
Remote sensing
Phyrophysiology

ABSTRACT

Live Fuel Moisture Content (LFMC) is one of the main factors affecting forest ignitability as it determines the availability of existing live fuel to burn. Currently, LFMC is monitored through spectral vegetation indices or inferred from meteorological drought indices. While useful, neither approach provides mechanistic insights into species-specific LFMC variation and they are limited in the ability to forecast LFMC under altered future climates. Here, we developed a semi-mechanistic model to predict daily variation in LFMC across woody species from different functional types by adjusting a soil water balance model which estimates predawn leaf water potential (Ψ_{pd}). Our overarching goal was to balance the trade-off between biological realism, which enhances model applicability, and parameterization complexity, which may limit its value within operational settings. After calibration, model predictions were validated against a dataset comprising 1659 LFMC observations across peninsular Spain, belonging to different functional types and from contrasting climates. The overall goodness of fit for our model ($R^2 = 0.5$) was better than that obtained by an existing models based on drought indices ($R^2 = 0.3$) or spectral vegetation indices ($R^2 = 0.1$). We observed the best predictive performance for seeding shrubs ($R^2 = 0.6$) followed by trees ($R^2 = 0.5$) and resprouting shrubs ($R^2 = 0.4$). Through its relatively simple parameterization, the approach developed here may pave the way for a new generation of process-based models that can be used for operational purposes within fire risk mitigation scenarios.

1. Introduction

Wildfires are a natural component of many terrestrial ecosystems, but they are becoming an increasing threat to civil protection, public health and national security worldwide (Borchers-Arriagada et al., 2021; Duane et al., 2021; Karavani et al., 2018; McDonald, 2020; Resco de Dios and Nolan, 2021; Tedim et al., 2020). Sustainable wildfire management should not seek to eliminate all fires in ecosystems that are naturally fire-prone. Instead, the target for wildfire management lies in creating fuel structures, from local to landscape scales, that reduce the risk for life and property while maintaining ecological functions. In this context, a key aspect for fire prevention and management actions is understanding the temporal changes that occur in the moisture content of both, dead and live fuels. Wildfires can only occur once critical fuel dryness thresholds are crossed (Jurdao et al., 2012; Luo et al., 2019; Nolan et al., 2016), and management can significantly alter fuel growth and provide a better knowledge of where and when live and dead fuels are in a critically dry state for assessing the risk of large wildfires

Abbreviations: LFMC, life fuel moisture content; Ψ_{pd}, predawn leaf water potential; Ψ_{soil}, soil water potential; DC, Drought Code; EVI, Enhanced Vegetation Index.

* Corresponding author at: Mathematical and Fluid Physics Department, Faculty of Sciences, Universidad Nacional de Educación a Distancia (UNED), Madrid 28040, Spain.
E-mail address: rodrigo.balaguer@ccia.uned.es (R. Balaguer-Romano).

https://doi.org/10.1016/j.agrformet.2022.109022
Received 10 December 2021; Received in revised form 17 May 2022; Accepted 22 May 2022

The 1st International Electronic Conference on Forests. Forests for a Better Future: Sustainability, Innovation, Interdisciplinarity.

Needle Senescence Affects Fire Behavior in Aleppo Pine (*Pinus halepensis* Mill.) Stands: A Simulation Study

Rodrigo Balaguer-Romano [1,*], Rubén Díaz-Sierra [1], Javier Madrigal [2], Jordi Voltas [3] and Víctor Resco de Dios [3,4]

[1]Mathematical and Fluid Physics Department, Faculty of Sciences, UNED. [2] Department of Forest Dynamics and Management, INIA–CIFOR. [3] Department of Crop and Forest Sciences Universitat Lleida. [4]School of Life Science and Engineering, Southwest University of Science and Technology.* Correspondence: rodrigo.balaguer.romano@gmail.com

INTRODUCTION

The brunt of the fire season in the Western Mediterranean Basin occurs at the beginning of July, when live fuel moisture content is near its maximum. We have tested whether a potential

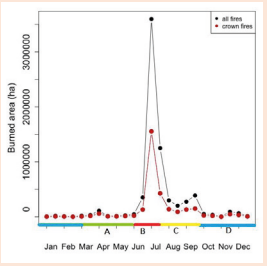

explanation to this conundrum lies in Aleppo pine needle senescence, which typically occurs in July. Our objective was to simulate the effects of needle senescence on fire behavior.

METHODS

We simulated in *BehavePlus6.* four scenarios that recreated the major annual physiological and structural changes in relation to needle senescence. That is; A: representing spring leaf sprout; B: representing the time of needle senescence; C: after dry leaves shed and D: later in the year after the onset of litter decomposition in the autumn. Simulations were carried out in two contrasting stands types: Forest and Shrubs.

Forest	A	B	C	D
Canopy Cover (%)	35	35	35	35
Canopy Height (m)	8	8	8	8
Canopy Base Height (m)	1.5	1.5	1.5	1.5
Canopy Bulk Density (kg/m³)	0.15	0.15	0.1	0.1
Fine Fuel Load (t/ha)	2.5	2.5	3	2.5
1-h Dead Surface Fuel Moisture (%)	6	5	5	9
Foliar Moisture Content (%)	105	74	100	100
Shrub	**A**	**B**	**C**	**D**
Canopy Cover (%)	100	100	100	100
Canopy Height (m)	5	5	5	5
Canopy Base Height (m)	1	1	1	1
Canopy Bulk Density (kg/m³)	0.22	0.22	0.15	0.15
Fine Fuel Load (t/ha)	10	10	10.7	10
1-h Dead Surface Fuel Moisture (%)	6	5	5	9
Foliar Moisture Content (%)	105	74	100	100

RESULTS

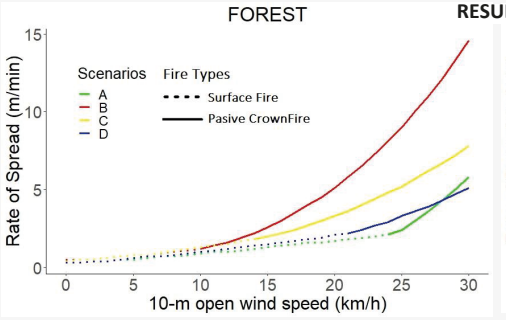

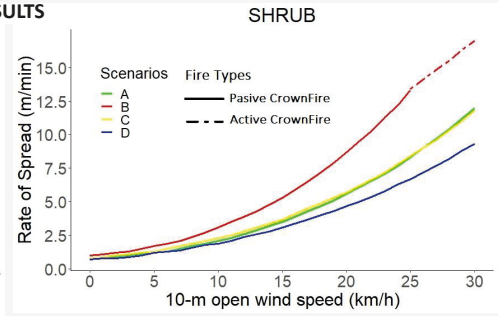

CONCLUSION

Changes in physiological and structural conditions following senescence enhance the probability of more intense and severe crown fires development and concentrate extreme tree mortality rates in senescence periods.

Balaguer-Romano, R.; Díaz-Sierra, R.; Madrigal, J.; Voltas, J.; Resco de Dios, V. Needle Senescence Affects Fire Behavior in Aleppo Pine (*Pinus halepensis* Mill.) Stands: A Simulation Study. *Forests* **2020**, *11*, 1054. https://doi.org/10.3390/f11101054

A3. Poster format presentation of Chapter III results in the 1st Electronic Conference on Forests.

LINKING FUEL MOISTURE WITH PLANT PHYSIOLOGY:

Coupling a water balance model with a LFMC model to predict species-specific LFMC values.

R. Balaguer-Romano [1,*] ,R. Díaz-Sierra [1], J. Voltas [2] & V. Resco de Dios [2,3]

[1]Mathematical and Fluid Physics Department, Faculty of Sciences, UNED. [2] Department of Crop and Forest Sciences, Universitat Lleida. [3]School of Life Science and Engineering, Southwest University of Science and Technology.

UNED

Universitat de Lleida

INTRODUCTION

Live Fuel Moisture Content (LFMC) is a critical determinant of forest flammability and thus fire behavior and severity in many ecosystems. Considering the limitations of current approaches (satellite remote sensing and drought indices) to estimate LFMC, we seek to estimate LFMC in a way that allows to obtain species-specific values and make future predictions

METHODS

To predict species-specific LFMC, we couple Medfate (1), a water balance model which uses meteorological, edaphic and forest inventory data to predict soil moisture dynamics, with Nolan et al., (2) model which estimates LFMC from leaf water potential (Ψleaf).

In all, we have analyzed more than 2500 LFMC data from 46 different species in 40 sites of the Iberian Peninsula.

Predicted LFMC values were calibrated and validated using field data from an independent LFMC data base (3). Finally, we estimate for the same study sites the drought code index (DC) and the normalized difference vegetation index (NDVI) with the aim of compare the predictive capabilities of the three approaches.

RESULTS

MEDFATE

All: R^2 = 0.5
Trees: R^2 = 0.41
Seeders: R^2 = 0.57
Resprouter: R^2 = 0.3

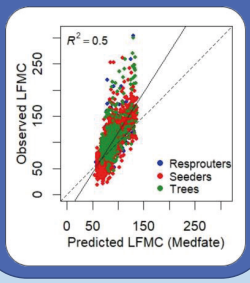

DROUGHT CODE

All: R^2 = 0.31
Trees: R^2 = 0.09
Seeders: R^2 = 0.5
Resprouter: R^2 = 0.005

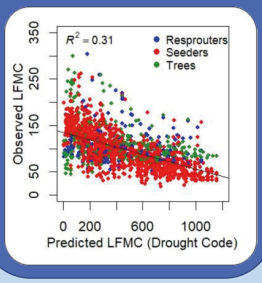

NDVI

All: R^2 = 0.28
Trees: R^2 = 0.06
Seeders: R^2 = 0.13
Resprouter: R^2 = 0.03

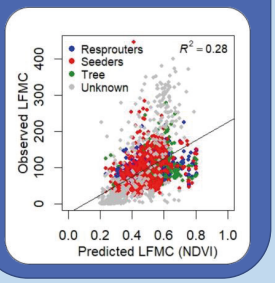

In conclusion we have linked fuel moisture with plant physiology to estimate LFMC values in a way that allow to obtain species-specific values and make future predictions.

1-Cáceres, M. De, Martínez-Vilalta, J., Coll, L., Llorens, P., Casals, P., Poyatos, R., Pausas, J. G., & Brotons, L. (2015). Coupling a water balance model with forest inventory data to predict drought stress: The role of forest structural changes vs. climate changes. Agricultural and Forest Meteorology, 213, 77–90. 2-Nolan, R. H., Hedo, J., Arteaga, C., Sugai, T., & Resco de Dios, V. (2018). Physiological drought responses improve predictions of live fuel moisture dynamics in a Mediterranean forest. Agricultural and Forest Meteorology, 263, 417–427. 3-Yebra, M., Scortechini, G., Badi, A. et al. (2019). Globe-LFMC, a global plant water status database for vegetation ecophysiology and wildfire applications. Sci Data 6, 305

A4. Poster format presentation of Chapter IV results in the 2nd Electronic Conference on Forests.

Un modelo semi-mecanicista para predecir las variaciones diarias de la humedad del combustible vivo a nivel de especie

Rodrigo Balaguer-Romano [1]

Rubén Díaz-Sierra [1], Miquel De Cáceres [2], Jordi Voltas [3], Víctor Resco de Dios [3].

[1] Departamento de Física Matemática y de Fluidos, Facultad de Ciencias, UNED, 28040 Madrid, España.

[2] CREAF, E08193 Bellaterra (Cerdanyola del Valles), Catalonia, España.

[3] Department of Crop and Forest Sciences, ETSEA-Universitat de Lleida, 25198 Lleida, España.

doi.org/10.1016/j.agrformet.2022.109022

8º CONGRESO FORESTAL ESPAÑOL

Introducción. Determinar la variación temporal de la humedad del combustible vivo (HCV) es un aspecto fundamental en la prevención y gestión de los incendios forestales. Teniendo en cuenta las limitación que presentan los métodos comúnmente utilizados para estimar la HCV (*Drought Code* e índices de vegetación espectral), en este estudio hemos desarrollado un método novedoso que permite modelizar diariamente el contenido de humedad de la vegetación obteniendo valores específicos a nivel de especie.

Métodos. La HCV se estima aplicando una relación lineal con los valores diarios del potencial hídrico de las hojas al amanecer (Ψ_{pd}), modelizados para cada especie con el modelo de balance hídrico MEDFATE. Las especies se han clasificado en tres grupos funcionales: arbustos germinadores (R-), arbustos rebrotadores (R+) y árboles (Ar). El método ha sido calibrado y validado con valores de HCV medidos en campo por un estudio independiente.

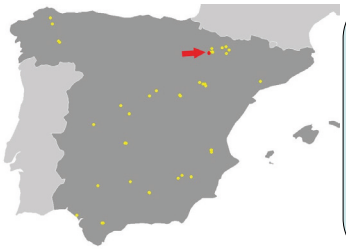

En total se han analizado 2512 datos de 37 especies, tomados entre 1996 y 2017, en 40 localizaciones con diferentes condiciones climáticas. Para evaluar la capacidad predictiva del método en términos comparativos, se ha estimado la HCV en las mismas localizaciones con *Drought Code* (DC) y el índice de vegetación *Enhanced Vegetation Index* (EVI), calculando para este último el espesor de agua equivalente (EAE).

Resultados. El método desarrollado ($MEDFATE_{HCV}$) permite estimar las variaciones diarias de la HCV considerando distintos géneros (Tabla 1) y especies, obteniendo mayor calidad de ajuste con los datos observados, que las estimaciones realizadas con Drought Code (DC_{HCV}) o con teledetección (EVI_{EAE}), en todos los grupos funcionales (Figura 1). En la Figura 2 se representan las dinámicas anuales de la HCV observada (línea negra discontinua) y predicha con MEDFATE (línea color continua) en una localización representativa (flecha roja) compuesta por el arbusto germinador *Genista scorpius (R-)*, el arbusto rebrotador *Quercus coccifera (R+)* y el árbol *Quercus ilex (Ar)*.

Tabla 1. Géneros analizados, numero de repeticiones (N), coeficiente de determinación (R^2) y error absoluto medio (EAM).

	N	R^2	EAM
Cistus (R-)	483	0.7	16.1
Lavandula (R-)	33	0.5	52.9
Salvia (R-)	473	0.6	24.0
Thymus (R-)	47	0.7	33.6
Ulex (R-)	46	0.5	20.5
Arbutus (R+)	29	0.5	50.5
Buxus (R+)	53	0.4	11.3
Erica (R+)	43	0.3	17.6
Genista (R+)	30	0.6	19.4
Pinus (Ar)	121	0.5	16.8
Quercus (Ar)	347	0.6	23.1

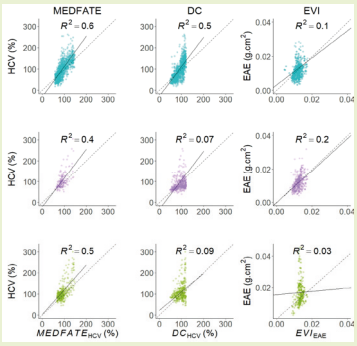

Figura 1. Calidad del ajuste entre la HCV (%) observada y predicha en cada grupo funcional: Germinadores (R-) azul; Rebrotadores (R+) morado; Árboles (Ar) verde.

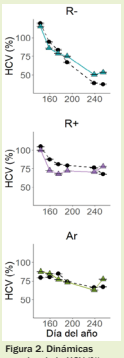

Figura 2. Dinámicas anuales de la HCV (%).

Conclusión. El método desarrollado permite predecir diariamente el contenido de humedad de la vegetación obteniendo valores específicos a nivel de especie. Nuestras estimaciones se ajustan mejor con los valores observados que las obtenidas con *Drought Code* o los índices de vegetación espectral.

La Ciencia forestal y su contribución a los Objetivos de Desarrollo Sostenible

Comunicación disponible en

8º CONGRESO FORESTAL ESPAÑOL 2022 Lleida 27·1 junio·juny julio·juliol Catalunya

Sociedad Española de Ciencias Forestales SECF

A5. Poster format presentation of Chapter IV results in the 8th Spanish Forestry Congress.

Fuel moisture content dynamics under climate change in Spanish forests.

R. Balaguer-Romano [1,*], R. Díaz-Sierra [1] & V. Resco de Dios [2,3]

[1]Mathematical and Fluid Physics Department, Faculty of Sciences, UNED. [2] Department of Crop and Forest Sciences, Universitat Lleida. [3]School of Life Science and Engineering, Southwest University of Science and Technology.

INTRODUCTION

Global warming is expected to increase water scarcity potentially enhancing the days with weather conditions conducive to wildfire spread. In order to asses how fuel moisture (FM) is going to be affected by increasing aridity, we used semi-mechanistic models to forecast changes in live and dead fuel moisture content (LFMC and DFMC) across the 21st century from medium and high greenhouse gas emission scenarios (RCP4.5 and 8.5).

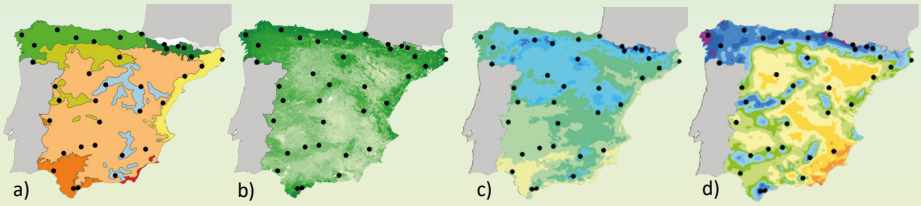

METHODS

We assessed LFMC and DFMC across 36 study sites which corresponds with forest inventory plots, covering ecoregions (a), productivity (b), temperature (c) and precipitation (d) gradients. Future meteorological data was obtained from regional climate models of the Euro-CORDEX adjusted grid. To analyse FM dynamics we assessed changes on the fire season length as the number of days per year (d yr^{-1}) when FM fell below wildfire occurrence thresholds. We established the minimum, critical and extreme threshold values at 120, 100 and 80 % for LFMC and at 12, 10 and 8 % for DFMC.

RESULTS

From 2020 to 2100, under RCP4.5 conditions fire season length increased in 15, 8, 2 d yr^{-1} (a) and in 20, 17, 15 d yr^{-1} (b) regarding minimum, critical and extreme LFMC and DFMC thresholds respectively. Under RCP 8.5 conditions fire season length increased in 50, 30, 5 d yr^{-1} (a) and in 46, 40, 33 d yr^{-1} (b) regarding minimum, critical and extreme LFMC and DFMC thresholds respectively.

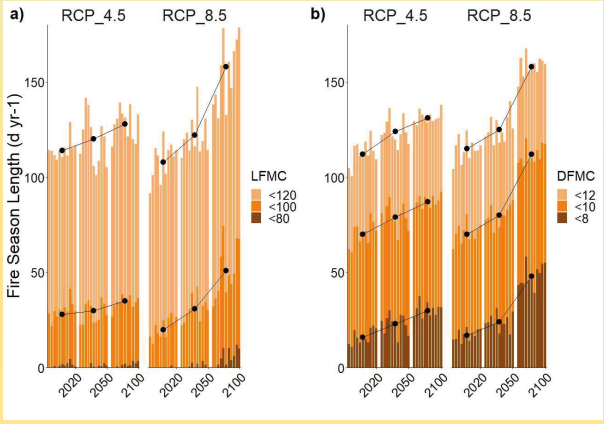

CONCLUSION

We recorded generalized fuel moisture declining trends from nowadays to the end of the century that are going to increase the number of days per year with FM values below wildfire occurrence thresholds, lengthening fire seasons.

A6. Poster format presentation of Chapter V results in the 3rd Electronic Conference on Forests.

2021

CONSECUENCIAS DEL CAMBIO CLIMÁTICO EN EL RÉGIMEN DE INCENDIOS DE LOS PINARES PIRENAICOS

Consequences of climate change on the fire regime of the Pyrenees pine forest

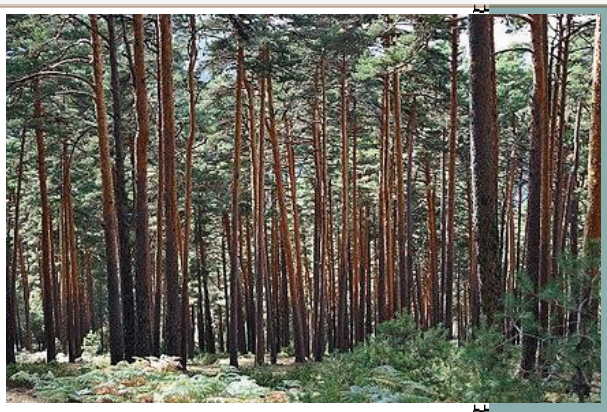

Tutores:

Rodrigo Balaguer-Romano

Rubén Díaz Sierra

Ana Renshaw Calderón 02717312T

Estudiante Ciencias ambientales

UNED (2020-2021)

30/06/2021

A7. Environmental Sciences Bachelor Thesis tutored during this PhD Thesis.

Universidad Nacional de Educación a Distancia
Facultad de Ciencias
Departamento de Física

Memoria del Trabajo Fin de Grado en Física

Optimización de un modelo de balance hídrico.

Gonzalo Figueroa Losana

Tutores: Rodrigo Balaguer Romano y Ruben Diaz Sierra

Curso 2021/2022

A8. Physics Bachelor Thesis tutored during this PhD Thesis.